AIR FORCE INSTITUTE OF TECHNOLOGY

AIR UNIVERSITY
UNITED STATES AIR FORCE

SCHOOL OF ENGINEERING

WRIGHT-PATTERSON AIR FORCE BASE, OHIO

AF-WP-O-MAY 62 3,500

ESCAPE TRAJECTORIES FOR LOW THRUST VEHICLES

Lt John J. Dell

GA/Phys/62-4

AF-WP-O-OCT 62 25

ESCAPE TRAJECTORIES FOR LOW THRUST VEHICLES

THESIS

Presented to the Faculty of the School of Engineering of
the Air Force Institute of Technology
Air University
in Partial Fulfillment of the
Requirements for the Degree of
Master of Science

By
John Joseph Dell, B.S. M.E.
1st Lt USAF

Graduate Astronautics

August 1962

Preface

A significant part of current space research and development programs are being directed toward low-thrust devices.

This study is concerned with determining the validity of various numerical and analytical equations and in performing a parametric performance investigation of these devices.

Since the mission duration for these devices can range from days to years, this paper will be confined to only one small aspect of the mission profile, that pertaining to escape missions from the earth's gravitational field.

Equations of motion in addition to Euler-Lagrange optimization equations were solved using certain simplifying assumptions.

Solutions were obtained from an IBM 7090 Low-Thrust Digital Computer Program. The solutions for the parametric investigations represent different combinations of specific impulse and electrical power requirements.

Computer data is represented in graphical form in Section V of this study. No attempt has been made to tabulate and report all the computer output since this data would contribute little toward analyzing the results.

I wish to acknowledge my indebtedness to Mr. Fred L'Hommedieu of the Propulsion Laboratory, ASD whose assistance made this study possible and to my advisor, Capt Richard C. Wingerson for his guidance and many helpful suggestions. I also wish to express my appreciation

to Mr. Carroll Fetter and Mr. Wayne A. Buchtel of the Digital Computation Group, ASD whose assistance was required in obtaining a workable computer program. Without their faithful co-operation, the computer results would not have been possible.

John J. Dell

Contents

Contents

List of Figures

List of Figures

List of Tables

List of Tables

Abstract

This study is concerned in determining: (1) the escape parameters (time, range angle and position) for achieving optimum escape missions using low-thrust vehicles, and (2) the magnitudes of deviation from previously reported analytical and numerical calculations.

The equations of motion in addition to Euler-Lagrange optimization equations were solved using an IBM 7090 Low-Thrust Digital Computer Program.

Specific impulses were varied from 1,000 to 25,000 seconds and electrical power outputs were varied from 100 KW to 100 MW. Planar orbits (initially circular) were assumed.

Results of the parametric investigation are presented both in tabular and graphical form. Analysis of generated escape data indicate that the analytical equations previously reported have deviations ranging from approximately -25% to 44%. Numerical results previously reported are in general agreement with this study.

I. Introduction

Space propulsion is here but due to present day payload limitations of conventional chemical rockets, low thrust propulsion devices are presently being evaluated by various governmental and civilian organizations in the United States.

Results of several ASD sponsored contracts on mission analysis have shown that these devices have the capability of transferring large payloads for interplanetary missions when compared to conventional chemical rockets (Ref 9: 151-152).

In evaluating these devices, parameters associated with the engine, vehicle and specific mission must all be taken into consideration for a complete analysis.

Engine parameters include thrust, specific impulse, electrical power requirements and efficiencies associated with the engine and the power plant. Vehicle parameters include the thrust - to - weight ratio and mass fractions allocated to each subsystem of the vehicle. Finally, mission parameters include mission time, velocity and energy requirements to successfully accomplish the mission.

The range of specific impulse, which is a measure of engine performance, is estimated to be between 1,200 to 30,000 seconds corresponding to thrust levels of 10 and 1 pounds respectively (Ref 18: 133).

The initial thrust - to - weight ratios will vary from 10^{-1} to 10^{-6} g's. This indicates that the use of low thrust devices is

restricted to outer space operations after these devices have been boosted into orbit by conventional chemical rockets.

Electrical power requirements will vary from a few kilo-watts for satellite sustainer missions to beyond the mega-watt region for interplanetary missions (Ref 11: 7).

Any interplanetary 1-way mission can be divided into five phases. The first phase includes the chemical boost phase from the earth's surface to a predetermined satellite orbit. The second phase includes the escape flight of the space vehicle where the low thrust device is continually in operation. The vehicle spirals slowly outward until escape conditions are achieved whereby the vehicle energy is greater that the earth's gravitational energy. The third phase includes the transfer trajectory to the target planet. The fourth phase includes a parking orbit for the space vehicle and finally the fifth phase involves descent to the planets surface.

Statement of the Problem

This study is concerned exclusively with the following two items:

1. Perform parametric investigations to determine escape parameters for achieving optimum escape missions (Phase 2) associated with an interplanetary mission.
2. Determine magnitudes of deviation from previously reported analytical and numerical calculations.

The parameter variations selected for this study are great enough to cover approximately the complete spectrum of low thrust engines that

are of current interest. For example, specific impulses varied from 1,000 to 25,000 seconds and electrical power outputs varied from 100 KW to 100 MW.

The problem is restricted, however, to initial circular orbits originating in the equatorial plane. Also, atmospheric drag and oblateness of the earth were not considered in this study.

The parametric investigation was performed by using an IBM 7090 Digital Low-Thrust Computer Program developed under contract AF 33(616)-7313 (Ref 10).

Organization

The study is presented in 7 major sections. Appropriate background material concerning analytical equations and previous reported investigations are presented initially.

Following these are sections covering the ASD low thrust computer program and the numerical results obtained therein. These results are presented in graphical form for a reference altitude of 1036.5 statute miles. Also, included are generalized graphs for determining the escape parameters for any other reference altitude. Following these are additional sections covering discussions and comparisons of other analytical and numerical results. A numerical example is also included to illustrate the use of the generalized data obtained in this study.

There are also 5 appendices which contain supplementary information necessary to thoroughly understand this study. Appendix A explains the differential equations of motion used in the ASD computer

program. Appendix B contains an analytical investigation to determine what engine parameters affect the escape trajectory. Appendix C discusses the variational approach to optimization while Appendix D explains the various formats in supplying input data to the ASD low thrust computer program. Finally, Appendix E includes a list of symbols used in this study.

II. Analytical Equations

Equations of Motion

The differential equations of motion, based on Kepler's Law of Planetary Motion, in polar co-ordinates are given below: (Ref 13: 81-82)

$$m\left(\ddot{r} - r\dot{\theta}^2\right) = -Gm\frac{M}{r^2} \tag{1}$$

$$m\left(2\dot{r}\dot{\theta} + r\ddot{\theta}\right) = \frac{1}{r}\frac{d\left(m r^2 \dot{\theta}\right)}{dt} = 0 \tag{2}$$

All symbols are defined in Appendix E.

When a constant thrust (F) (Fig 24(a)) is applied to the space vehicle, Eqs (1) and (2) are modified as follows:

$$m\left(\ddot{r} - r\dot{\theta}^2\right) = -Gm\frac{M}{r^2} + F\sin\beta \tag{3}$$

$$m\left(2\dot{r}\dot{\theta} + r\ddot{\theta}\right) = \frac{1}{r}\frac{d\left(m r^2 \dot{\theta}\right)}{dt} = F\cos\beta \tag{4}$$

where

m = instantaneous vehicle mass.

r = radial distance from the center of the earth to the vehicle in orbit.

θ = range angle.

G = universal gravitational constant.

M = mass of central body.

F = engine thrust.

β = in-plane throw off angle measured from unit vector $\bar{\bar{T}}$ to F (See Fig 24a).

Conservation of Energy and Angular Momentum

The total energy, V.E., per unit mass for an object describing a conic is given by

$$V.E. = \frac{1}{2}\left[(\dot{r})^2 + (r\dot{\theta})^2\right] - \frac{G\,M}{r} \qquad \text{(Ref 13: 60) (5)}$$

For a space vehicle to have sufficient energy to escape the earth's gravitational field, the escape condition is determined when the total vehicle energy is zero.

The total angular momentum per unit mass, h, is given by

$$h = r^2\dot{\theta} \qquad \text{(Ref 13: 81) (6)}$$

Vehicle Velocity Increment

The maximum velocity change, ΔV, that a vehicle may attain in a field free space is expressed by

$$\Delta V = c \ln \frac{M_o}{M_1} \qquad \text{(Ref 17: 4) (7)}$$

where

c = exhaust velocity of vehicle

M_o = initial mass of vehicle

M_1 = mass of vehicle at escape

Specific Impulse

Specific impulse is a measure of engine performance and is given by

$$I_{sp} = \frac{F}{\dot{W}} = \frac{c}{32.172} \qquad (8)$$

where

$$F = \dot{m} c \tag{9}$$

The conversion factor 32.174, is in $lb_{(mass)}$ - $ft/lb_{(force)}$ - sec^2 and the vehicle exhaust velocity, c, is in ft/sec.

Jet Power and Specific Weight

The power in the exhaust jet of the low thrust device is given by

$$P = \frac{1}{2} \dot{m} c^2 \tag{10}$$

Introducing Eqs (8) and (9) into (10) yields

$$P = \frac{F I_{sp}}{45.854} \tag{11}$$

where the electric power, P, is expressed in KW, F is the engine thrust expressed in pounds, and I_{sp} is given in seconds.

The specific weight of the electrical power plant is equal to the weight of the power plant, W_{pp}, divided by the electrical output, P, to the low thrust device.

$$\alpha = \frac{W_{PP}}{P} \tag{12}$$

Unclassified data on electrical power plants are shown on Figures (1) and (2) (Ref 6: 23). From these figures, the specific weight parameter is related to electrical power output by the following approximate equation:

$$\alpha = 514.2 \, P^{-0.6746} \qquad \text{(Ref 10: II-4)} \tag{13}$$

where the electrical power output, P, is expressed in KW.

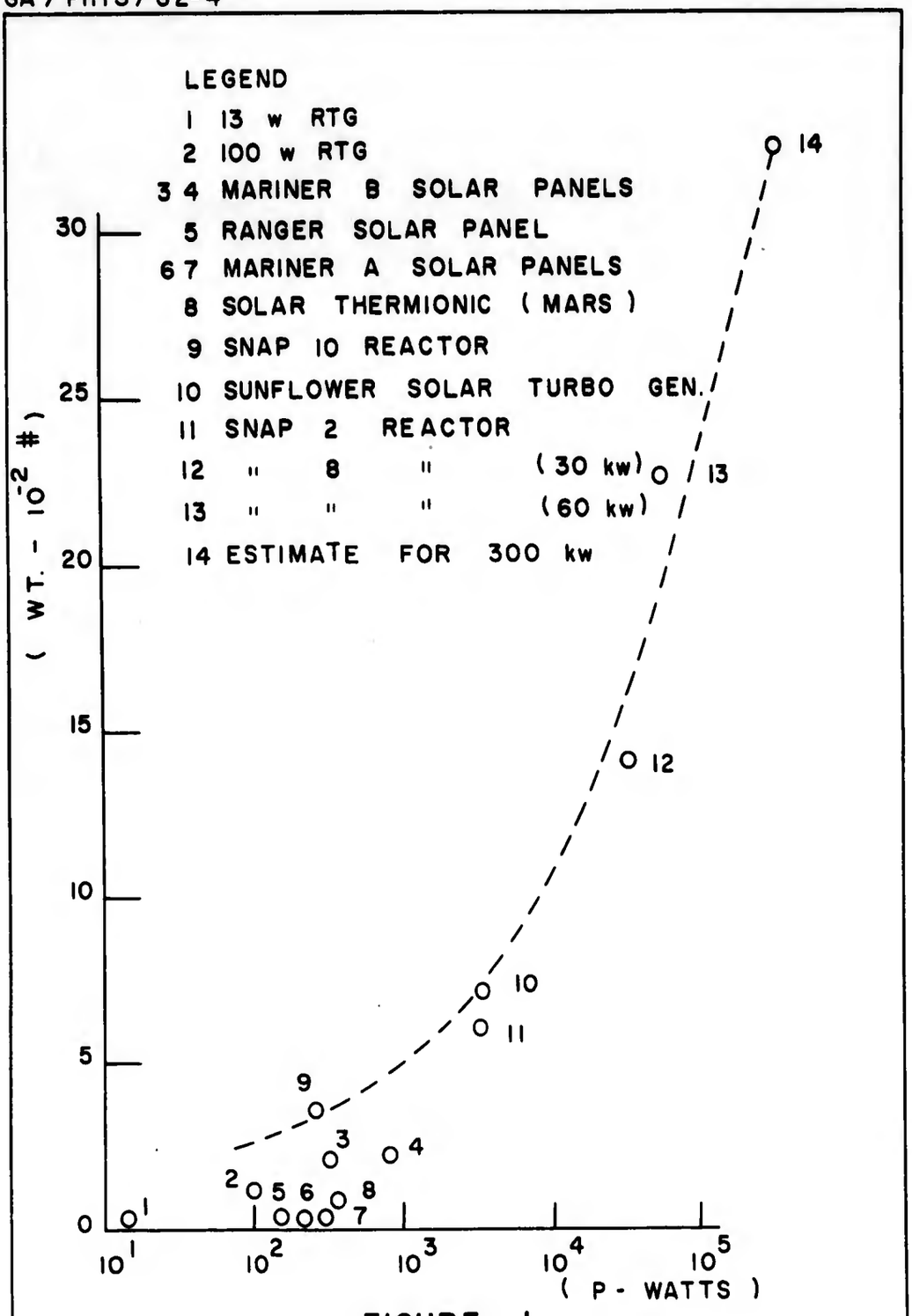

FIGURE 1

POWER PLANT WEIGHT

vs POWER LEVEL

(REF 6:23)

GA / PHYS / 62-4

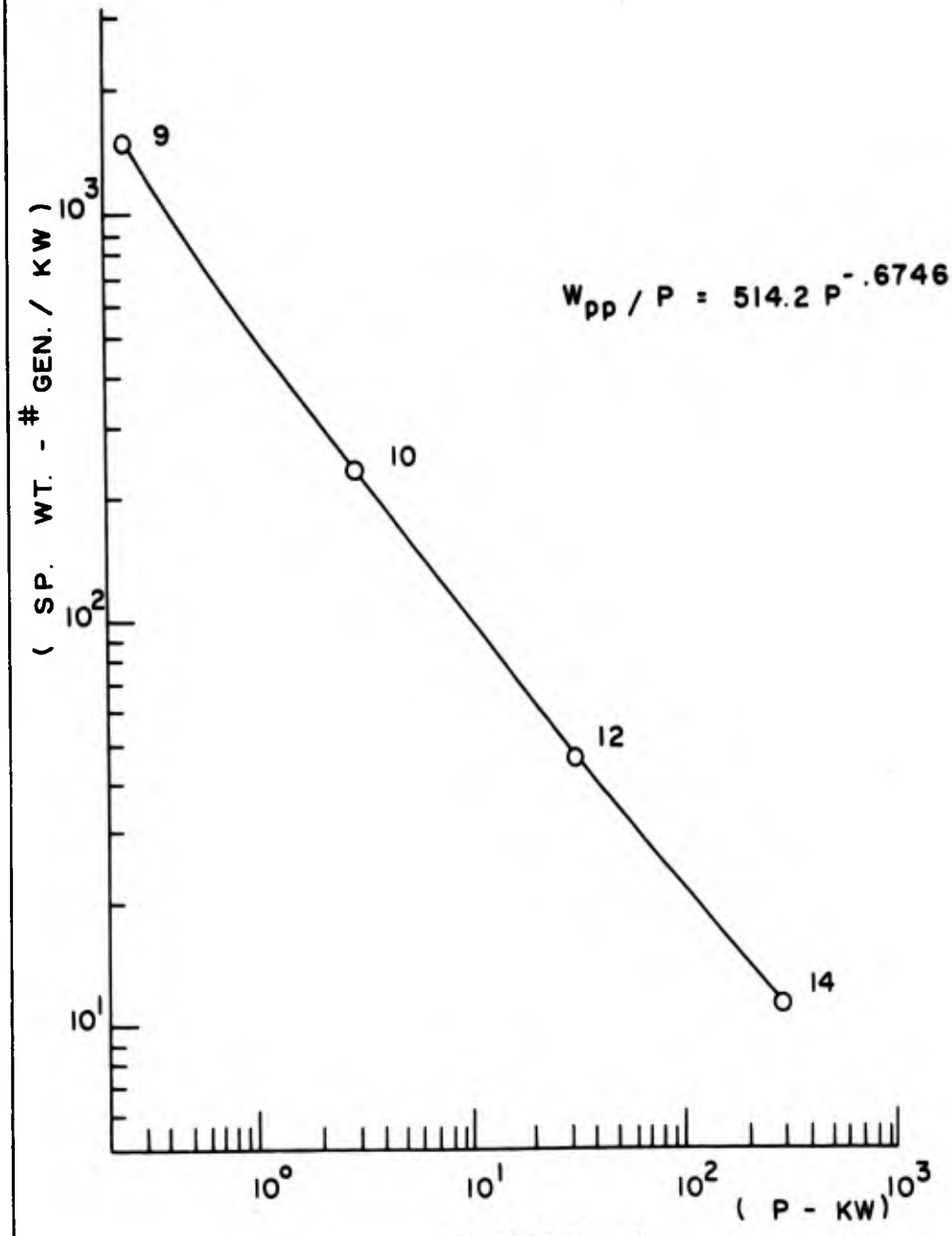

FIGURE 2

POWER PLANT SPECIFIC WEIGHT

vs POWER LEVEL

(REF 6 : 23)

Equation (13) is incorporated in the ASD computer program where specific weight requirements are calculated for given input power levels.

Circular Velocity

The velocity (V_{c_o}) of a vehicle in a circular orbit is given by

$$V_{c_o}^2 = r_o \, g_o \tag{14}$$

where

$$g_o = g_E \left[\frac{R_E}{r_o} \right]^{+2} \tag{15}$$

The symbols g_o and r_o represent the acceleration of gravity and the orbital radius taken at initial conditions; and R_E is the earth's radius taken as 3963.5 stat. miles.

Nondimensional Parameters

Nondimensional terms, used throughout this study, are defined below.

The nondimensional escape time, ($T_{1_{nd}}$), is given by

$$T_{1_{nd}} = T_1 \times \frac{V_{c_o}}{r_o} = T_1 \times \omega_o \tag{16}$$

where T_1 is the actual escape time expressed in seconds; and ω_o is the angular velocity of the vehicle taken at r_o.

The nondimensional escape radius, (ρ), is given by

$$\rho = \frac{r_1}{r_o} \tag{17}$$

where r_1 represents the actual escape radius.

The nondimensional angular momentum, (h_{nd}), per unit mass is given by

$$h_{nd} = \frac{h}{r_o V_{c_o}} \tag{18}$$

where h is given by Eq (6).

The nondimensional vehicle energy, $(V.E._{nd})$, per unit mass is given by

$$(V.E._{nd}) = \frac{V.E.}{V_{c_o}^2} \tag{19}$$

where V.E. is given by Eq (5).

The nondimensional vehicle velocity, (V_{nd}), is given by

$$V_{nd} = \frac{V}{V_{c_o}} \tag{20}$$

where V represents the vehicle velocity on the escape trajectory.

The nondimensional vehicle thrust, (F_{nd}), is given by

$$F_{nd} = \frac{F}{W_o \cdot \frac{g_E}{g_o}} \tag{21}$$

where F is engine thrust expressed in pounds force; W_o represents the initial vehicle weight at the reference altitude and is expressed in pounds.

The nondimensional thrust acceleration, (A_o), is given by

$$A_o = \left[\frac{A}{g_E}\right] \frac{g_E}{g_o} \tag{22}$$

where A represents the vehicle acceleration on the escape trajectory expressed in ft/sec^2. The bracket term of Eq (22) is computer output data and represents the thrust-to-weight ratio of the vehicle.

Specific Mission Energy

The specific mission energy, E, associated with each escape mission is defined as follows:

$$E = \frac{PT}{W_o \times \frac{g_E}{g_o}} \tag{23}$$

This parameter represents the energy expended by the vehicle per pound of vehicle weight in escaping the earth's gravitational field.

Optimization of Mass Fraction Equations

Space missions involving optimization programs are concerned in answering the following questions:

1. Given a fixed mission time, what is the maximum possible payload?
2. Given a fixed payload, what is the minimum flight time?

Irving (Ref 5: 4) has shown that a low-thrust device should operate at the maximum achievable power level for minimum propellant consumption. This was substantiated by the following equation

$$\frac{M_o}{M_1} = 1 + \frac{M_o}{M_{pp}} \times \frac{\alpha_m}{2} \int_o^T A^2 \, dT \qquad \text{(Ref 5:4)} \tag{24}$$

where

M_o = initial vehicle mass

M_1 = vehicle mass @ escape

M_{PP}= power plant mass

α_m = specific mass of power plant

A = vehicle acceleration

T = time

Equation (24) may be rewritten as

$$\frac{M_o}{M_1} = 1 + \frac{M_o}{M_{PP}} * \alpha_m \quad J \tag{25}$$

or

$$\frac{M_o}{M_1} = 1 + \frac{M_o}{P} * J \tag{25a}$$

where the propellant utilization factor, J, is defined as

$$J = \frac{1}{2} \int_o^T A^2 \, dT = \frac{P}{M_o} \left[\frac{M_o}{M_1} \quad -1 \right] \tag{26}$$

and

$$P = \frac{M_{PP}}{\alpha_m} \tag{12}$$

Therefore, for minimum propellant consumption, Eq (26) must be minimized.

It was also stated (Ref 4: 32) that the minimization of propellant consumption is achieved by optimizing both the thrust magnitude and direction for a given power plant and mission time.

From an engineering standpoint, subsystems required for optimization of the thrust magnitude as a function of time or range angle will require additional vehicle weight. To keep these subsystem weights to

a minimum, it was assumed for this study that only the direction of the thrust vector be optimized for maximum payload.

The initial mass of a space vehicle is given by

$$M_o = M_{PL} + M_{ST} + M_{PP} + M_P \tag{27}$$

or

$$1 = \frac{M_{PL}}{M_o} + \frac{M_{ST}}{M_o} + \frac{M_{PP}}{M_o} + \frac{M_P}{M_o} \tag{27a}$$

where

M_{PL} = payload mass

M_{ST} = vehicle structure mass

M_P = propellant mass

For maximum payload, exclusive of the power plant, M_{PP} must be selected which maximize $M_{PL} + M_{ST}$ (Ref 5: 5).

The ratio of payload and structure mass to original vehicle mass is given by

$$\frac{M_{PL} + M_{ST}}{M_o} = \frac{M_1 - M_{PP}}{M_o} \tag{28}$$

Introducing Eqs (25) and (12) into (28) and simplifying yields

$$\frac{M_{PL} + M_{ST}}{M_o} = \frac{M_{PP}}{M_o} \times \left[\frac{1}{\frac{M_{PP}}{M_o} + \alpha_m J} - 1 \right] \tag{29}$$

The maximum $M_{PL} + M_{ST}$ is obtained by taking it's differential with respect to M_{PP} and equating it to zero.

$$\frac{d\left[\frac{M_{PL}+M_{ST}}{M_o}\right]}{d\left[\frac{M_{PP}}{M_o}\right]} = \frac{1}{\left[\frac{M_{PP}}{M_o}+\alpha_m{}^J\right]} - \frac{M_{PP}}{M_o\left[\frac{M_{PP}}{M_o}+\alpha_m{}^J\right]^2} - 1 = 0$$

or

$$\frac{M_{PP}}{M_o} = \left[\alpha_m{}^J\right]^{1/2} - \alpha_m{}^J \tag{30}$$

The ratio of propellant to original vehicle mass is given by

$$\frac{M_P}{M_o} = \frac{M_o - M_1}{M_o} \tag{31}$$

Using Eqs (31) and (30) into (25) and simplifying yields

$$\frac{M_P}{M_o} = \left[\alpha_m{}^J\right]^{1/2} \tag{32}$$

Introducing Eqs (30) and (32) into (27a) yields

$$\frac{M_{PL}+M_{ST}}{M_o} = 1 - 2\left(\alpha_m{}^J\right)^{1/2} + \alpha_m{}^J = \left[1 - \left(\alpha_m{}^J\right)^{1/2}\right]^2 \tag{33}$$

Equation (33) may be expressed in terms of the original and final mass fraction by re-introducing Eq (32) into Eq (33) which gives

$$\frac{M_{PL}+M_{ST}}{M_o} = \left[1 - \frac{M_P}{M_o}\right]^2 = \left[\frac{M_1}{M_o}\right]^2 \tag{34}$$

For optimum conditions, Eqs (26), (31), (34) and (27a) are used in determining the various mass fractions of the vehicle. The propellant

utilization factor, J, is a function of mission duration and is graphically plotted on Figure 16.

III. Previous Analytical and Numerical Investigations

Circumferential Thrust

The solutions of the equations of motion for a vehicle in orbit are frequently based on certain simplifying assumptions.

A preliminary analytical study involving an escape mission was reported by Tsien (Ref 19: 233-236).

His assumptions included:

1. Initial orbit is circular.
2. Thrust acceleration (A_o) is constant and is directed either in the radial or circumferential direction.
3. At time equal to zero, $\dot{\rho} = \ddot{\rho} = 0$, $\rho = 1$ and $\dot{\theta} = 1$.

Making use of these assumptions, the following equations were obtained (Ref 19: 236);

$$\rho = \left[\frac{1}{1 - A_o T_{1_{nd}}}\right]^2 = \frac{1}{\sqrt{2A_o}} \tag{35}$$

$$T_{1_{nd}} = \frac{1 - (2\ A_o)^{\frac{1}{4}}}{A_o} \tag{36}$$

and

$$\frac{I_{sp}\ g_E}{\sqrt{g_o\ r_o}}\ \log_e \left[\frac{M_o}{M_1}\right] = A_o\ T_{1_{nd}} \tag{37}$$

where

ρ = nondimensional escape radius $\left[\frac{r_1}{r_o}\right]$

A_o = nondimensional thrust acceleration

$T_{1_{nd}}$ = nondimensional escape time

Tsien concludes from his approximate solution that the most efficient means for minimum fuel expenditure is to maintain the thrust direction in a circumferential direction instead of the radial direction. Circumferential direction is defined as being perpendicular to the radius vector and contained in the equatorial plane. The radial direction is measured outward from the center of the earth and is also contained in the equatorial plane. These directions are illustrated in Figure (24a).

Tangential Thrust

Lawden (Ref 7: 43) has shown analytically that thrust directed in the tangential direction results in the greatest instantaneous rate of energy change with respect to the vehicle mass by the following equation.

$$\frac{d(V.E.)}{dt} = v \cdot c \left[\frac{d(\log M)}{dt}\right] \qquad \text{(Ref 7: 43)} \qquad (38)$$

The object here is to raise the energy as quickly as possible for minimum fuel expenditure. This, however, does not maximize the energy change during engine operation but is a good approximation to optimum. Lawdens (Ref 7: 51) numerical results indicate the optimum thrust

direction lies between the circumferential and tangential directions of the trajectory.

Benny (Ref 1: 167-169) has also analytically investigated the case of tangential thrust. His assumptions included:

1. Initial orbit is circular.
2. Thrust acceleration is constant.
3. $\frac{d^2\rho}{ds^2} = 0$ through out the mission.
4. $s = \frac{d\rho}{ds} = 0$ at $\rho = 1$ and $T_o = 0$.

where

s = distance traveled on trajectory.

The analytical investigation yielded the following equations (Ref 1: 169)

$$\rho = \frac{1}{(20\ A_o^2)^{\frac{1}{4}}} \tag{39}$$

$$\theta = \frac{180}{4\pi A_o} \tag{40}$$

$$T_{lnd} = \frac{1}{A_o}\left[1 - 20^{1/8}\ A_o^{1/4}\right] \tag{41}$$

$$\frac{I_{sp}\ g_E}{\sqrt{g_o\ r_o}}\ \log_e\left[\frac{M_o}{M_1}\right] = (1 - 20^{1/8}\ A_o^{1/4}) \tag{42}$$

Previous numerical investigations have been accomplished by Perkins (Ref 15: 291-297). His numerical results are plotted in generalized trajectory curves relating nondimensional parameters that

include vehicle velocity, radial distance and time.

Perkins assumptions included:

1. Initial orbit is circular.
2. Constant thrust acceleration.

The nondimensional Perkin's parameters for initial circular orbits are defined as (Ref 15: 294):

$$X \triangleq A_o^{\frac{1}{2}} \frac{r}{r_o} \tag{43}$$

$$Y \triangleq A_o^{\frac{1}{4}} \frac{V}{V_{c_o}} \tag{44}$$

$$T \triangleq \left[\frac{V_{c_o}}{r_o}\right] A_o^{3/4} T \tag{45}$$

These parameters are introduced into the differential equations of motion so that the equations of motion are independent of $\underline{GM}$ and $\frac{\underline{F}}{m}$.

For $A_o \leq 10^{-2}$, Perkins obtains a single curve of Y as a function of X and Y as a function of $\underline{T-T_1}$. Perkins data are shown on Figures (22) and (23).

IV. ASD Low-Thrust Computer Program

The analytical solutions involving earth - escape missions have been presented in the preceding section. It should be noted that all the analytical and numerical solutions incorporated simplifying assumptions in order to obtain approximate solutions.

Since a major effort of this study was devoted to obtaining a workable low-thrust computer program, it was necessary to use the following assumptions:

1. Motion of space vehicle takes place around a point mass so that there are no perturbations acting on the vehicle due to atmospheric drag and central body oblateness. Dr. Strughold*, among others, have stated that aerodynamic drag is effectively terminated at an altitude of approximately 120 miles. Since all escape missions originated at altitudes of 1036.5 miles and 300 miles, this assumption is valid.
2. Initial orbits are circular so that the computer results are compatible with the analytical assumptions.
3. Effects of the sun, moon, and other planets are neglected. The only external force acting on the vehicle is the central gravitational force field.

* Paper "Extraterrestrial Environment" presented to the Graduate Astronautics students in April 1962 by the Aerospace Medical Laboratory.

4. The computer program was restricted to a two dimensional study. All trajectories were in the equatorial plane.
5. Low-thrust devices are operating at 100% efficiency. Since these devices operate at various efficiencies depending upon their operating mode, the intent of this study is to obtain general results. Therefore, for indicating "trends", this assumption is valid.
6. For equal basis of comparison, the weight of the electrical powerplant is assumed to be 25 percent of the initial gross weight of the vehicle. Irving's graphical results (Ref 5: 14), indicating distribution of masses for maximum payload, clearily shows that the powerplant mass fraction is approximately 25% except at the end points of the curve where it approaches zero. Therefore, this assumption is justified.

The equations of motion and the Euler-Lagrange equations were numerically integrated by an IBM 7090 Digital Computer program outlined in Appendix C.

Computer Options

The computer program is basically divided into nine different options involving various combinations of thrust magnitude and direction. The options used in this study are defined as:

Option 4 - Engine thrust is constant.
Thrust direction is optimized.

Option 5 - Specific impulse is constant.
Thrust direction is optimized.

Option 6 - Thrust acceleration, β and γ are constant throughout the mission profile.

Option 9 - Engine thrust, β and γ are constant throughout the mission profile.

Approximately 85% of all computer runs involved Option #5. Other options were run essentially to note any differences in output data.

Error Bounds

It must be emphasized that the numerical integration on the digital computer is subject to a compromise between truncation and round-off errors (Ref 3: 3D-15). Truncation error is due to finiteness of a particular series being expanded about a point where the integrand is being evaluated. This error can be reduced by decreasing the integration step size. The round-off error is due to the finite number of digits being carried in each calculation and the error increases when the number of computations is increased.

The computer program (Ref 10: II-37) uses the Runge-Kutta integration procedure. Its advantage over other techniques is that it is able to integrate to a specified point in advance. The integration procedure is started with ease and the integration step size can be changed for any specified error control (Ref 3: 3D-16). If the calculated error exceeds the maximum stipulated error, then

1. The integrated value of the dependent variable is rejected by the computer.

2. The interval size is reduced by $\frac{1}{2}$ and the integration procedure is resumed.

Thus, the choice of the integration step size and the error bound is critical in determining the accuracy required in the final result.

Table I summarizes the step sizes and error bounds used in this investigation.

Printed Output and Stopping Conditions

The computer program will print out, for each numerical integration, the parameters listed in Table II.

Table II

ASD Computer Print Out Data

Orbit	Vehicle	Trajectory
Total Energy	Thrust Acceleration	Time
Angular Momentum	Thrust Magnitude	Range Angle
Eccentricity	Specific Impulse	Radius
Semi-Major Axis	Efficiency	Velocity
Semi Latus Rectum	Mass Ratio	Attack Angle
Inclination	Longitude	Thrust Angles (β & γ)
Node Location	Latitude	

The computer program will automatically stop under the following conditions:

Run No.	Option No.	Integ Step Size	Error Bound	I_{sp} (sec)	Power (KW)
16-1	5	10^{o}	10^{-4}	1,000	100,000
26-1	5	1^{o}	10^{-5}	1,000	100,000
17-2	9	10^{o}	10^{-4}	5,000	100,000
16-2	5	10^{o}	10^{-4}	5,000	100,000
17-3	6	10^{o}	10^{-4}	5,000/ 5501.7	100,000
17-1	4	10^{o}	10^{-4}	5,000	100,000
21-4	5	10^{o}	10^{-5}	25,000	100,000
16-4	5	10^{o}	10^{-4}	1,000	10,000
21-3	5	10^{o}	10^{-5}	5,000	10,000
21-7*	5	10^{o}	10^{-5}	25,000	10,000
21-1	5	10^{o}	10^{-5}	1,000	1,000
21-2	5	10^{o}	10^{-5}	5,000	1,000
23-2*	5	10^{o}	10^{-5}	25,000	1,000
21-6	5	10^{o}	10^{-5}	1,000	100
22-1*	5	10^{o}	10^{-5}	5,000	100
19-2	5	30^{o}	10^{-4}	5,000	100
23-1*	5	10^{o}	10^{-5}	25,000	100
21-5	5	10^{o}	10^{-5}	5,000	3,500

Notes:

$M_{PP} = .25M_{o}$

* Based on extrapolated data.
See Figures (1) and (2).

TABLE I

ASD Computer Input Parameters

1. Designated range angle is exceeded.
2. Weight of vehicle becomes greater than unity.
3. Weight of vehicle becomes negative.
4. Numerical value from the transversality equation exceeds 100. For optimum trajectories, this value should be close to zero.

From variational calculus, the transversality condition is a necessary condition in determining a minimum solution of Euler's equation with a variable end-point (Ref 2: 166-167). Equation (103) in Appendix C represents the transversality condition that is used in the low-thrust computer program.

V. Discussion of Results

Parametric Investigations

Numerical results of the ASD low-thrust computer program are shown in graphical form in Figures 3 through 15 and are tabulated in Tables III and IV. The tabulated data represents interpolated escape data obtained between two integration calculations. The ASD computer program was not programmed to print output data at escape conditions. Printed output intervals were based on integration step sizes and error bounds. Therefore, the escape point was determined where vehicle energy changed from a negative to a positive value. A linear interpolation between these two points was accomplished to determine exactly the escape position. A scale factor resulting from this interpolation was then applied to the printed output data, obtained prior to escape, in order to obtain low-thrust vehicle escape data.

The term "escape parameters" used in this section will pertain to escape time, escape radius, and final range angle.

These figures show the escape parameters as functions of initial thrust - to - weight ratios and specific impulses for various electrical power plant levels. The use of these two independent parameters is justified in Appendix B.

For each figure, the electrical power spectrum was varied from 100,000 to 100 KW and the spectrum of specific impulse was varied from 25,000 to 1,000 seconds.

Run No.	Escape Time ($T_{1_{nd}}$)	Escape Range Angle	$\frac{F_o}{W_o}\frac{g_E}{g_o}$	$\frac{F_1}{W_1}\frac{g_E}{g_1}$	$\frac{M_1}{M_o}$	$\frac{r_1}{r_o}$	β_1^o
16-1	5.2490	208.34	5.2624×10^{-2}	7.6945×10^{-2}	0.68420	2.4831	13.942
26-1	5.2508	208.47	5.2624×10^{-2}	7.6779×10^{-2}	.68407	2.4823	13.881
17-2	40.865	892.55	1.0525×10^{-2}	1.1673×10^{-2}	.90164	6.2803	0
16-2	40.115	881.84	1.0525×10^{-2}	1.165×10^{-2}	.90346	6.2804	13.292
17-3	43.382	916.50	9.5300×10^{-3}	1.0525×10^{-2}	.90549	6.6248	0
17-1	40.111	881.81	1.0525×10^{-2}	1.1650×10^{-2}	.90328	6.2791	13.289
21-4	237.66	4,297.4	2.1050×10^{-3}	2.1543×10^{-3}	.97712	14.583	17.747
16-4	30.396	754.50	1.1133×10^{-2}	1.8165×10^{-2}	.61311	5.1536	17.423
21-3	212.96	3,975.3	2.2265×10^{-3}	2.4973×10^{-3}	.89158	13.600	17.623
21-7*	1,200.	20,200.	4.4530×10^{-4}	4.5646×10^{-4}	.97556	32.2	
21-1	158.96	3,380.5	2.3551×10^{-3}	4.1178×10^{-3}	.57196	10.747	14.694
21-2	1,083.1	18,605.	4.7102×10^{-4}	5.5323×10^{-4}	.88334	29.373	15.957
23-2*	6,200.	98,000.	9.4203×10^{-5}	9.6788×10^{-5}	.97329	70.5	
21-6	799.23	15,789.	4.9821×10^{-4}	9.1466×10^{-4}	.54473	22.635	16.352
22-1*	5,360.	87,761.	9.9643×10^{-5}	1.1351×10^{-4}	.87787	64.467	
19-2	5,360.3	87,760.	9.9643×10^{-5}	1.1328×10^{-4}	.87785	64.472	16.071
23-1*	32,500.	460,000.	1.9929×10^{-5}	2.0537×10^{-5}	.97038	159.	
21-5	455.34	8,067.5	1.0966×10^{-3}	1.2051×10^{-3}	.91002	19.579	15.153

Notes:

$M_{pp} = .25\ M_o$

*Based on extrapolated data.
See Figures (1) and (2).

TABLE III

ASD Computer Output Data

Run No.	V_{1nd}	h_{1nd}
16-1	0.89838	1.8035
16-2	.56497	2.9175
21-4	.37084	4.4132
16-4	.64055	2.6744
21-3	.38419	4.2660
21-1	.43156	3.8243
21-2	.26142	6.2953
21-6	.29743	5.5506

TABLE III (CONT'D)

ASD Computer Output Data

Run No.	Δ V (ft/sec)	J (KW/slug)	$W_o\left[\frac{g_E}{g_o}\right]$ (lbs)	A_o	E $\frac{(KW\text{-}sec)}{lbs}$
16-1	12,186	17.057	87,135	8.3745×10^{-2}	6.8875×10^{3}
26-1	12,226	17.067	87,135	8.3745×10^{-2}	6.8898×10^{3}
16-2	16,350	3.9489	87,133	1.6749×10^{-2}	5.2637×10^{4}
21-4	18,620	0.8654	87,134	3.3499×10^{-3}	3.1184×10^{5}
16-4	15,753	4.9335	41,187	1.7717×10^{-2}	8.4377×10^{3}
21-3	18,477	0.9506	41,189	3.5432×10^{-3}	5.9116×10^{4}
21-7*	19,908	0.1958	41,189	7.0864×10^{-4}	3.3310×10^{5}
21-1	17,990	1.2377	19,470	3.7479×10^{-3}	9.3348×10^{3}
21-2	19,971	0.2184	19,470	7.4957×10^{-4}	6.3603×10^{4}
23-2*	21,816	0.0454	19,470	1.4991×10^{-4}	3.6408×10^{5}
21-6	19,561	0.2924	9,203.8	7.9284×10^{-4}	9.9285×10^{3}
22-1*	20,968	0.0487	9,203.7	1.5857×10^{-4}	6.6589×10^{4}
23-1*	24,231	0.0107	9,203.5	3.1715×10^{-5}	4.0374×10^{5}
21-5	15,180	0.3807	29,270.3	1.2689×10^{-3}	4.9057×10^{4}

Note:

*Based on extrapolated data.
See Figures (1) and (2).

TABLE IV

Calculated Data from ASD Computer Runs

The numerical results of computer runs 21-7, 23-2, 22-1 and 23-1 are based on extrapolated data as shown on Figures 3 and 4. It can be easily seen from Figure 4 that the extrapolation of r_1/r_o is extremely risky and unreliable. Therefore, in conjunction with this particular extrapolation, Figures 6 and 8 were used to indicate the correct trends. This approach is more reliable since r_1/r_o appears to vary linearily at high specific impulses. This action was necessary due to the excessively large amount of computer time necessary to reach escape conditions for these runs. On all figures, unless otherwise noted, dash lines will represent extrapolated data points.

Initially, all ASD computer runs incorporated step sizes of 30^o. Dr. Stan E. Ross, Project Manager under contract AF 33(616)-7313 (Ref 10) of Lockheed Aircraft Corporation said in an interview on 4 April 1962 that the computer results would be questionable using this step size and suggested that the step size be reduced. Hence, the integration step sizes were reduced and are tabulated in Table I. For comparison purposes, Tables III and V shows the numerical results for integration step sizes of 30^o and 10^o. It will be noted that the computer output data differ only in the last two significant digits out of five digits. The percent error is less than 1%. Therefore, if accuracy requirements are not stringent, the 30^o integration step sizes may be used for indicating "trends" in the numerical computer program.

GA / PHYS / 62-4

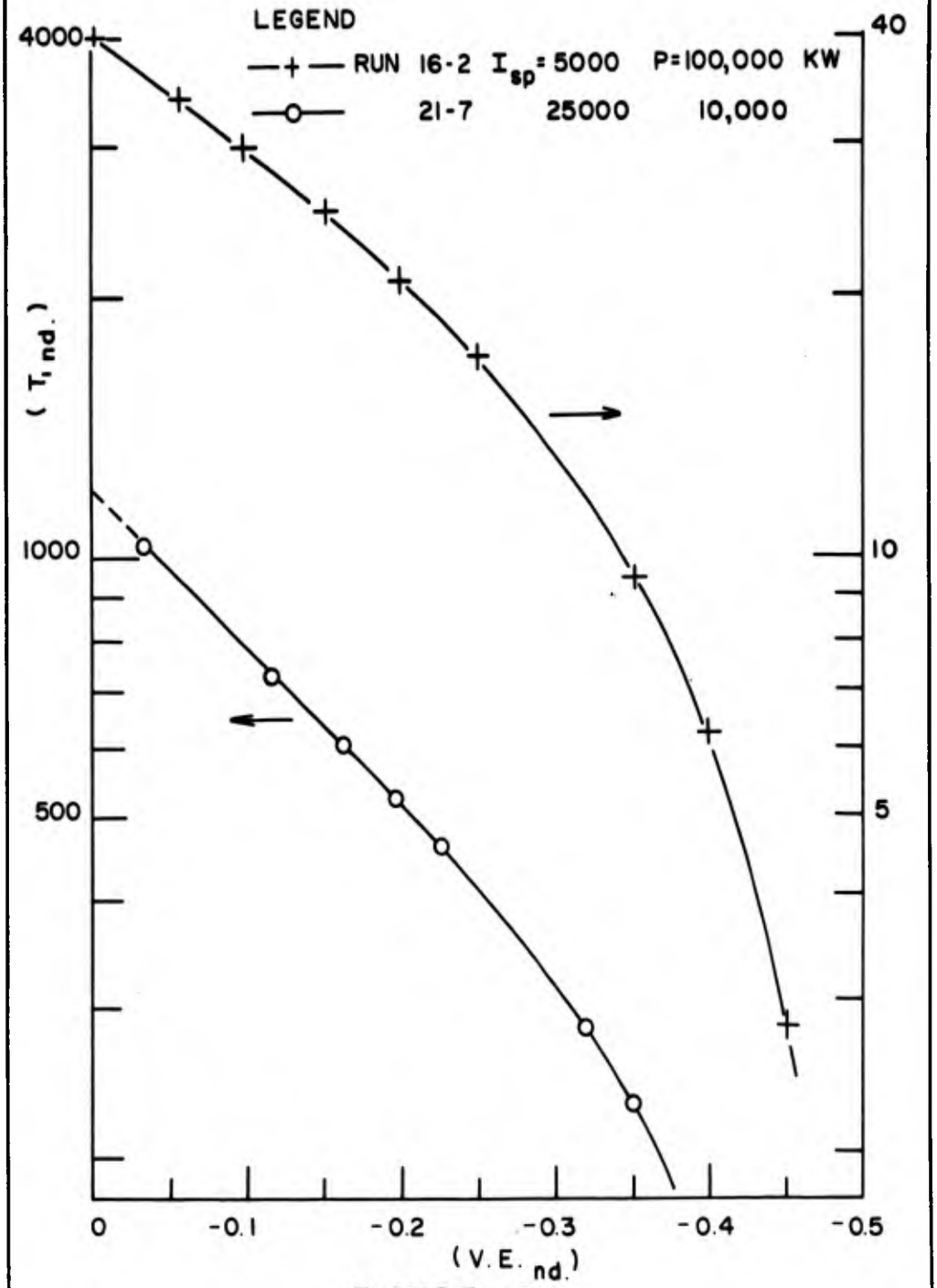

FIGURE 3
EXTRAPOLATION CURVE
ESCAPE TIME vs VEHICLE ENERGY

GA / PHYS / 62-4

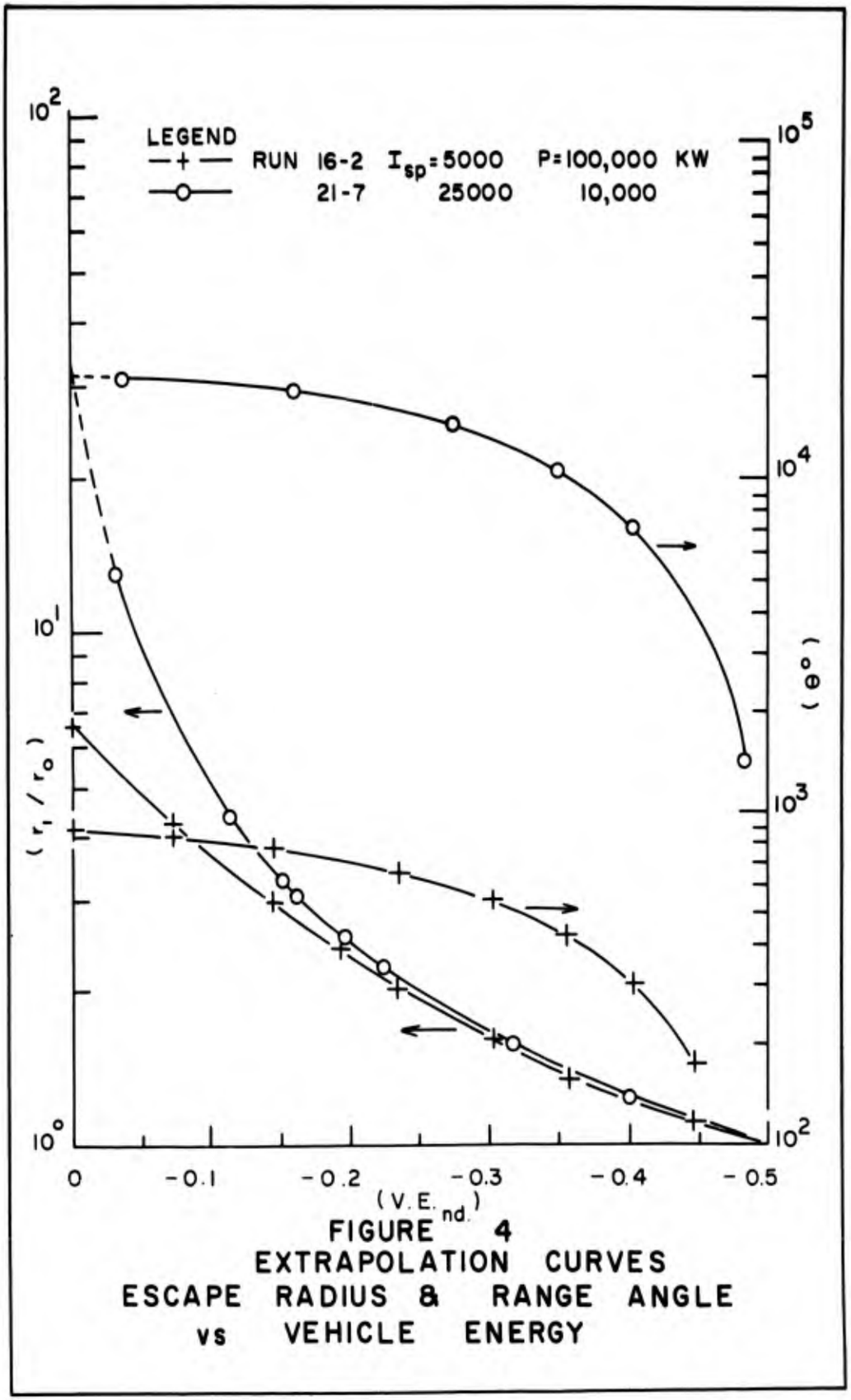

FIGURE 4
EXTRAPOLATION CURVES
ESCAPE RADIUS & RANGE ANGLE
vs VEHICLE ENERGY

Range Angle	Time (T_{nd}) Run 19-2	Time (T_{nd}) Run 22-1	Vehicle Energy (V.E.) 19-2	Vehicle Energy (V.E.) 22-1	Mass Ratio $\left[\frac{M}{M_o}\right]$ 19-2	Mass Ratio $\left[\frac{M}{M_o}\right]$ 22-1	$\left[\frac{r}{r_o}\right]$ 19-2	$\left[\frac{r}{r_o}\right]$ 22-1
2,010	35.377	35.377	-.49440	-.49440	.99919	.99919	1.0115	1.0115
4,020	71.366	71.366	-.48873	-.48873	.99837	.99837	1.0228	1.0228
6,000	107.44	107.44	-.48307	-.48308	.99755	.99755	1.0353	1.0353
8,010	144.72	144.71	-.47726	-.47726	.99670	.99670	1.0473	1.0473
10,020	182.69	182.68	-.47137	-.47137	.99584	.99583	1.0610	1.0610
12,000	220.79	220.79	-.46548	-.46549	.99497	.99496	1.0739	1.0738
14,010	260.23	260.23	-.45943	-.45944	.99407	.99407	1.0885	1.0884
16,020	300.46	300.46	-.45329	-.45330	.99315	.99315	1.1030	1.1030
18,000	340.91	340.90	-.44715	-.44717	.99223	.99223	1.1182	1.1182
20,010	382.83	382.82	-.44083	-.44085	.99127	.99127	1.1343	1.1343
23,730	462.89	462.87*	-.42887	-.42888	.98945	.98944	1.1661	1.1660
25,020	491.44		-.42463		.98880		1.1774	
30,000	605.87		-.40785		.98619		1.2256	
35,010	728.53		-.39019		.98340		1.2812	
40,050	860.85		-.37152		.98038		1.3455	
45,000	1001.2		-.35217		.97718		1.4199	
50,010	1155.9		-.33135		.97366		1.5092	
55,050	1327.7		-.30891		.96974		1.6189	
60,031	1517.6		-.28489		.96541		1.7552	
65,011	1734.7		-.25853		.96047		1.9339	
68,161	1890.7		-.24028		.95691		2.0807	

Notes:
Run 19-2 Step Size 30° Error Bound 10^{-4}
Run 22-1 Step Size 10° Error Bound 10^{-5}
*Computer Run Stopped

TABLE V

Comparison of ASD Computer Runs
Variation of Integration Step Sizes

Figures 5 through 7 describe in detail the variation of these escape parameters as functions of specific impulse and electrical power levels. Figures 8 through 11 show also the escape parameters as a function of an additional parameter, namely the initial thrust - to - weight ratio taken at the initial reference orbit under consideration.

It will be noted from these figures that small power levels and low thrust - to - weight ratios result in large magnitudes of the escape parameters.

One may observe from Figures 5 through 7 that the escape parameters may be reduced in magnitude by:

1. Increasing the electrical power output for a constant specific impulse engine at a constant gross weight. This would also increase the payload fraction as indicated on Figure 15.
2. Decreasing the specific impulse but maintaining a fixed power level at the expense of reducing the payload fraction.

Figures 8 through 11 indicate that the conditions stated above would result in larger thrust - to - weight ratios. This is to be expected if the initial vehicle mass is constant and is further justified by Eq 11 in Section II. For constant thrust - to - weight ratios, specific impulse and electrical power level would both be decreased for achieving smaller escape parameters as shown on Figures 8 and 9.

GA / PHYS / 62 - 4

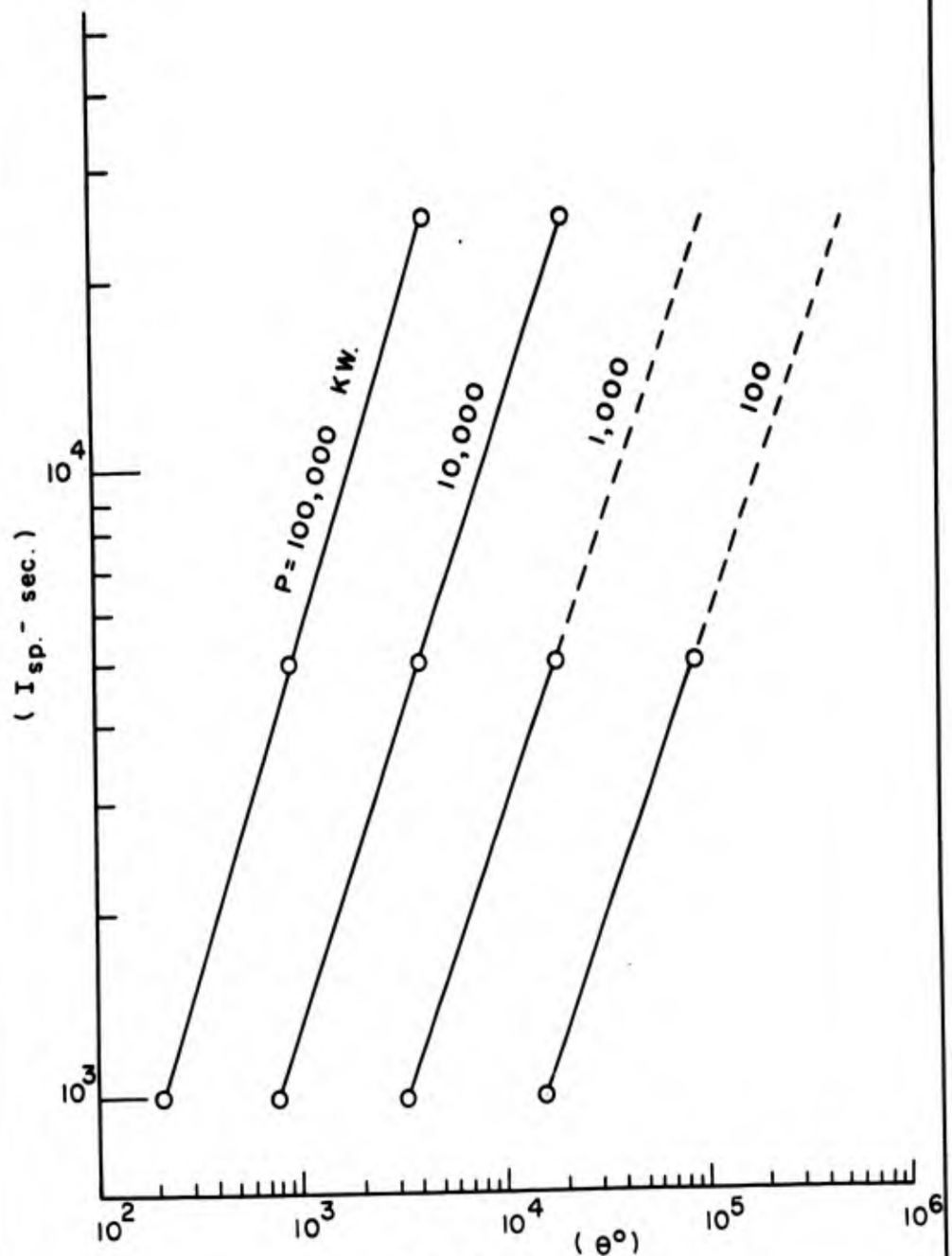

FIGURE 5

SPECIFIC IMPULSE vs ESCAPE RANGE ANGLE

GA / PHYS / 62-4

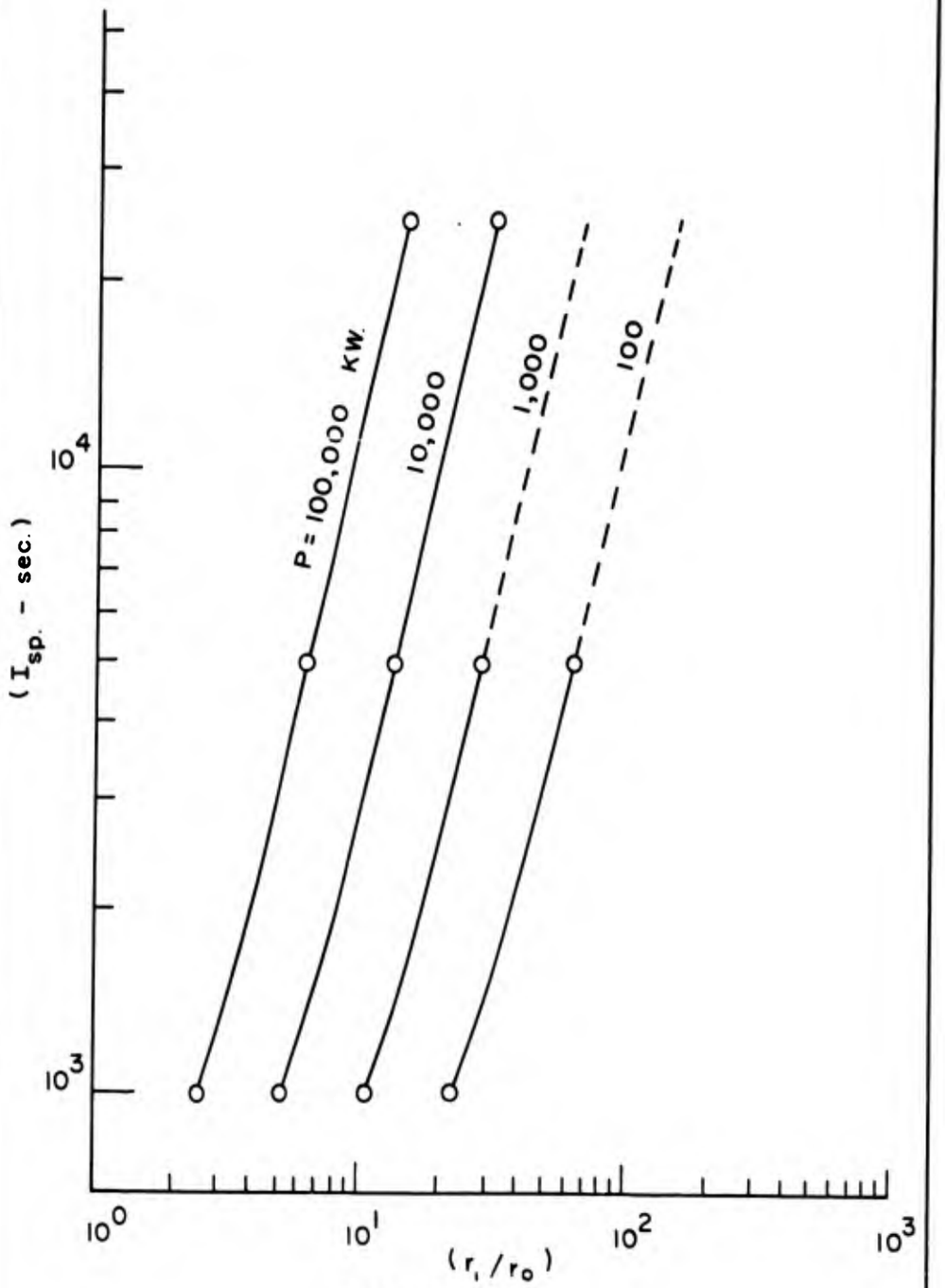

FIGURE 6

SPECIFIC IMPULSE vs ESCAPE RADIUS

GA / PHYS / 62-4

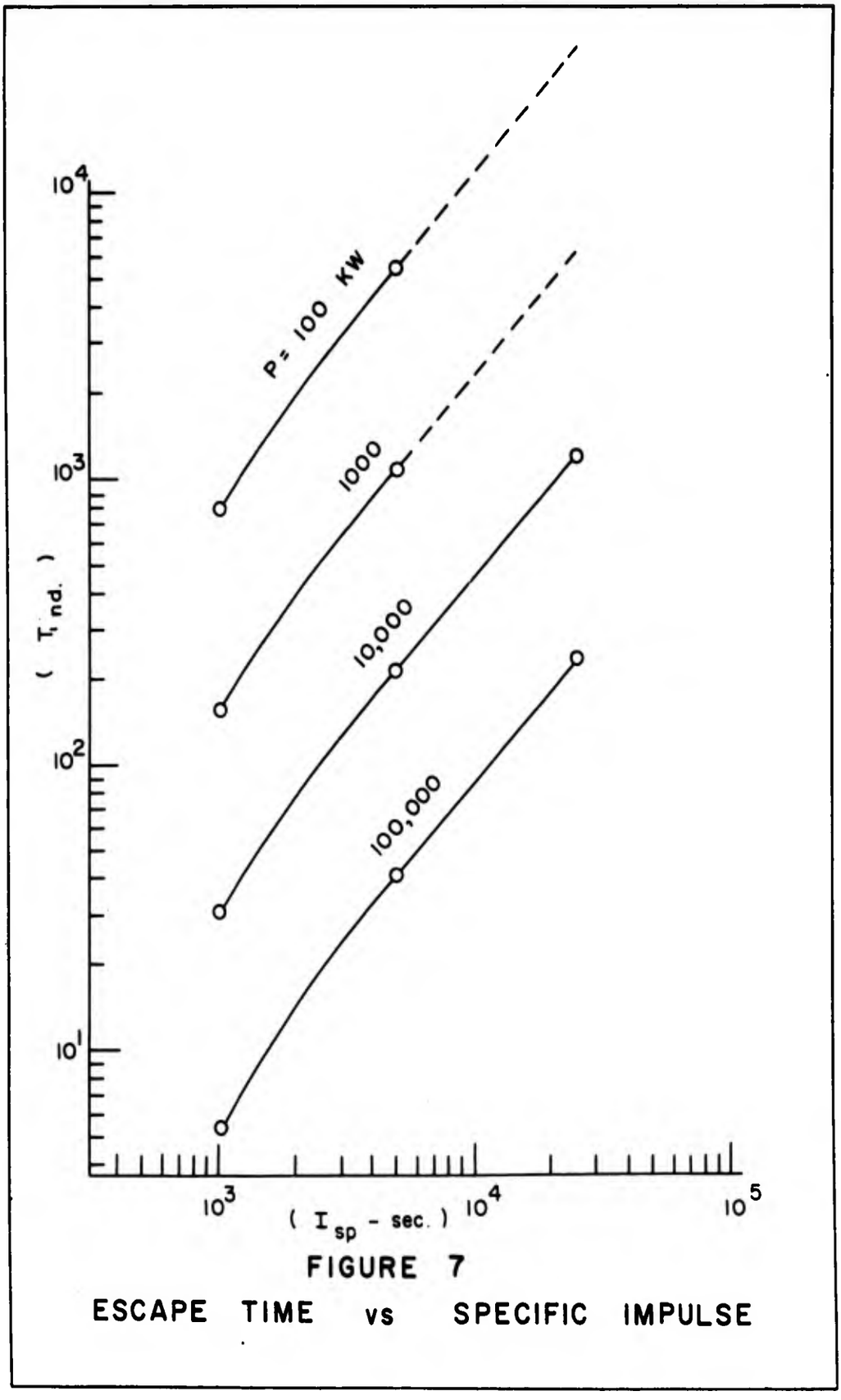

FIGURE 7

ESCAPE TIME vs SPECIFIC IMPULSE

GA / PHYS / 62-4

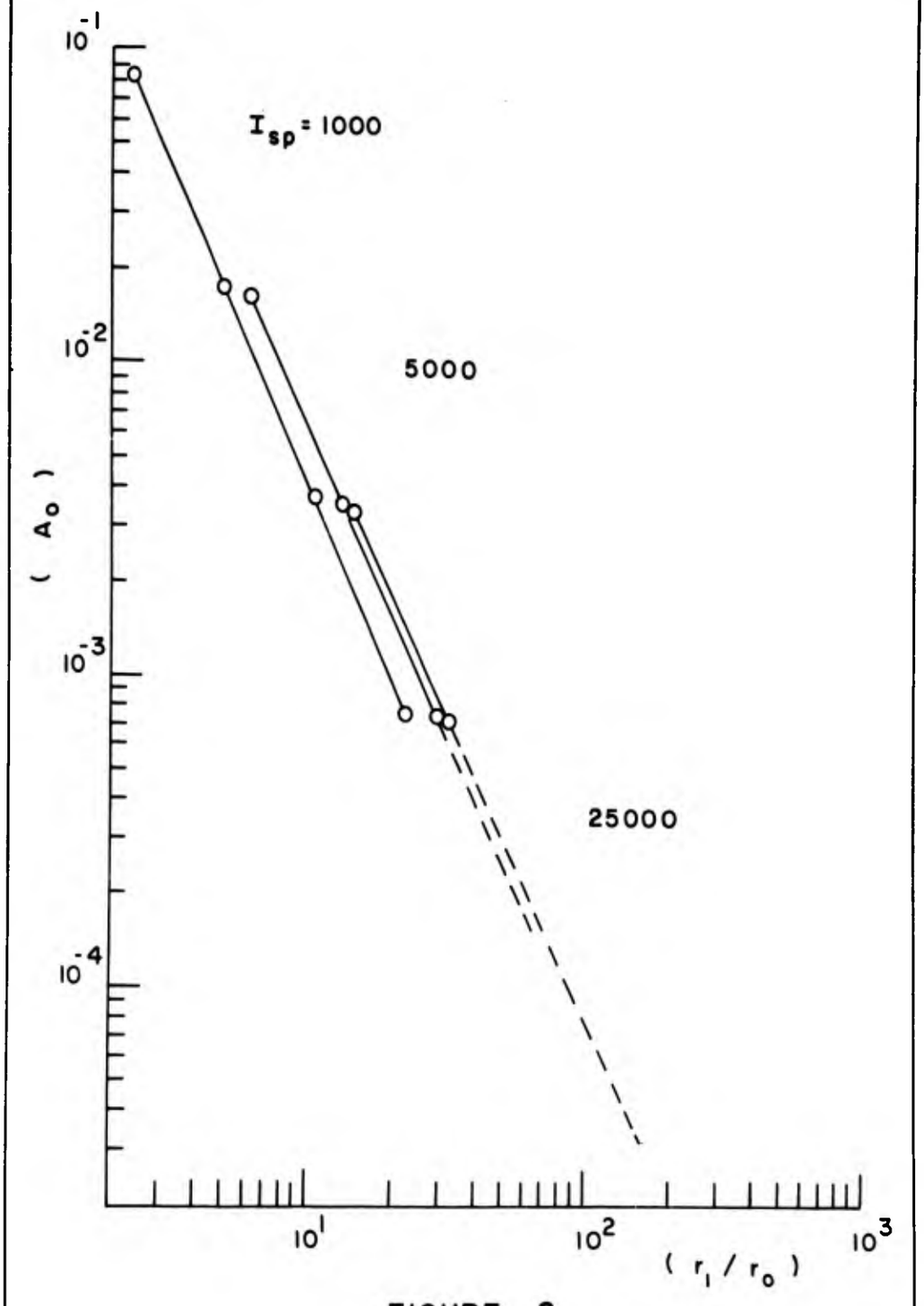

FIGURE 8

THRUST ACCELERATION vs ESCAPE RADIUS

GA / PHYS / 62-4

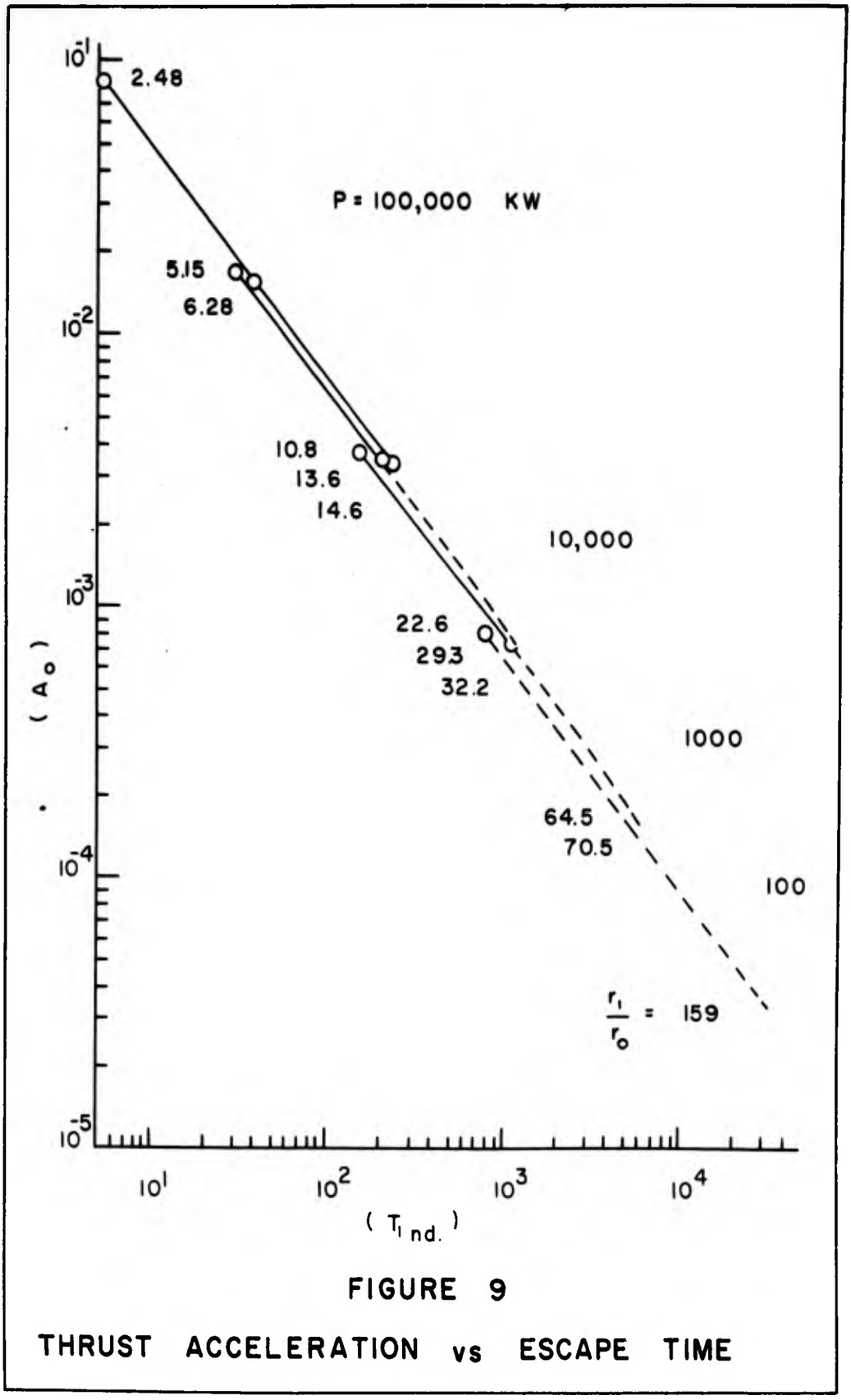

FIGURE 9

THRUST ACCELERATION vs ESCAPE TIME

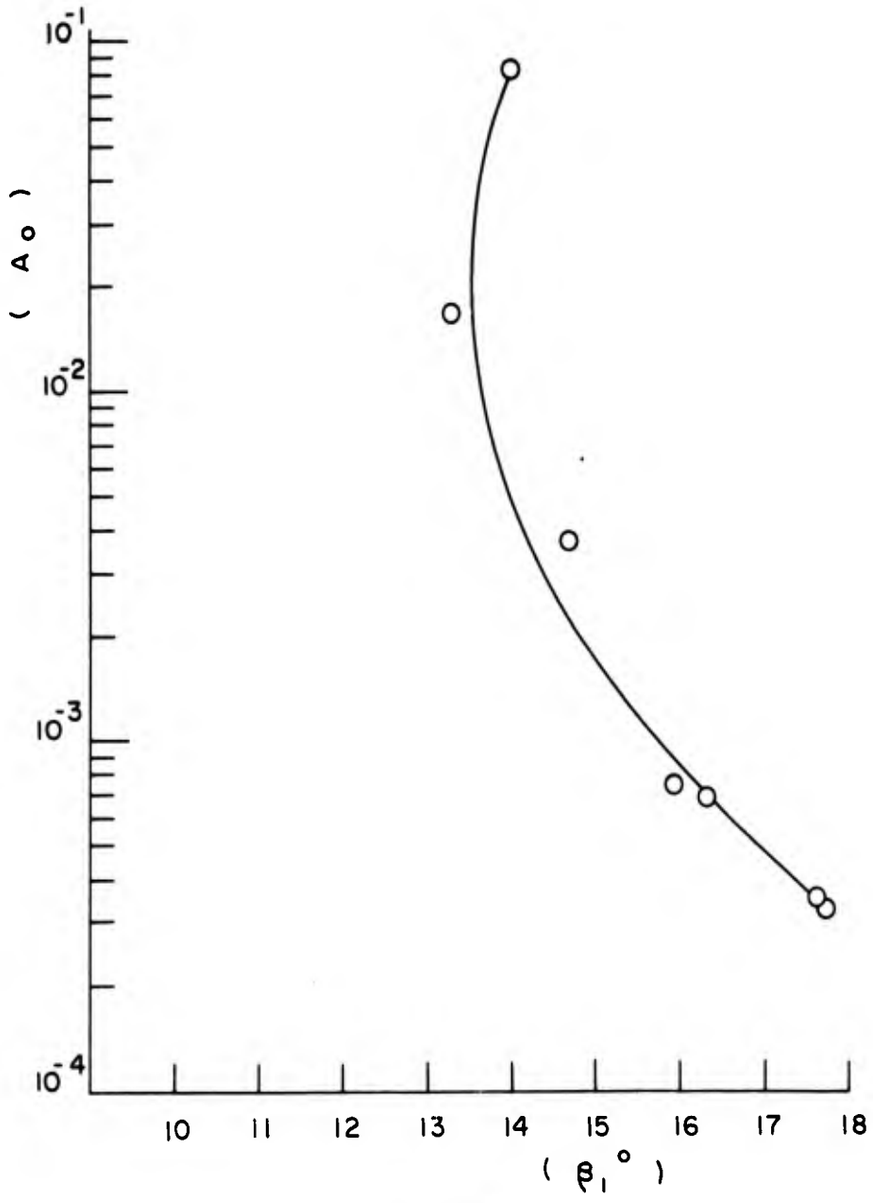

FIGURE 10
THRUST ACCELERATION
vs THROW OFF ANGLE

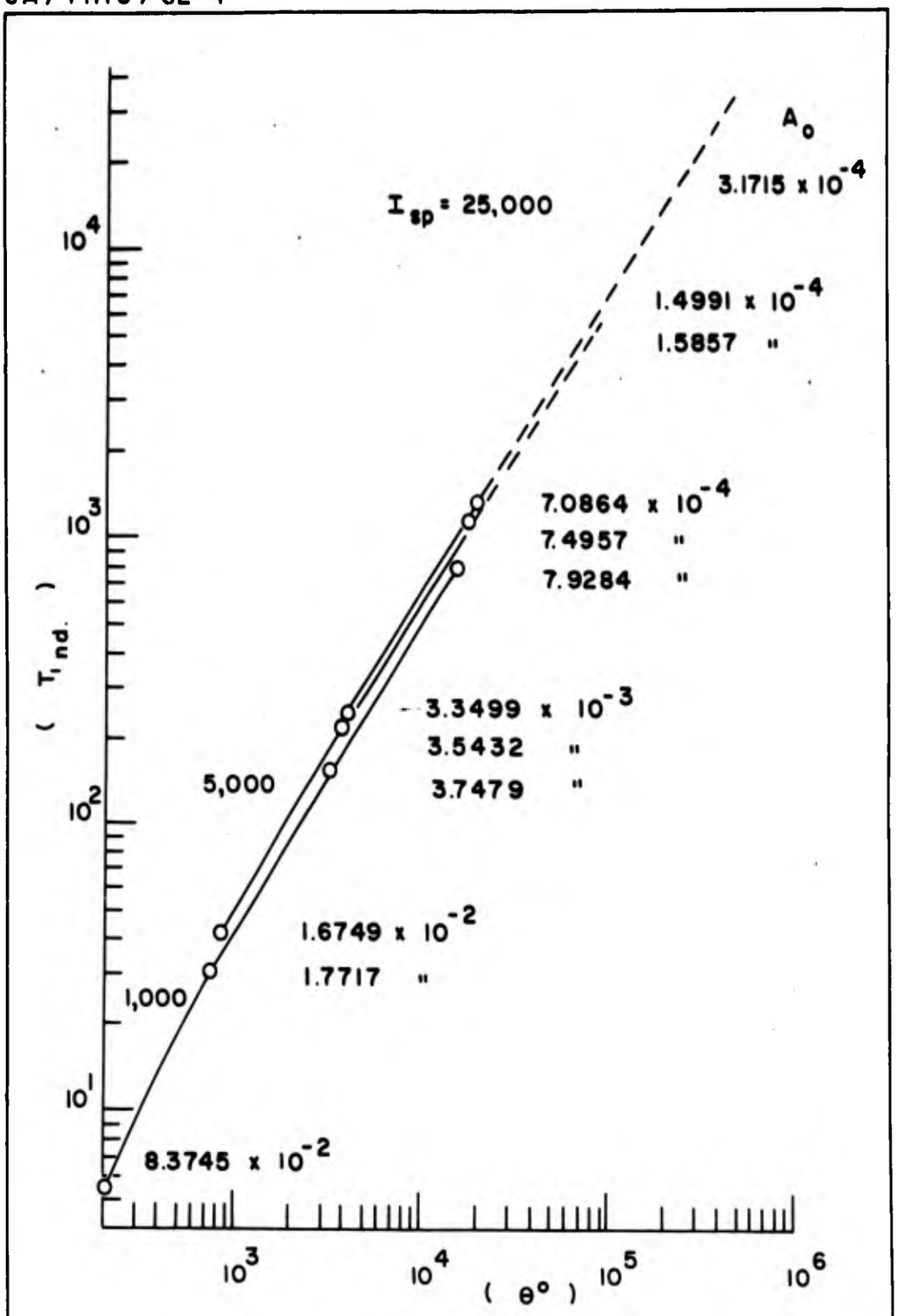

FIGURE 11

ESCAPE TIME vs RANGE ANGLE

Figure 10 shows the variation of the in-plane throw off angle at escape as a function of thrust acceleration. The scatter is due to interpolation but the graph clearily shows that the optimum thrust vectoring requirements for these engines are not severe.

If mission requirements dictate long mission times, substantial increases in payload fractions can be obtained by using higher specific impulse engines as shown on Figure 15. It will be noted from Figure 15 (b) that it depicts a family of curves for a powerplant mass fraction of 0.25. If other powerplant mass fractions were used, it would merely shift the curve up or down and would still indicate the same general trends. Also, if the specific gross weight of the vehicle per KW of electricity were extended to infinity, Figure 15 would indicate the minimum escape time for zero payload. This would result in a lower limit on the escape mission spectrum.

Figure 12 shows a typical escape spiral trajectory of a low-thrust device escaping from the earth's gravitational field as a function of position radii and range angle. It will be noted that escape occurred at approximately 2.5 revolutions from the initial launch point on the trajectory and the initial thrust acceleration is 1.675×10^{-2}.

Figure 13, which is representative of the data obtained in all of the computer runs, indicate the trend of range angle as a function of time. It is interesting to note that a family of curves for three computer runs initially all lie on a common line with a slope of + 1 prior to reaching the escape point.

GA / PHYS / 62 - 4

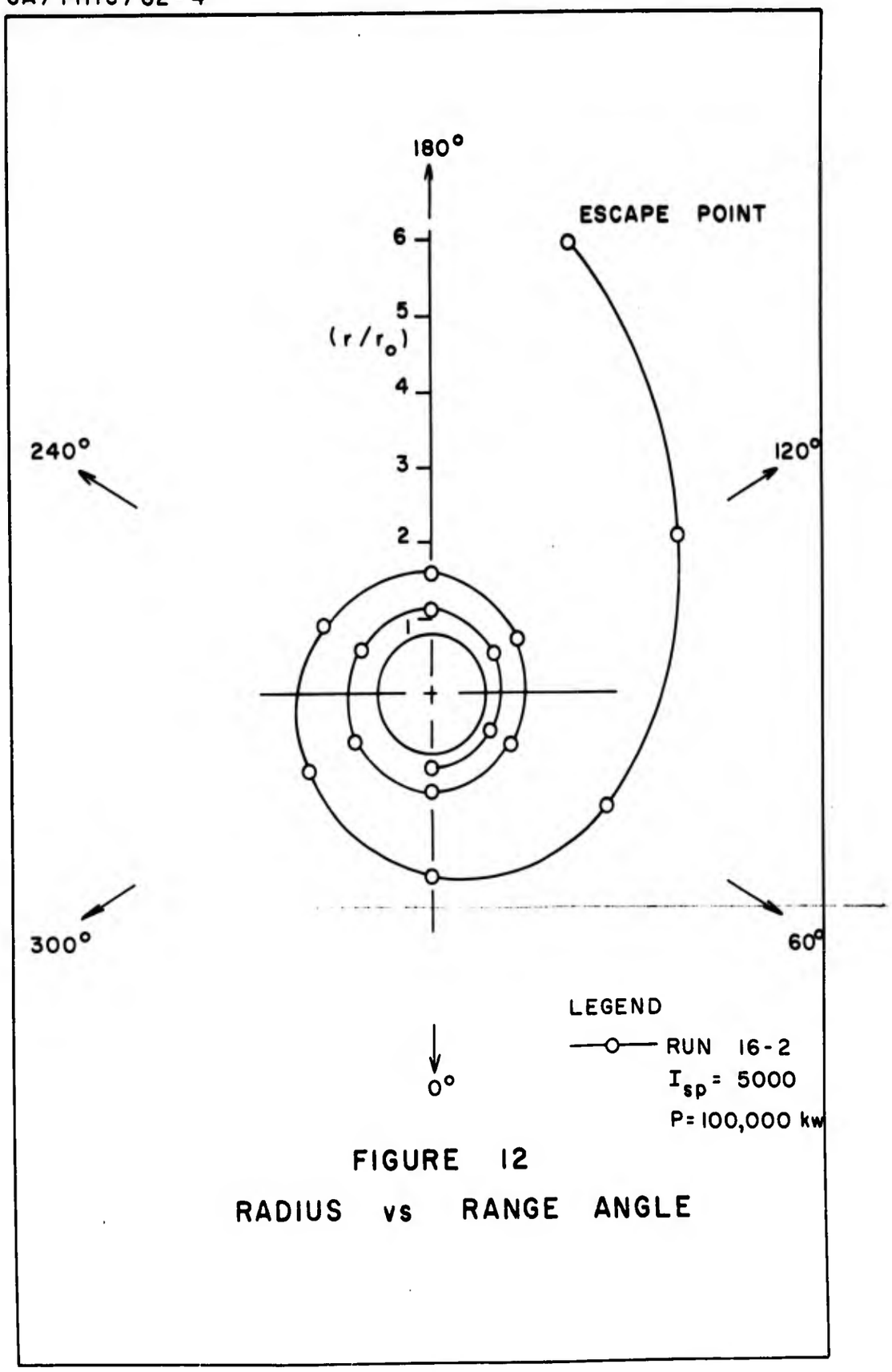

FIGURE 12

RADIUS vs RANGE ANGLE

GA / PHYS / 62-4

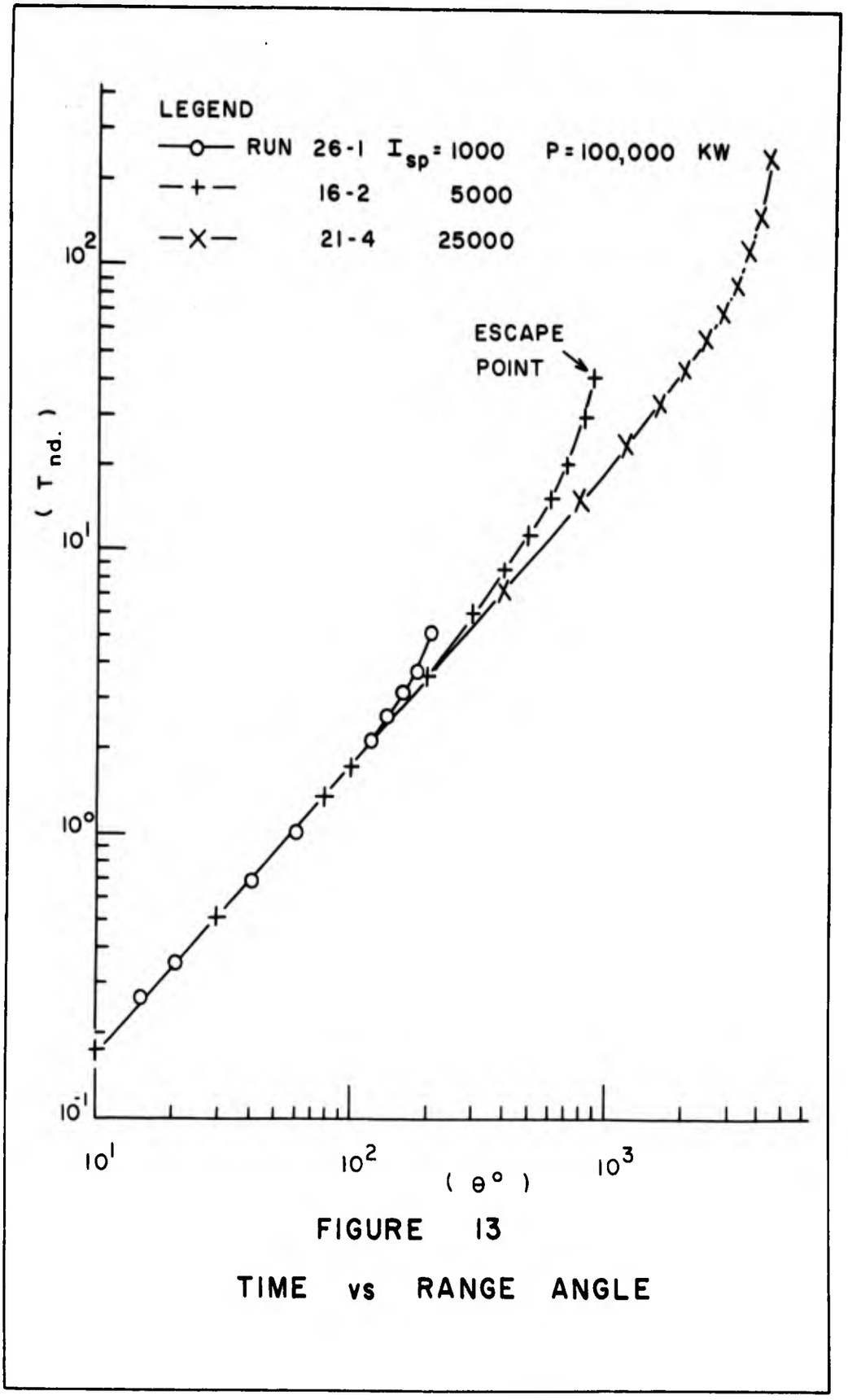

FIGURE 13

TIME vs RANGE ANGLE

Figures 14A and 14B represent the trend of eccentricity, e, as a function of time. Figure 14A clearly shows the oscillation of eccentricity as time is increased. This oscillation is not apparent from Figure 14B since it only represents the lower portion of the escape mission spectrum. From Figure 14A, the average rate of eccentricity change is constant for $e < 0.025$. From Figure 14B, the rate of eccentricity change is constant for $e < 0.275$ which agrees with Shapiro's (Ref 14: 2) results of $e < 0.30$.

The next graph (Figure 16), shows the propellant utilization factor as a function of escape time for all computer runs. This factor is an indication of propellant requirements and is used in conjunction with the optimization mass fraction equations outlined in Section II. Also, if propellant requirements are specified for the vehicle, in addition to the initial vehicle mass and powerplant output, the propellant utilization factor can be calculated by Eq (25). Using Figure 16, the escape time can be obtained.

Figures 17 and 18 show the specific energy and velocity increment requirements as a function of initial thrust - to - weight ratios. For high specific impulse engines, the operating time in the gravitational field is longer and as expected, the specific energy requirements would be large as depicted on Figure 17. Figure 18 indicates the escape velocity increment requirements for a reference altitude of 1036.5 miles.

GA / PHYS / 62-4

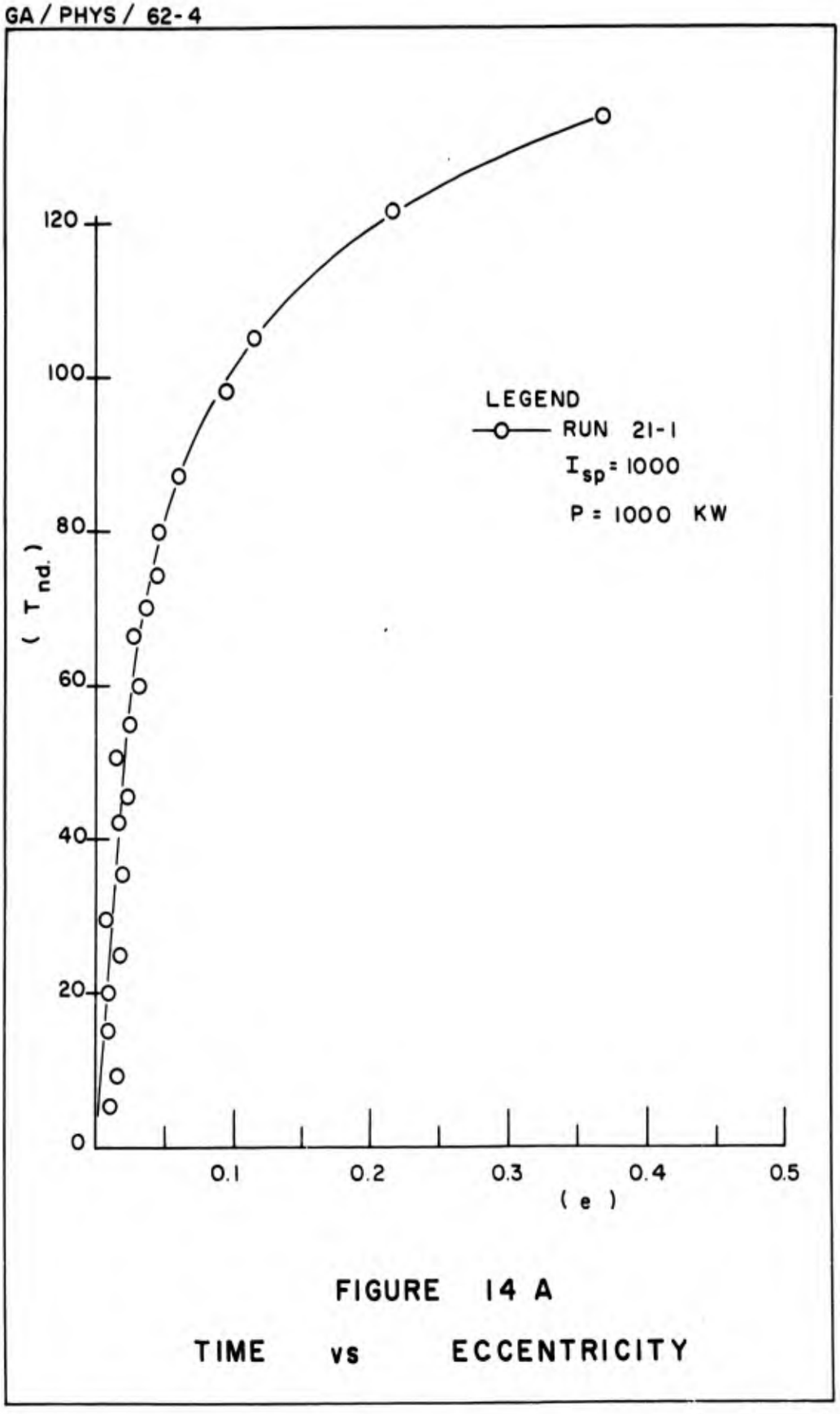

FIGURE 14 A

TIME vs ECCENTRICITY

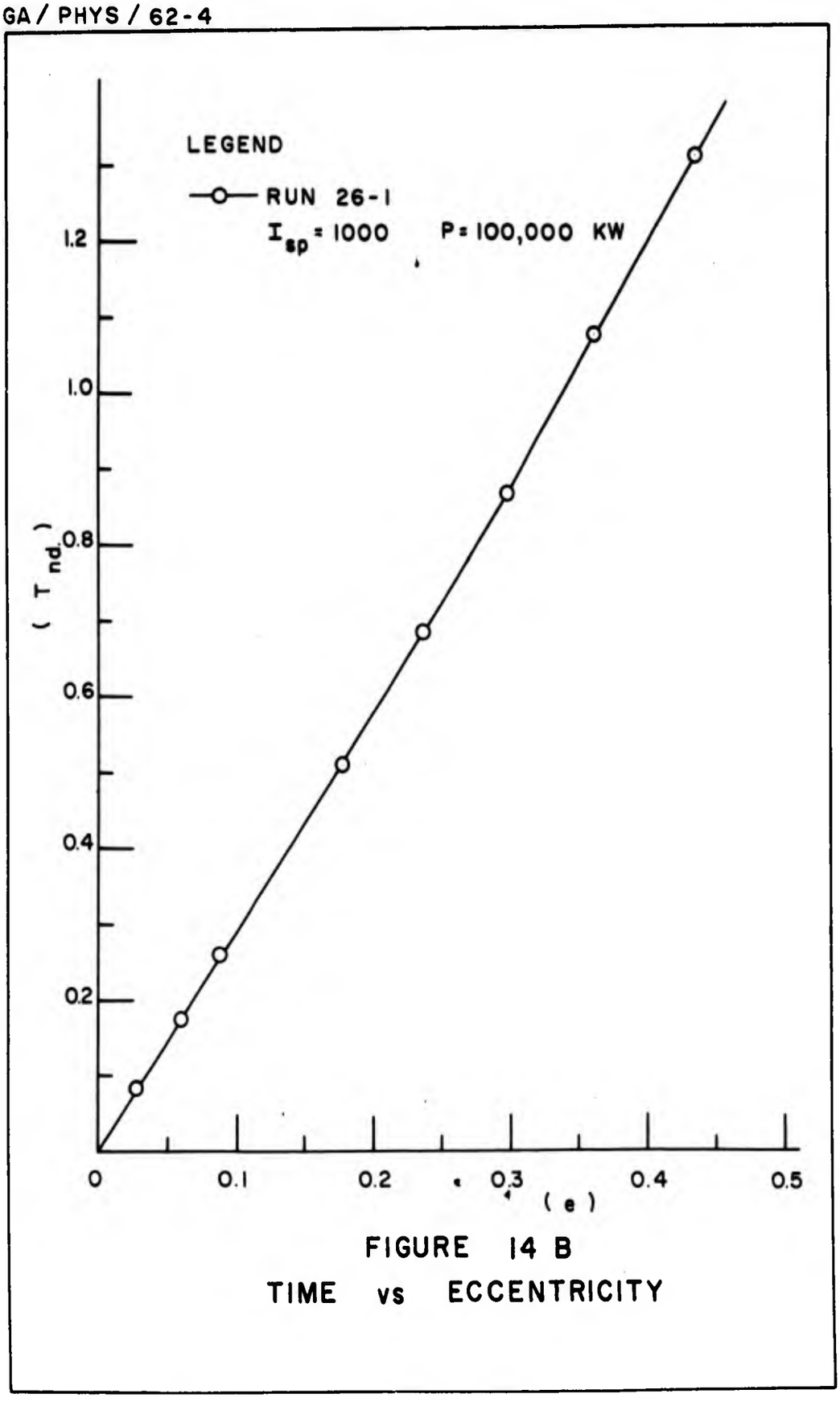

FIGURE 14 B
TIME vs ECCENTRICITY

GA / PHYS / 62-4

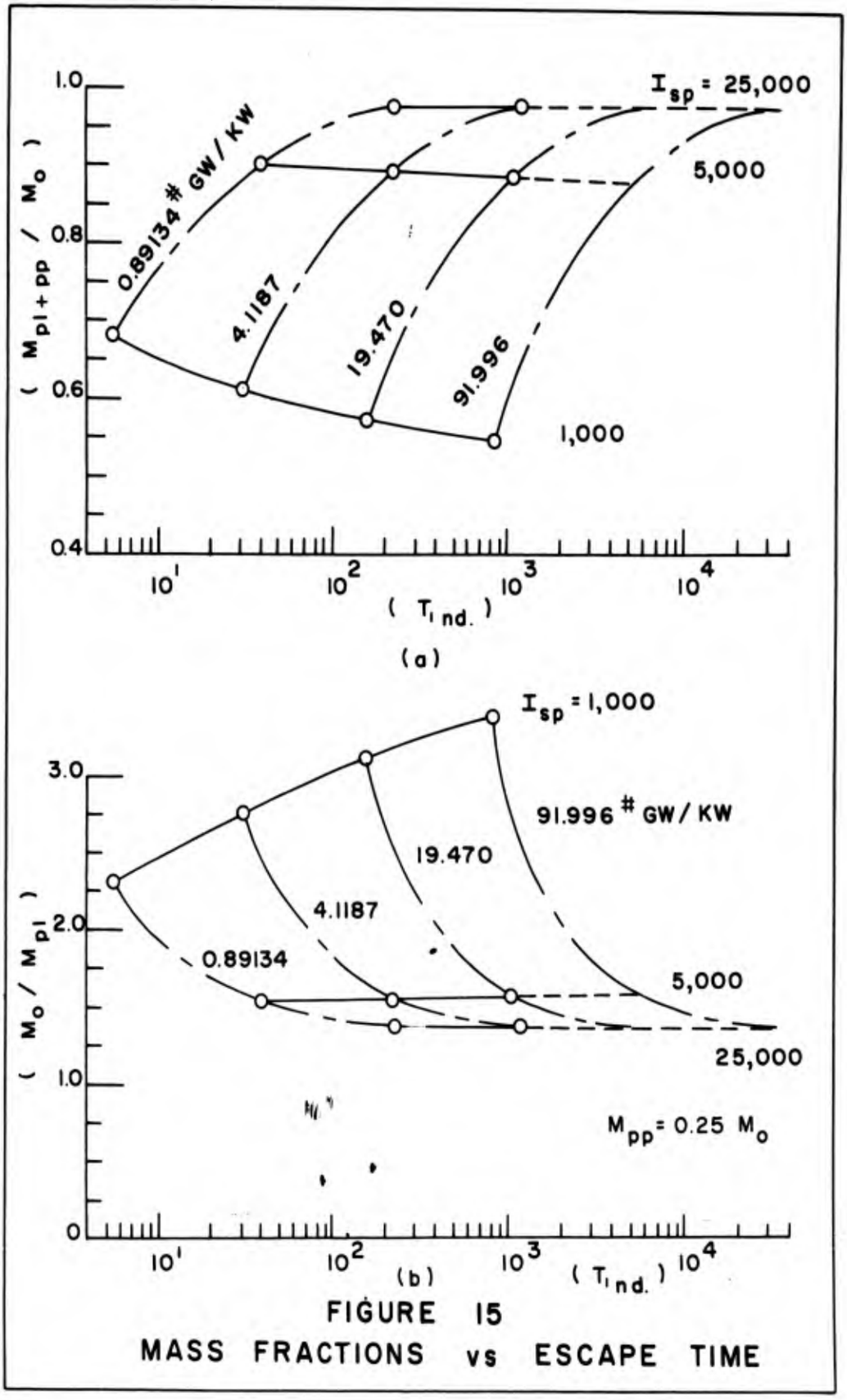

FIGURE 15
MASS FRACTIONS vs ESCAPE TIME

GA / PHYS / 62-4

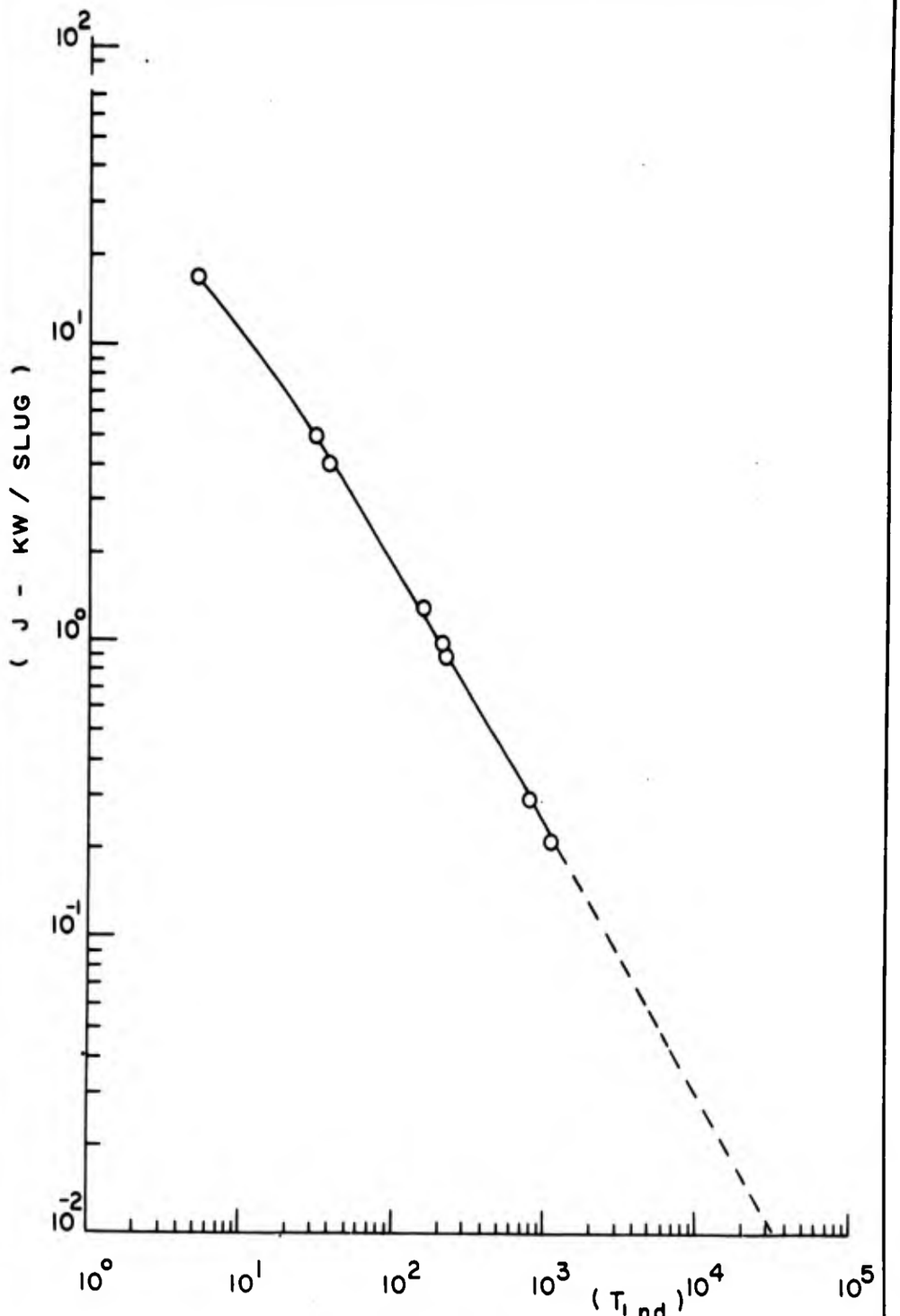

FIGURE 16
PROPELLANT UTILIZATION FACTOR
vs ESCAPE TIME

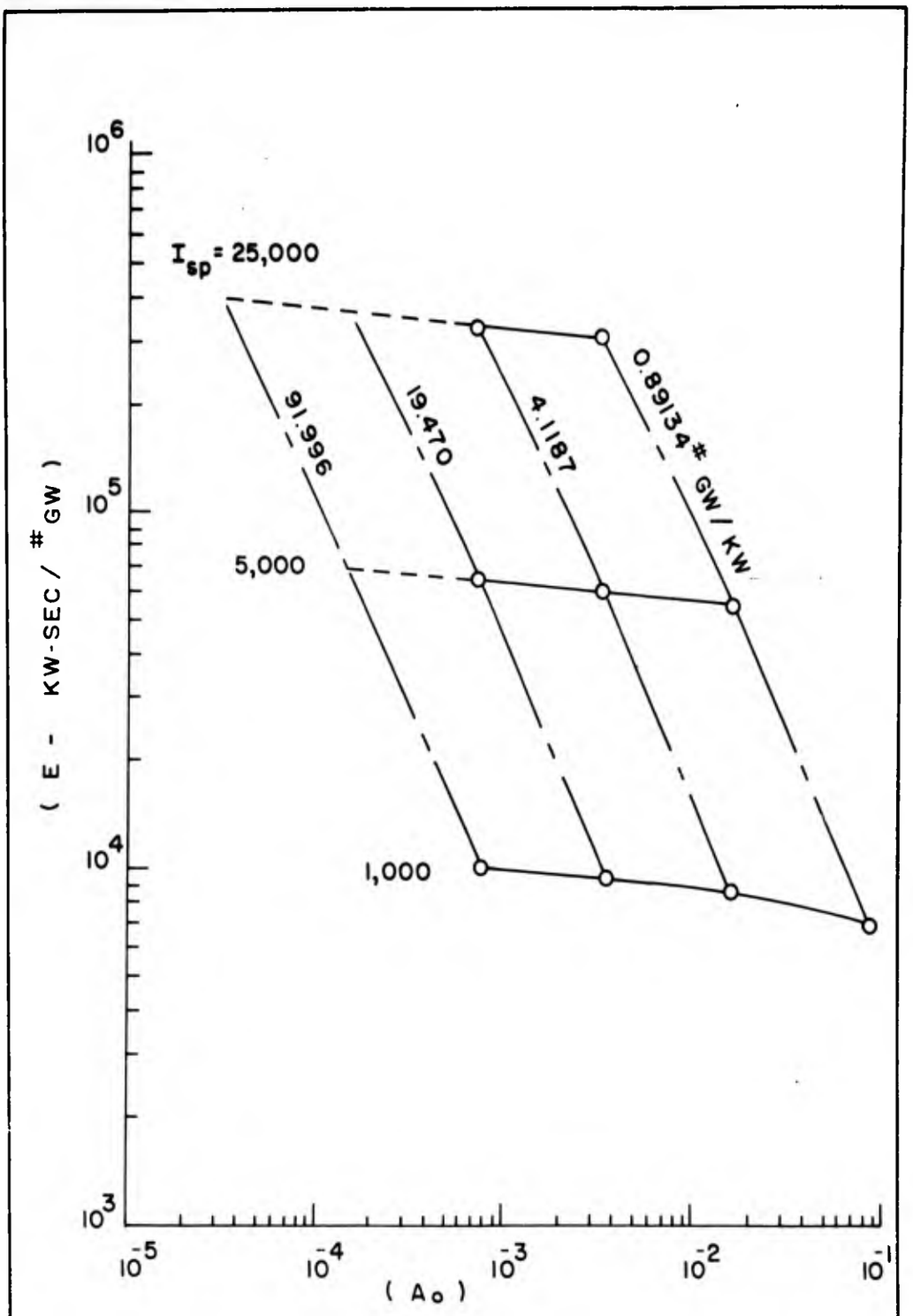

FIGURE 17

SPECIFIC ENERGY vs THRUST ACCELERATION

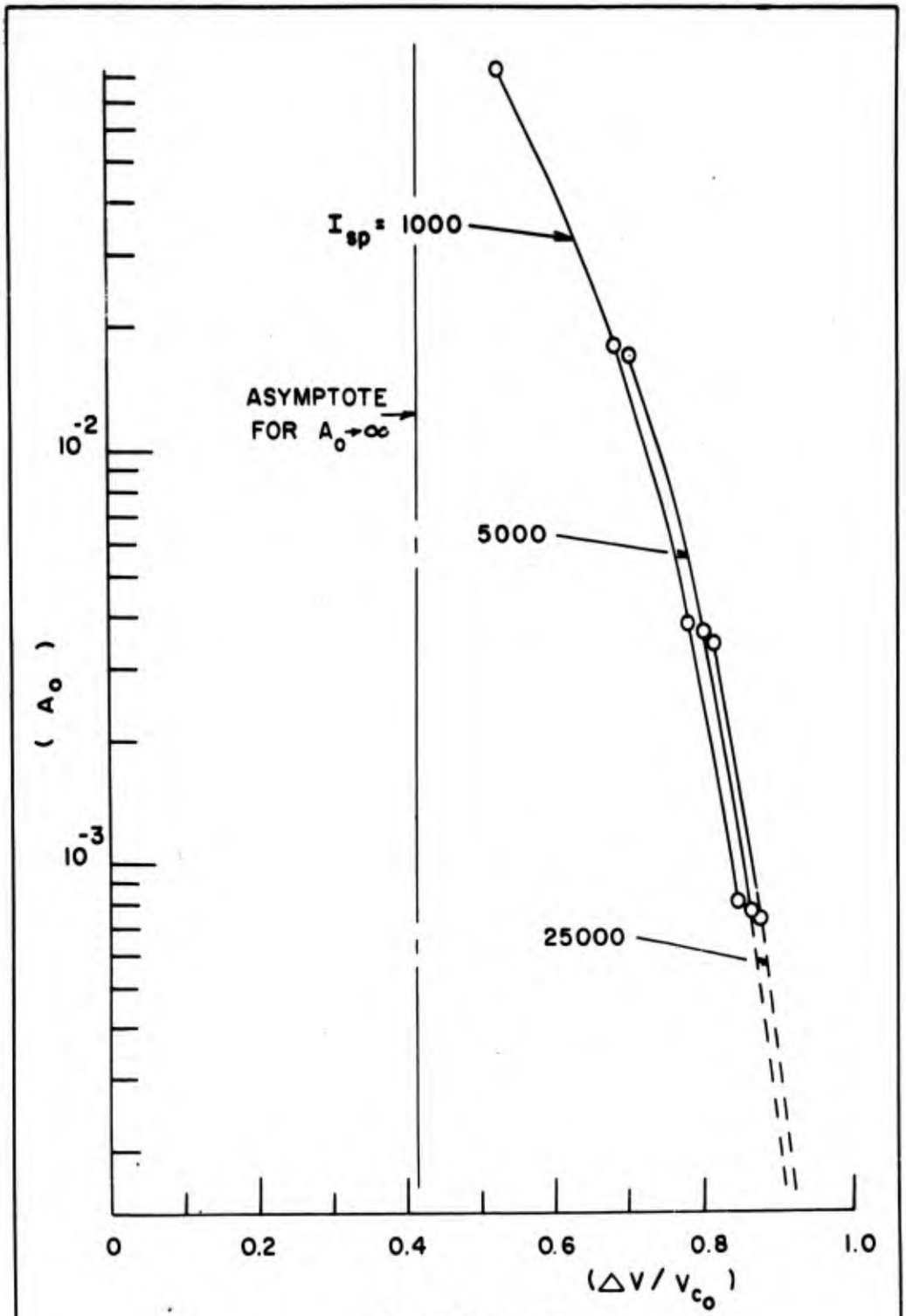

FIGURE 18
THRUST ACCELERATION
vs VELOCITY INCREMENT

The most useful data for detailed escape missions originating at an altitude of 1036.5 miles are Figures 5, 6, 7, 9, 11, 15, 16 and 17. For example, if I_{sp} and P are given initially, Figures 5, 6, 7 and 11 are used to obtain the escape parameters. Figure 9 is used to obtain the initial thrust - to - weight ratio at the reference altitude. Figures 15 and 16 are used to obtain the various mass ratios while Figure 17 is used to obtain the specific energy requirement of the escape mission.

It must be emphasized at this point that Figures 3 through 23 are only applicable for a reference altitude of 1036.5 miles. Figures 25, 26, 27 and 28, may be used in conjunction with any initial reference altitude since all terms have been nondimensionalized. To illustrate this important point, computer Run 21-5 was initiated at an initial altitude of 300 miles and the numerical results were compared to data obtained from the generalized figures.

Table V-1 shows some of the comparison data and indicates good agreement between the two sets of data. The results obtained from the generalized data will depend on how well a person can "eye ball" the graphical data.

Table V-1

Comparison of Escape Parameters

(Generalized Results)

Figure Number	Escape Parameters		% Deviation
	Generalized Data	Computer Run 21-5 (Ref. Alt. = 300 miles)	
26	Θ = 8270	8067.5	-2.55
27	r_1/r_o = 17.95	19.579	7.30
28	$T_{1^{nd}}$ = 473	455.34	-3.88
29	$T_{1^{nd}}$ = 473	455.34	-3.88

(Slide Rule Accuracy)

A detailed example of the use of these figures for an escape mission is included in Section VI.

Comparison of ASD Computer Options

The parametric data presented above were based exclusively on Option 5 of the ASD computer program. This option optimizes the thrust direction for reasons outlined in Section II. A comparison seems appropriate in analyzing the escape parameters obtained from other options and the results are tabulated in Table V-2. For Options 4 and 5, there should have been good agreement between these two

Table V-2

Comparison of Escape Parameters

from Various ASD Computer Options

Option No.	Computer Run	$T_{1^{nd}}$	Θ (Degrees)	$\frac{r_1}{r_o}$	$\frac{m_1}{m_o}$
4	17-1	40.111	881.81	6.2791	0.90328
5	16-2	40.115	881.84	6.2804	.90346
6	17-3	43.382	916.50	6.6248	.90549
9	17-2	40.865	892.55	6.2803	.90164

particular options. For Option 5, I_{sp} was specified and for Option 4, the engine thrust was specified. All remaining input data was the same. Therefore, these numerical results indicate some probability of error in completing the trajectory analysis by various options. The remaining two computer runs were not optimized. Interestingly enough, the results of computer run 17-3 are also sufficiently close to optimum. Computer Run 17-3 assumed that the thrust - to-weight ratio was constant throughout the mission profile. Since the vehicle mass is decreasing, the thrust level must also be decreasing to maintain a constant thrust - to - weight ratio. Since the power level is fixed, then the I_{sp} is increased which essentially reduces the propellant requirements. Therefore, the final mass ratio is higher when compared to other runs.

Validity of Analytical and Other Numerical Results

The analytical results of Tsien's and Benny's analytical equations are tabulated in Tables VI through XII. The percent deviations from the ASD numerical results were obtained and are graphically shown on Figures 19 through 21 and do not represent any extrapolated data.

The percent deviation was obtained by the following equation:

$$\% \text{ Deviation} = \frac{\text{ASD Numerical Result} - \text{Analytical Result}}{\text{ASD Numerical Result}} \times 100 \qquad (46)$$

It must be emphasized that these results are based on computer runs involving variable thrust - to - weight ratios. The basic assumption used by Tsien and Benny involved constant thrust - to - weight ratios in their derivations. Therefore, computer run 17-3 (constant thrust - to - weight ratio) was made and results compared to run 16-2. It can be seen from Tables VI through XII that the range of deviations from run 16-2 varied from approximately -0.20% to 3.2%. These deviations are small when compared to the original deviations of the escape parameters.

Figures 19 through 21 clearly indicate that for large specific impulses, the percent deviation of Tsien's analytical equations is much less than that of Bennys.

As mentioned previously in Section III, Tsien's and Benny's solutions were obtained by making certain simplifying assumptions. The effect of these assumptions is rather forcefully brought out by these figures.

1

Run No.	A_o	Benny Solution (r_1/r_o)	Computer Solution (r_1/r_o)	% Deviation
16-1	8.3745×10^{-2}	1.6340	2.4831	34.195
16-2	1.6749×10^{-2}	3.6538	6.2804	41.822
21-4	3.3499×10^{-3}	8.1702	14.583	43.976
16-4	1.7717×10^{-2}	3.5525	5.1536	31.068
21-3	3.5432×10^{-3}	7.9442	13.600	41.588
21-7*	7.0864×10^{-4}	17.764	32.200	44.832
21-1	3.7479×10^{-3}	7.7243	10.747	28.129
21-2	7.4957×10^{-4}	17.272	29.373	41.198
23-2*	1.4991×10^{-4}	38.621	70.500	45.218
21-6	7.9284×10^{-4}	16.794	22.635	25.805
22-1*	1.5857×10^{-4}	37.553	64.467	41.748
23-1*	3.1715×10^{-5}	83.968	159.00	47.190
17-3	1.6749×10^{-2}	3.6538	6.1079	40.179

Note:
*Based on extrapolated data.
See Figures (1) and (2).

1

$$\frac{r_1}{r_o} = \left[\frac{1}{20}\right]^{1/4} \times A_o^{-1/2}$$

TABLE VI

Comparison of Benny Solutions $\left[\frac{r_1}{r_o}\right]$ vs ASD

Numerical Calculations

1

Run No.	A_o	Benny Solution ($T_{1_{nd}}$)	Computer Solution ($T_{1_{nd}}$)	% Deviation
16-1	8.3745×10^{-2}	2.5996	5.2490	50.474
16-2	1.6749×10^{-2}	28.470	40.115	29.029
21-4	3.3499×10^{-3}	194.08	237.66	18.337
16-4	1.7717×10^{-2}	26.497	30.396	12.827
21-3	3.5432×10^{-3}	182.10	212.96	14.491
21-7*	7.0864×10^{-4}	1,076.3	1,200.0	1.9725
21-1	3.7479×10^{-3}	170.81	158.96	- 7.4547
21-2	7.4957×10^{-4}	1,013.1	1,083.1	4.6164
23-2*	1.4991×10^{-4}	5,597.2	6,200.0	9.7226
21-6	7.9284×10^{-4}	953.51	799.23	-19.304
22-1*	1.5857×10^{-4}	5,277.3	5,360.3	1.5484
23-1*	3.1715×10^{-5}	28,090.	32,500.	13.569
17-3	1.6749×10^{-2}	28.470	41.695	31.718

Note:
*Based on extrapolated data.
See Figures (1) and (2).

1

$$T_{1_{nd}} = \frac{1}{A_o}\left[1-20^{1/8}\ A_o^{1/4}\right]$$

TABLE VII

Comparison of Benny Solutions ($T_{1_{nd}}$) vs

ASD Numerical Calculations

Run No.	A_o	I_{sp} (sec)	Benny Solution $\frac{M_1}{M_o}$	Computer Solution $\frac{M_1}{M_o}$	% Deviation
16-1	8.3745×10^{-2}	1,000	0.85528	0.68420	-25.004
16-2	1.6749×10^{-2}	5,000	.93379	.90346	- 3.3570
21-4	3.3499×10^{-3}	25,000	.98155	.97712	- .45337
16-4	1.7717×10^{-2}	1,000	.71387	.61311	-16.434
21-3	3.5432×10^{-3}	5,000	.91149	.89158	- 1.1115
21-7*	7.0864×10^{-4}	25,000	.97828	.97556	- .27[illegible]1
21-1	3.7479×10^{-3}	1,000	.63159	.57196	-10.426
21-2	7.4957×10^{-4}	5,000	.89670	.88334	- 1.5124
23-2*	1.4991×10^{-4}	25,000	.97618	.97328	- .29796
21-6	7.9284×10^{-4}	1,000	.58122	.54473	- 6.6987
22-1*	1.5857×10^{-4}	5,000	.88676	.87787	- 1.0127
23-1*	3.1715×10^{-5}	25,000	.97475	.97038	- .45033
17-3	1.6749×10^{-2}	5,000	.93685	.90880	- 3.0864

Note:

*Based on extrapolated data.
See Figures (1) and (2).

$$\frac{I_{sp} \times g_E}{\sqrt{g_o \; r_o}} \times \log_e \left[\frac{M_o}{M_1}\right] = \left(1 - 20\,\frac{1}{8} \times A_o\,\frac{1}{4}\right)$$

TABLE VIII

Comparison of Benny Solutions $\left[\frac{M_1}{M_o}\right]$ vs

ASD Numerical Calculations

1

Run No.	A_o	Benny Solution (θ)	Computer Solution (θ)	% Deviation
16-1	8.3745×10^{-2}	171.04	208.34	17.903
16-2	1.6749×10^{-2}	855.21	881.84	3.0198
21-4	3.3499×10^{-3}	4,276.0	4,297.4	.49798
16-4	1.7717×10^{-2}	808.49	754.50	- 7.1557
21-3	3.5432×10^{-3}	4,042.7	3,975.3	- 1.6955
21-7*	7.0864×10^{-4}	20,214.	20,200.	- .06931
21-1	3.7479×10^{-3}	3,821.9	3,380.5	-13.057
21-2	7.4957×10^{-4}	19,110.	18,605.	- 2.7143
23-2*	1.4991×10^{-4}	95,550.	98,000.	2.5020
21-6	7.9284×10^{-4}	18,067.	15,789.	-14.428
22-1*	1.5857×10^{-4}	90,333.	87,761.	- 2.9307
23-1*	3.1715×10^{-5}	451,650.	460,000.	1.8152
17-3	1.6749×10^{-2}	885.21	910.00	6.0209

Note:
*Based on extrapolated data.
See Figures (1) and (2).
1

$$\theta = \frac{180}{4 \pi A_o}$$

TABLE IX

Comparison of Benny Solutions (θ) vs

ASD Numerical Calculations

1

Run No.	A_o	Tsien Solution $\frac{r_1}{r_o}$	Computer Solution $\frac{r_1}{r_o}$	% Deviation
16-1	8.3745×10^{-2}	2.4434	2.4831	1.5988
16-2	1.6749×10^{-2}	5.4636	6.2804	13.006
21-4	3.3499×10^{-3}	12.217	14.583	16.224
16-4	1.7717×10^{-2}	5.3121	5.1536	- 3.0755
21-3	3.5432×10^{-3}	11.879	13.600	12.654
21-7*	7.0864×10^{-4}	26.563	32.200	17.506
21-1	3.7479×10^{-3}	11.550	10.747	- 7.4718
21-2	7.4957×10^{-4}	25.828	29.373	15.473
23-2*	1.4991×10^{-4}	57.750	70.500	18.085
21-6	7.9284×10^{-4}	25.113	22.635	-10.948
22-1*	1.5857×10^{-4}	56.155	64.467	12.893
23-1*	3.1715×10^{-5}	125.56	159.00	21.031
17-3	1.6749×10^{-2}	5.4636	6.1079	10.549

Note:
*Based on extrapolated data.
See Figures (1) and (2).

1

$$\frac{r_1}{r_o} = \frac{1}{2^{1/2} \quad A_o^{1/2}}$$

TABLE X

Comparison of Tsien Solutions $\left[\frac{r_1}{r_o}\right]$ vs

ASD Numerical Calculations

1

Run No.	A_o	Tsien Solution ($T_{1_{nd}}$)	Computer Solution ($T_{1_{nd}}$)	% Deviation
16-1	8.3745×10^{-2}	4.3020	5.2490	18.042
16-2	1.6749×10^{-2}	34.162	40.115	14.840
21-4	3.3499×10^{-3}	213.11	237.66	10.330
16-4	1.7717×10^{-2}	31.953	30.396	- 5.1224
21-3	3.5432×10^{-3}	200.34	212.96	5.9260
21-7*	7.0864×10^{-4}	1,137.3	1,200.0	5.2250
21-1	3.7479×10^{-3}	188.31	158.96	-18.464
21-2	7.4957×10^{-4}	1,071.6	1,083.1	1.0618
23-2*	1.4991×10^{-4}	5,792.7	6,200.0	6.5694
21-6	7.9284×10^{-4}	1,009.6	799.23	-26.322
22-1*	1.5857×10^{-4}	5,464.8	5,360.3	-19.495
23-1*	3.1715×10^{-5}	28,717.	32,500.	11.640
17-3	1.6749×10^{-2}	34.162	41.695	18.067

Note:
*Based on extrapolated data.
See Figures (1) and (2).

1

$$T_{1_{nd}} = \frac{1 - (2A_o)^{1/4}}{A_o}$$

TABLE XI

Comparison of Tsien Solution ($T_{1_{nd}}$)

vs ASD Numerical Calculations

Run No.	A_o	$T_{1_{nd}}$	I_{sp}	Tsien Solution $\frac{M_1}{M_o}$	Computer Solution $\frac{M_1}{M_o}$	% Deviation
16-1	8.3745×10^{-2}	4.3020	1,000	0.77208	0.68420	-12.844
16-2	1.6749×10^{-2}	34.162	5,000	.92114	.90346	- 1.9569
21-4	3.3499×10^{-3}	213.11	25,000	.97971	.97712	- .2651
16-4	1.7717×10^{-2}	31.953	1,000	.66608	.61311	- 8.6395
21-3	3.5432×10^{-3}	200.34	5,000	.90399	.89158	- 1.3919
21-7*	7.0864×10^{-4}	1137.3	25,000	.97713	.97556	- .1609
21-1	3.7479×10^{-3}	188.31	1,000	.60255	.57196	- 5.3482
21-2	7.4957×10^{-4}	1071.6	5,000	.89110	.88334	- .8785
23-2*	1.4991×10^{-4}	5792.7	25,000	.97532	.97328	- .2096
21-6	7.9284×10^{-4}	1009.6	1,000	.56296	.54473	- 3.3466
22-1*	1.5857×10^{-4}	5464.8	5,000	.88300	.87787	- .5844
23-1*	3.1715×10^{-5}	28717.	25,000	.97418	.97038	- .3916
17-3	1.6749×10^{-2}	34.162	5,000	.92472	.90880	- 1.7517

Note:
*Based on extrapolated data.
See Figures (1) and (2).

$$\frac{I_{sp} \times g_E}{\sqrt{g_o \times r_o}} \times \log_e \frac{(M_o)}{(M_1)} = A_o \times T_{1_{nd}}$$

TABLE XII

Comparison of Tsien Solution $\left[\frac{M_1}{M_o}\right]$ vs ASD Numerical Calculations

GA / PHYS / 62-4

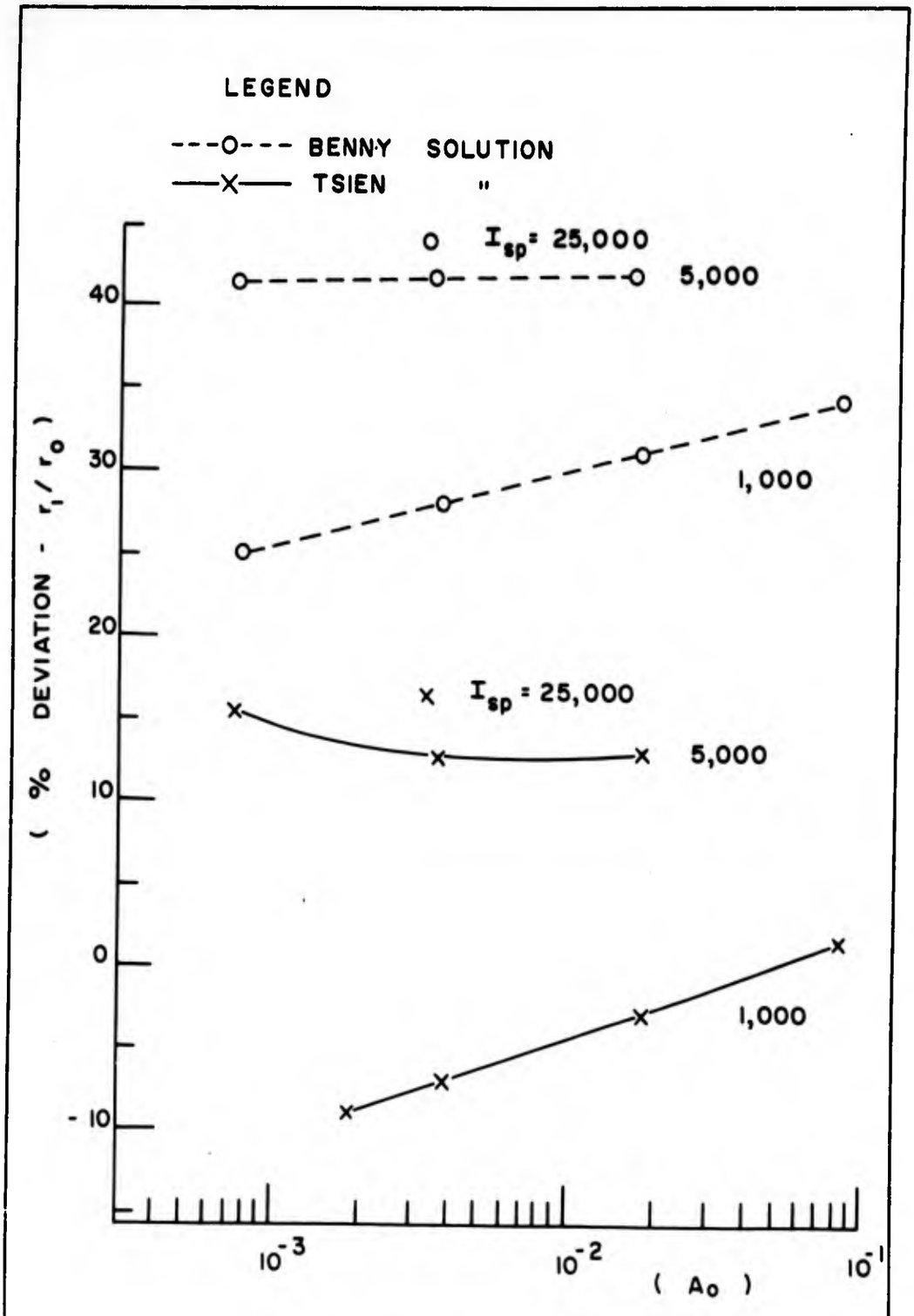

FIGURE 19
PERCENT DEVIATION (r_1 / r_o)
FROM ASD COMPUTER PROGRAM

GA / PHYS / 62-4

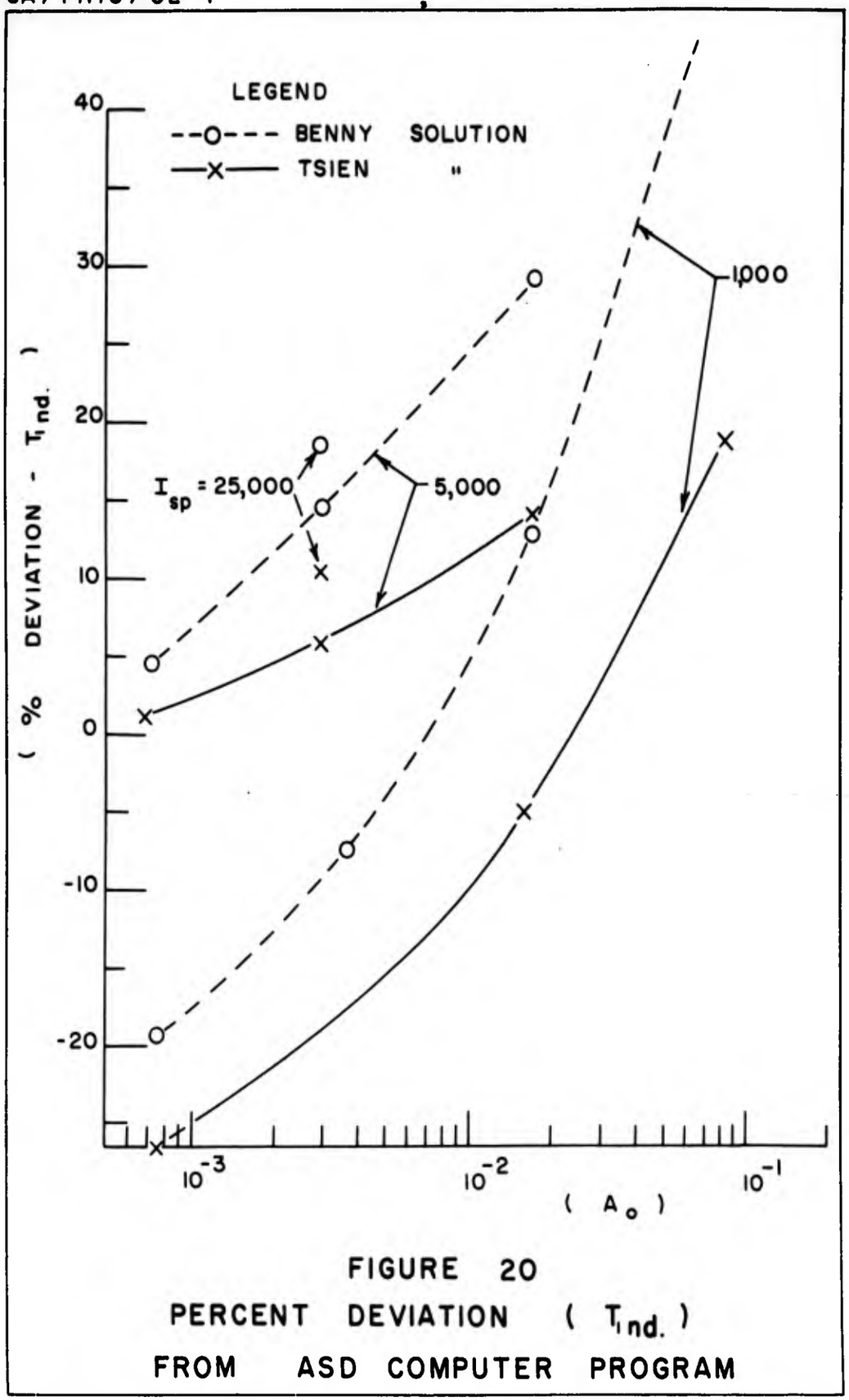

FIGURE 20
PERCENT DEVIATION ($T_{i\,nd.}$)
FROM ASD COMPUTER PROGRAM

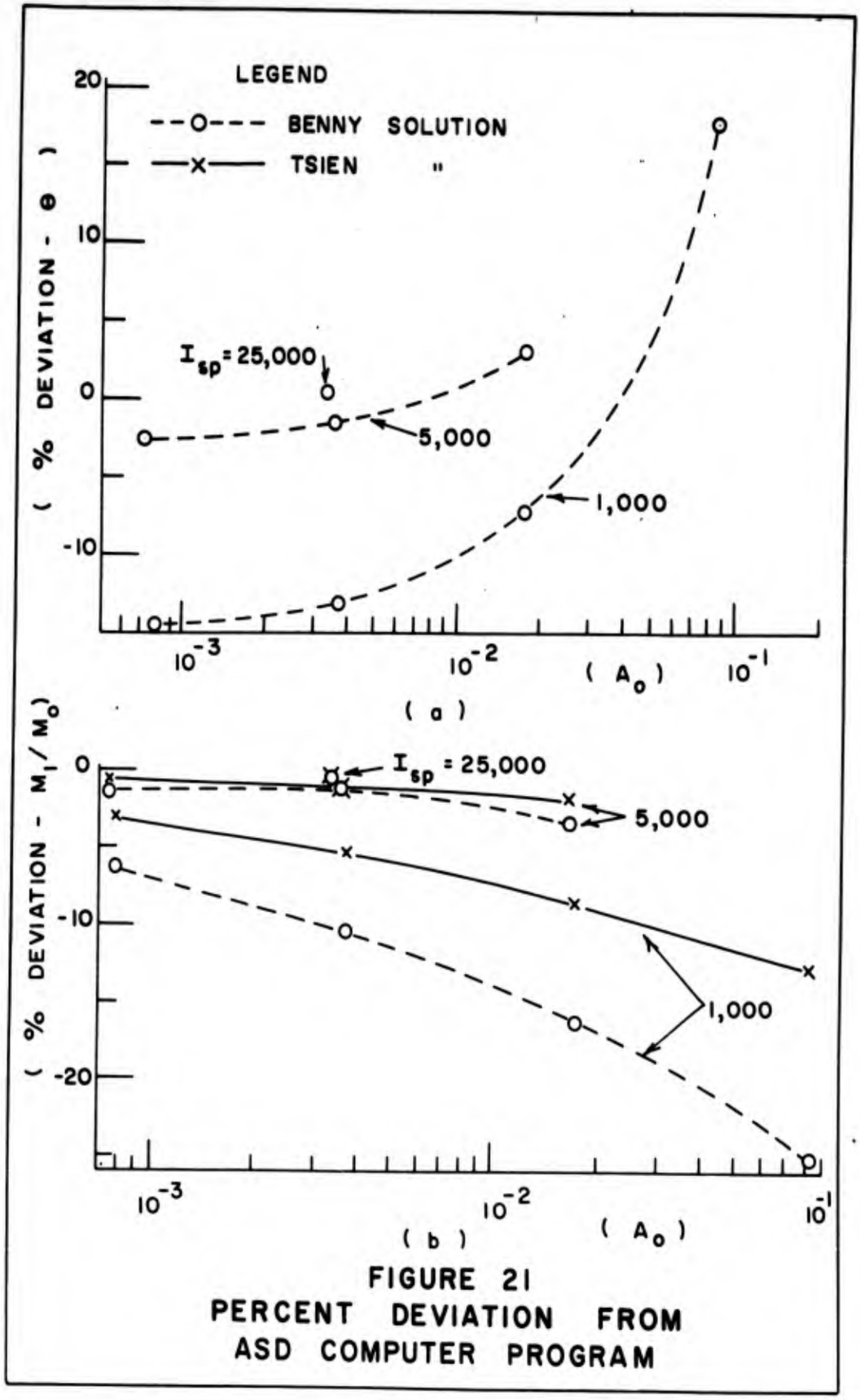

FIGURE 21
PERCENT DEVIATION FROM
ASD COMPUTER PROGRAM

From Figure 21 (b), it is shown that the mass fractions deviate from the numerical results by less than - 3.4 percent for $I_{sp} \geq 5000$ seconds. Therefore, Figure 21 (b) may be used for estimating preliminary mass fraction deviations.

Figures 22 and 23 indicate the variation of Perkins parameters as functions of time and velocity.

The ASD numerical data for these figures are tabulated in Tables XIII through XV.

These figures represent generalized trajectory charts and can be used for obtaining position radii and time as a function of initial thrust - to - weight ratio at the reference altitude.

Figures 22 and 23 also represent exact duplicates of Perkins curves up to and including the escape point. Beyond escape, the transversality condition, associated with the ASD computer program, approaches very rapidly the magnitude of 100 and optimization accuracy is lost. For thrust accelerations less than 10^{-2}, single curves independent of thrust accelerations are obtained. As pointed out by Perkins (Ref 15: 293), if the equation of motion involving radial acceleration was not put into a simple form, the general result of ΔV and Δr would contain in addition to sine terms an exponential damping coefficient. The simplified form assumes that $\dot{r}$ is approximately zero. Since this simplified form was not used in the ASD computer program, these oscillations are readily apparent from Figures 22 and 23.

T_{nd}	V_{nd}	Y	$\frac{r}{r_o}$	X	$\left[T-T_1\right]_{nd}$	$\left[\underline{T}-\underline{T}_1\right]_{nd}$
0	1.0000	1.77	1.0000	0.321	-5.2508	-0.956
.35276	1.0287	1.82	1.0012	.321	-4.8980	- .891
.68992	1.0503	1.85	1.0092	.324	-4.5609	- .830
1.0268	1.0614	1.87	1.0297	.331	-4.2240	- .769
1.3730	1.0599	1.87	1.0680	.343	-3.8778	- .706
1.7411	1.0451	1.84	1.1299	.363	-3.5097	- .639
2.1481	1.0182	1.80	1.2230	.393	-3.1090	- .566
2.6169	.98229	1.73	1.3578	.436	-2.6339	- .479
3.1800	.94274	1.66	1.5513	.498	-2.0708	- .377
3.8849	.90823	1.60	1.8321	.588	-1.3659	- .249
4.8029	.89315	1.58	2.2538	.724	-0.4479	- .0815
5.1930	.89662	1.58	2.4520	.787	-0.0578	- .0105
5.2508	(ESCAPE POINT)			.797	0	0
6.0416	.92273	1.63	2.9257	.939	0.7908	.144
7.7615	1.0456	1.85	4.0945	1.59	2.5107	.457

Notes:

$$Y = A_o^{-1/4} \frac{V}{V_{c_o}}$$

$$X = A_o^{1/2} \frac{r}{r_o}$$

$$\underline{T} = \frac{V_{co}}{r_o} A_o^{3/4} T$$

A_o AVG = 0.10296, V_{c_o} = 23,112.63 ft/sec, r_o = 5000 miles

TABLE XIII

Perkins Parameters for ASD

Computer Run 26-1

(P=100 MW I_{sp} = 1000)

T_{nd}	V_{nd}	Y	$\frac{r}{r_o}$	X	$\left[T-T_1\right]_{nd}$	$\left[\underline{T}-\underline{T}_1\right]_{nd}$
0	1.0000	2.76	1.0000	0.133	-40.115	- 1.93
1.7432	1.0047	2.77	1.0254	.136	-38.372	- 1.85
3.6792	.93492	2.58	1.1419	.152	-36.435	- 1.76
6.0273	.87929	2.43	1.2668	.168	-34.087	- 1.64
8.6269	.87363	2.41	1.3412	.178	-31.488	- 1.52
11.507	.82849	2.29	1.5041	.200	-28.608	- 1.38
15.216	.74258	2.05	1.8277	.243	-24.899	- 1.20
20.308	.67601	1.87	2.2878	.304	-19.807	- .955
23.606	.64307	1.78	2.6528	.353	-16.509	- .796
29.984	.58582	1.62	3.6717	.488	-10.131	- .488
39.661	.56337	1.55	6.1301	.815	- 0.45350	- .0219
40.115	(ESCAPE POINT)				0	0
45.040	.58873		8.0190		4.9250	.237

Notes:

$$Y = A_o^{-\frac{1}{4}} \frac{V}{V_{c_o}}$$

$$X = A_o^{\frac{1}{2}} \frac{r}{r_o}$$

$$\underline{T} = \frac{V_{co}}{r_o} A_o^{3/4} T$$

$A_{o\ AVG}$ = 0.017645 , V_{co} = 23,112.63 ft/sec , r_o = 5000 miles

TABLE XIV

Perkins Parameters for ASD

Computer Run 16-2

(P = 100 MW I_{sp} = 5000)

T_{nd}	V_{nd}	Y	$\frac{r}{r_o}$	X	$\left[T-T_1\right]_{nd}$	$\left[\frac{T-T_1}{}\right]_{nd}$
0	1.0000	4.15	1.0000	0.0582	-237.66	- 3.30
7.2363	.97984	4.07	1.0460	.0609	-230.42	- 3.20
15.052	.95548	3.97	1.1023	.0642	-222.61	- 3.09
23.574	.92590	3.84	1.1729	.0683	-214.09	- 2.98
32.979	.89131	3.70	1.2618	.0734	-204.68	- 2.85
43.518	.85255	3.54	1.3740	.0800	-194.14	- 2.70
55.571	.80999	3.36	1.5184	.0884	-182.09	- 2.53
69.760	.76233	3.16	1.7143	.0998	-167.90	- 2.33
87.244	.70528	2.93	2.0081	.117	-150.42	- 2.09
110.65	.62913	2.61	2.5365	.148	-127.01	- 1.77
148.94	.50704	2.10	3.9809	.232	- 88.72	- 1.23
237.66	(ESCAPE POINT)		14.583	.849	0	0
314.57	.50835	2.11	39.285	2.29	76.91	1.07

Notes:

$$Y = A_o^{-\frac{1}{4}} \frac{V}{V_{c_o}}$$

$$X = A_o^{\frac{1}{2}} \frac{r}{r_o}$$

$$\frac{T}{} = \frac{V_{c_o}}{r_o} A_o^{3/4} T$$

$A_{o\ AVG} = 0.0033891$, $V_{c_o} = 23{,}112.63$ ft/sec, $r_o = 5000$ miles

TABLE XV

Perkins Parameters for ASD

Computer Run 21-4

(P = 100 MW I_{sp} = 25,000)

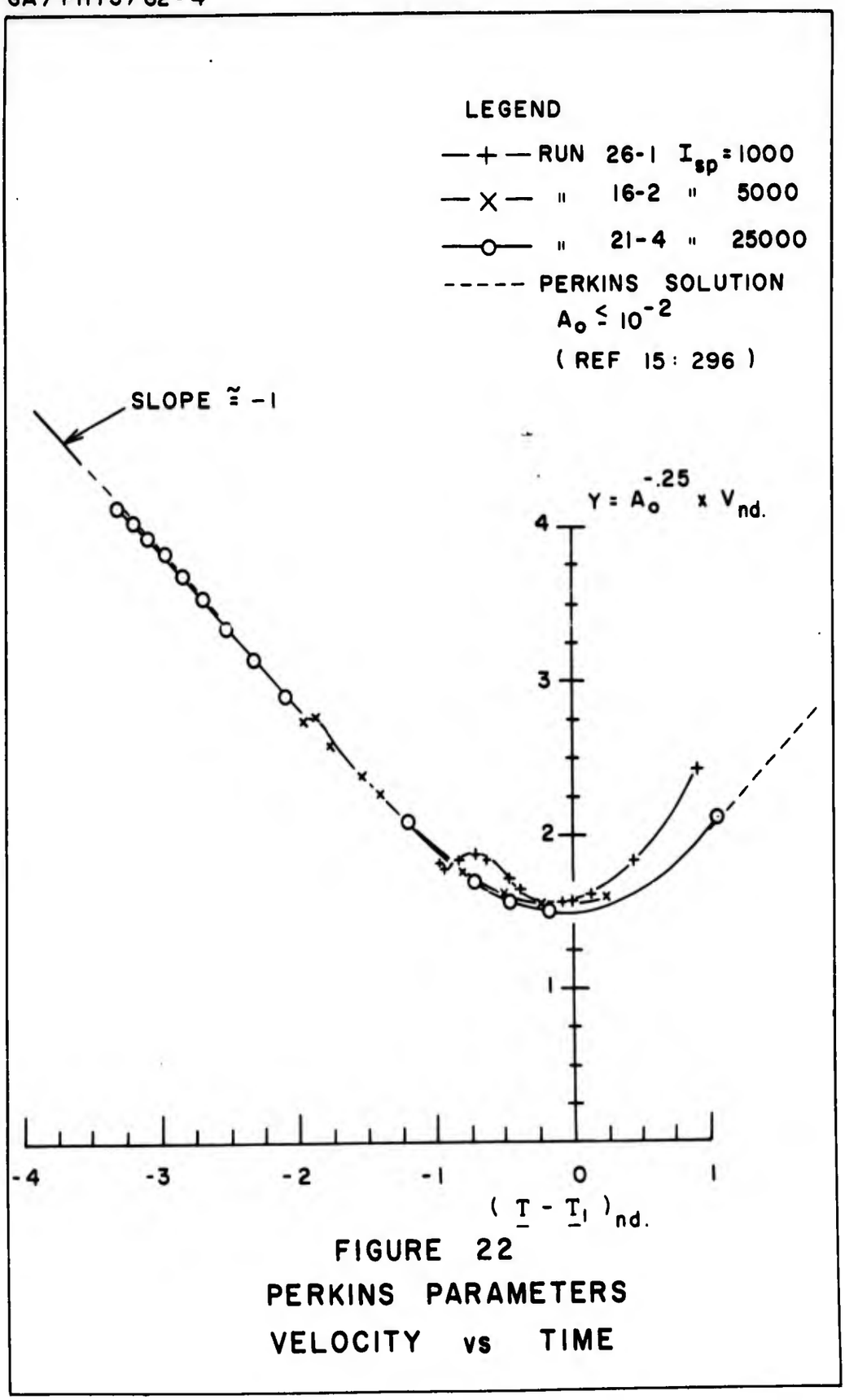

FIGURE 22
PERKINS PARAMETERS
VELOCITY vs TIME

GA / PHYS / 62-4

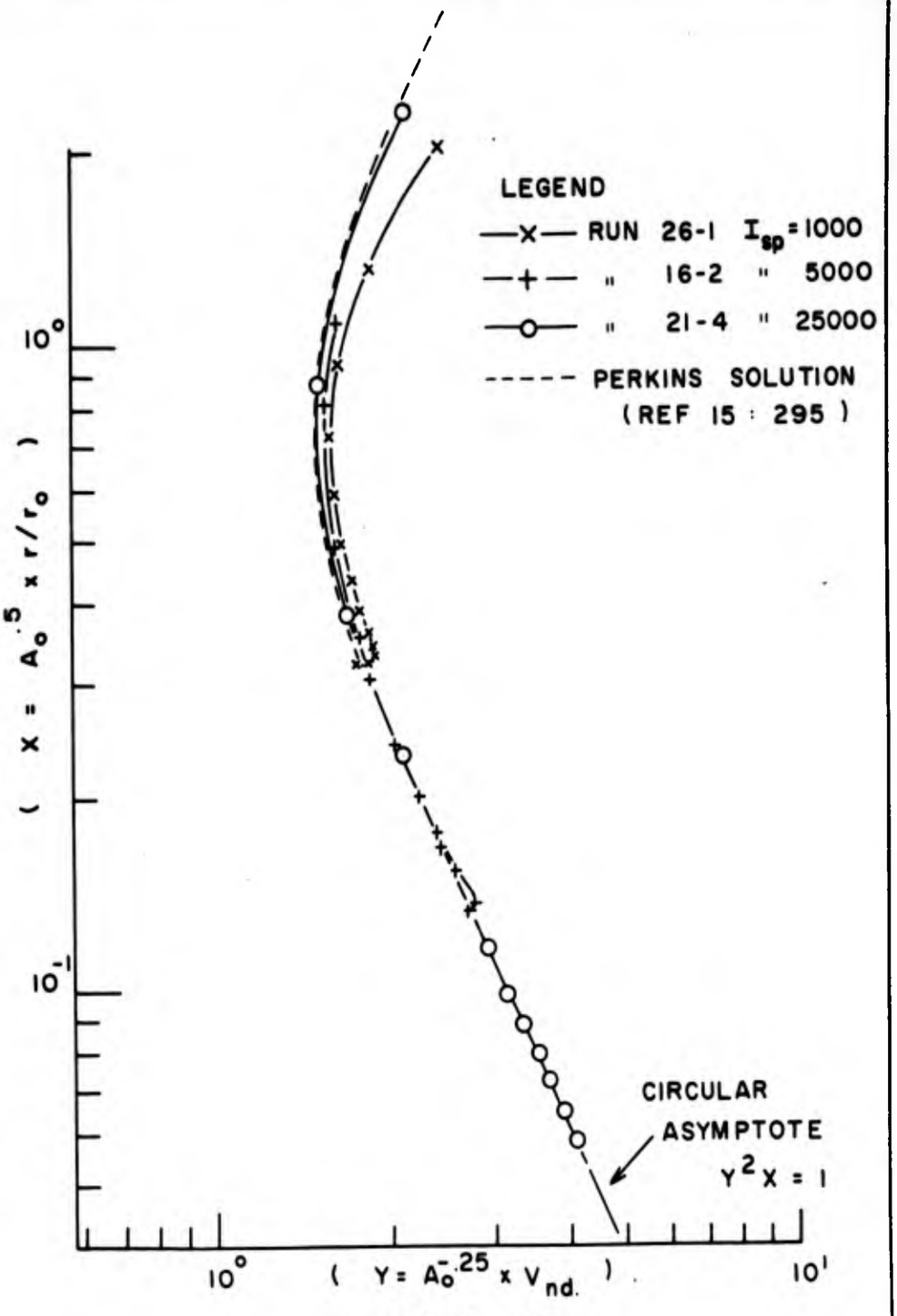

FIGURE 23

PERKINS PARAMETERS
RADIUS RATIO vs VELOCITY

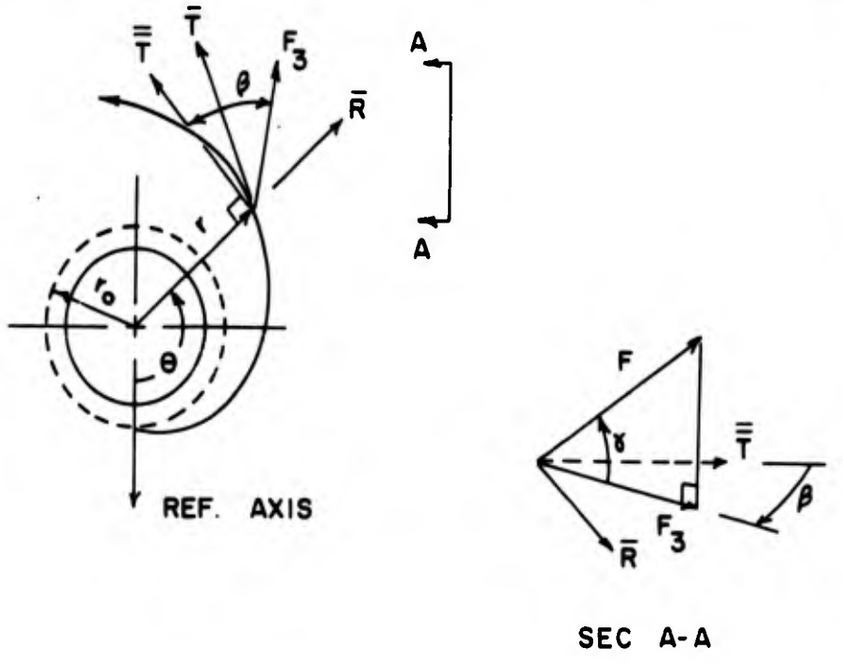

(a)

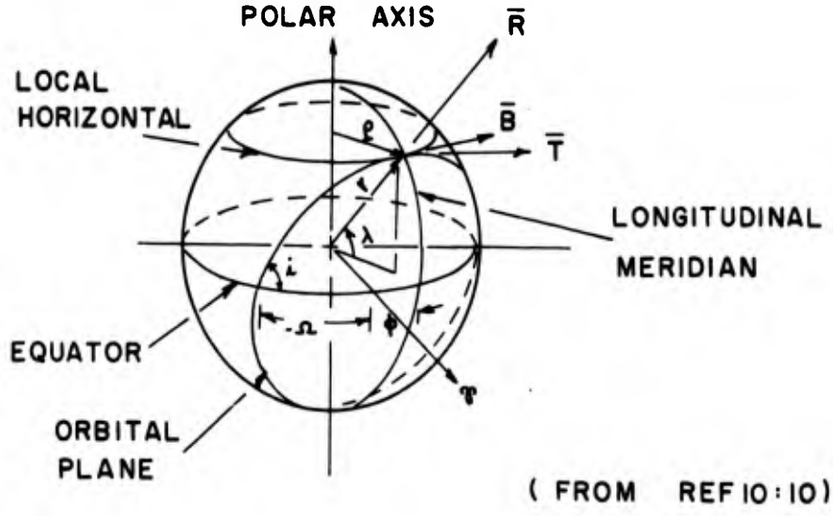

(b)

FIGURE 24

COORDINATE SYSTEM

GA / PHYS / 62-4

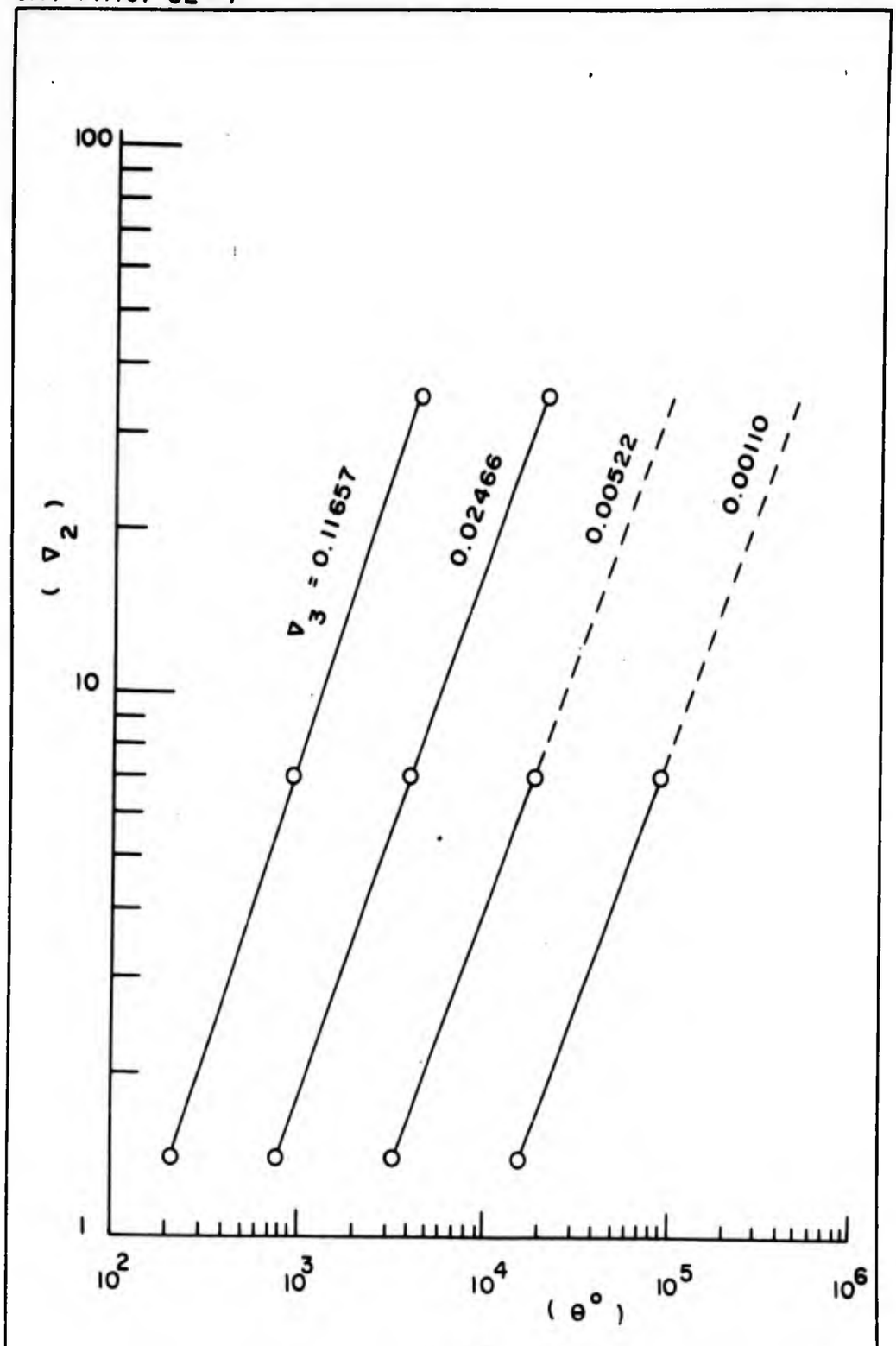

FIGURE 25

∇_2 vs ESCAPE RANGE ANGLE

GA/PHYS/62-4

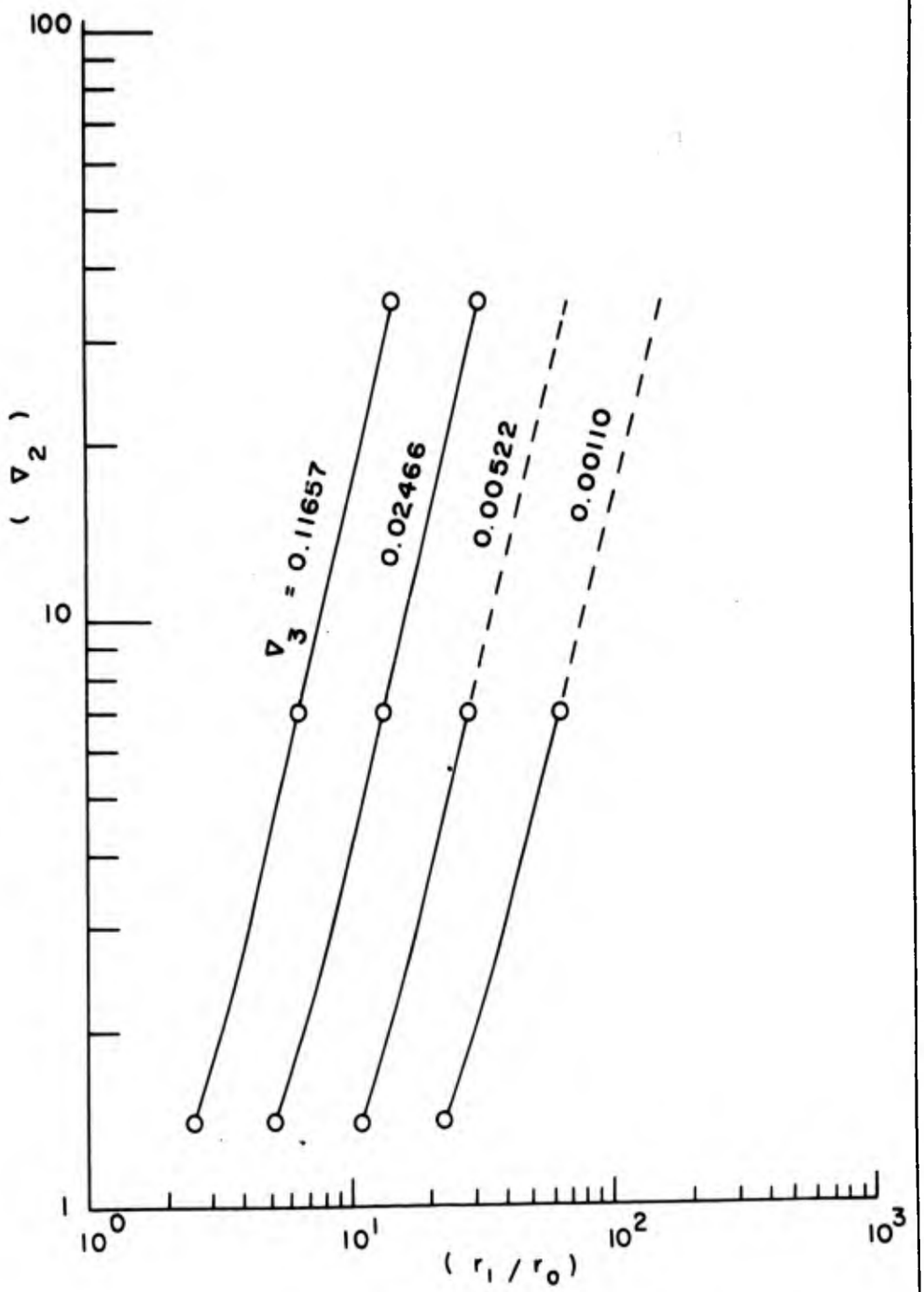

FIGURE 26

∇_2 vs ESCAPE RADIUS

GA / PHYS / 62-4

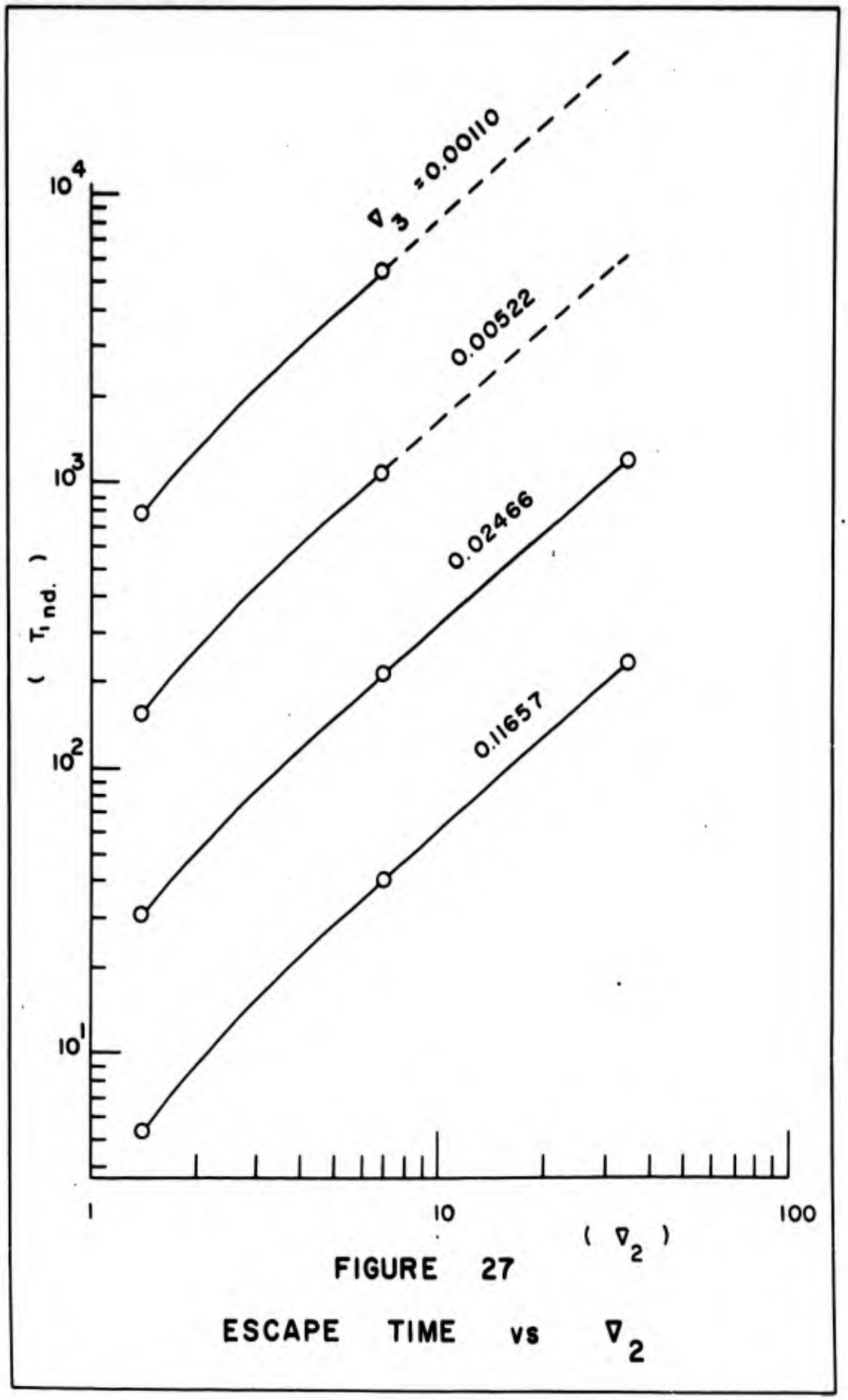

FIGURE 27

ESCAPE TIME vs ∇_2

GA / PHYS / 62-4

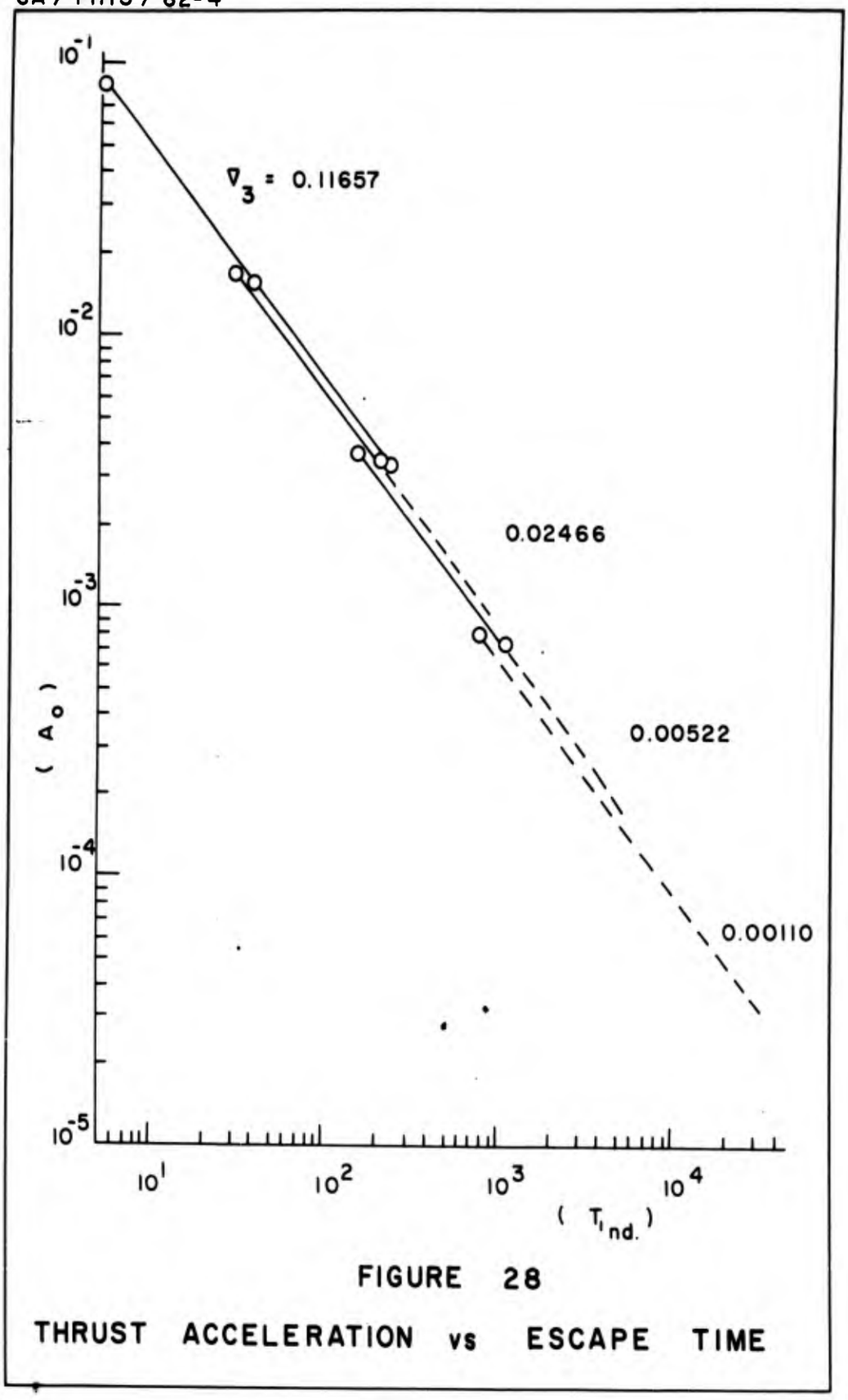

FIGURE 28

THRUST ACCELERATION vs ESCAPE TIME

The angular direction of the vehicle escape velocity must be known if the escape trajectory is to successfully match the interplanetary transfer trajectory. Using angular momentum and vehicle velocity data tabulated in Table III, the direction can readily be calculated for a reference altitude of 1036.5 miles. This angular direction, which is measured perpendicular from the escape radius vector, is simply equal to the arc $\cos^{-1}$ ratio of circumferential escape velocity divided by the vehicle escape velocity. For example, the angular deviation for run 16-1 was found to be approximately 45.8°.

VI. Numerical Example of Escape Mission

As an illustration in the use of the graphical data presented in this study, the electrical power output, payload and powerplant mass fractions are specified. The vehicle is assumed to be placed in an initial circular orbit by a conventional chemical rocket and it is required to obtain the escape parameters associated with this mission. (Slide rule accuracy will only be required since values will be read off figures generated in Section V).

Before attempting the problem, it is suggested that the reader review Appendix B since this particular example involves the use of generalized parameters.

The basic constants and assumed parameters for this analysis are as follows:

r_o = 4500 stat. miles

$g_E/g_o = \frac{1}{.77577} = 1.2890$

V_{c_o} = 24,362 ft/sec

$\frac{r_o}{V_{c_o}} = 975.29$

P = 60 KW

$M_{PL+ST} = 0.50\ M_o$ (Space Tug)

$M_{PP} = 0.25\ M_o$

eff. = 100%

As previously defined in Section II, the specific weight of the electrical power plant is given by

$$\alpha = 514.2\ P^{-.6746} \tag{13}$$

Therefore,

$$\alpha = 514.2\ (60)^{-.6746} = 32.4 \text{ lbs powerplant/KW.}$$

The expression for the gross weight of the vehicle measured at the surface of the earth is given as:

$$W_E = \alpha \times P \times \frac{M_o}{M_{PP}} \tag{47}$$

or

$$W_E = 32.4\ (60)\ \frac{1}{.25} = 7750 \text{ lbs.}$$

The propellant utilization factor for this mission is given by

$$J = \frac{P}{M_o} \times \left[\frac{M_o}{M_1} - 1 \right] \tag{25}$$

where

P = electrical power in KW

M_o = initial vehicle mass

M_1 = vehicle mass at escape

Therefore,

$$J = \frac{60 \times 32.2}{7750} \times \left[\frac{1}{.75} - 1 \right] = 0.083\ \frac{KW}{SLUG}$$

From Figure 16, for $J = 0.083$ KW/SLUG,

$$T_{l_{nd}} (5000) \cong 3150$$

which represents the nondimensional escape time for a reference radius of 5000 miles.

Since the reference radius of this example is 4500 miles, a correction factor must be calculated and it is given by

$$C.F. = \frac{\omega_o^{-1}}{1143.34} = \frac{975.29}{1143.34} = 0.8530 \qquad (104)$$

The nondimensional escape time for a reference radius of 4500 miles is given by

$$T_{l_{nd}} (4500) = C.F. \quad T_{l_{nd}} (5000) \qquad (101)$$

or

$$T_{l_{nd}} (4500) = 0.853 \ (3150) \cong \underset{(726 \text{ HRS})}{2680}$$

The propellant consumption of the vehicle is given by

$$W_P = {}^{1/4} W_E = \frac{F}{I_{sp}} \times T_{l_{(4500)}} \qquad (48)$$

where

$$T_{l_{nd}} (4500) = T_l (4500) \times \frac{V_{c_o}}{r_o} \qquad (16)$$

The jet power is related to the engine thrust and specific impulse by the following expression

$$P = \frac{F \ I_{sp}}{45.854} \qquad (11)$$

or

$$F = 45.854 \frac{P}{I_{sp}} \tag{11a}$$

Substituting Eq (11a) into (48) yields

$$W_p = \frac{1}{4} W_E = \frac{45.854 \times T_1(4500) \underline{\times P}}{I_{sp}^2}$$

or

$$I_{sp}^2 = \frac{45.854 \times 4 \times T_1(4500) \underline{\times P}}{W_E} \tag{49}$$

Introducing Eq (16) yields

$$I_{sp}^2 = \frac{45.854 \times 4 \times T_{1_{nd}}(4500)}{W_E} \frac{r_o \times P}{V_{c_o}} \tag{49a}$$

$$I_{sp}^2 = \frac{45.854 \times 4 \times 2680 \times 975.29 \times 60}{7750}$$

$$= 3.72 \times 10^6$$

$$I_{sp} = 1930 \text{ seconds}$$

Substituting I_{sp} into Eq (11a) yields

$$F = 1.425 \text{ lbs.}$$

The nondimensional thrust acceleration is given by

$$A_o = \frac{A}{g_E} \times \frac{g_E}{g_o} = \frac{F}{W_E} \times \frac{g_E}{g_o} \tag{22}$$

or

$$A_o = \frac{1.425}{7750} \times 1.289$$

$$= 2.36 \times 10^{-4}$$

The normalized specific impulse parameter, ∇_2, is given by

$$\nabla_2 = \frac{g_E \quad I_{sp}}{\omega_o \quad r_o} = \frac{g_E \quad I_{sp}}{V_{c_o}} \tag{96}$$

or

$$\nabla_2 = \frac{32.2\ (1930)}{24,362}$$

$$\nabla_2 = 2.56$$

The normalized power parameter, ∇_3, is represented by

$$\nabla_3 = A_o \quad x \quad \nabla_2 \tag{98}$$

or

$$\nabla_3 = 2.36 \times 10^{-4} \times 2.56$$
$$= 6.04 \times 10^{-4}$$

From Figure 25, for $\nabla_2 = 2.56$ and $\nabla_3 = 6.04 \times 10^{-4}$,

$$\Theta_{(5000)} = 48,000^{\circ}$$

The escape range angle for a reference altitude of 4500 miles is given by

$$\Theta_{(4500)} = C.F. \times \Theta_{(5000)} \tag{102}$$

or

$$\Theta_{(4500)} = 0.8530\ (48,000) = 41,000^{\circ}$$

From Figure 26, for $\nabla_2 = 2.56$ and $\nabla_3 = 6.04 \times 10^{-4}$,

$$\rho = \frac{r_1}{r_{o\,(5000)}} = 49$$

The nondimensional escape radius for a reference altitude of 4500 miles is given by

$$\rho_{(4500)} = \text{C.F.} \times \rho_{(5000)} \tag{103}$$

or

$$\rho_{(4500)} = 0.8530\,(49) \cong 41.8$$

Figure 27 will now be used to obtain a preliminary check on escape time at a reference readius of 5000 miles. For $\nabla_2 = 2.56$ and $\nabla_3 = 6.04 \times 10^{-4}$

$$T_{1_{nd(5000)}} = 3200$$

The escape parameters are summarized in Table XVI.

Table XVI

Illustrative Example Results

Mission Parameter ($r_o = 4500$)	Approximate Results
Nondimensional Escape Time ($T_{1_{nd}}$)	2680 (726 HRS)
Specific Impulse (I_{sp})	1930 seconds
Engine Thrust	1.425 lbs.
Escape Range Angle (Θ)	41,000° (114 Rev.)
Nondimensional Escape Radius $\frac{r_1}{r_o}$	41.8

VII. Conclusion and Recommendations

Analysis of the data obtained in this study indicate the following general results:

1. The escape parameters are dependent upon the initial thrust - to - weight ratios and specific impulses of the low thrust devices.
2. The escape parameters can be reduced in magnitude by:
    a. Using electrical power plants with low specific weights.
    b. Using engines with high thrust - to - weight ratios or low specific impulses.
3. For maximum payload capability of a "space-freight - ferry", with no restrictions on the escape parameters, engines with high specific impulses or low thrust - to - weight ratios would be required.
4. The results obtained from the analytical equations previously reported have percent deviations ranging from approximately - 25% to 44%.
5. The graphical curves generated from Perkins parameters are in general agreement with Perkins generalized curves as shown in Figures (22) and (23).
6. Regardless of the initial reference altitude, Figures (25) (26) (27) and (28) are directly applicable in determining the escape parameters for any interplanetary

mission. This simply requires the rescaling of the initial thrust acceleration, specific impulse and electrical power. This is accomplished by calculating A_o, ∇_2, ∇_3 and ω_o^{-1} at the reference altitude under consideration.

From the results reached in this study, a number of areas require further investigation. They are:

1. Determine analytically and numerically the effects of atmospheric drag and central body oblateness acting on the vehicle for various combinations of eccentricities and inclination angles.
2. The ASD computer option involving ballistic trajectories was not attempted due to time limitations. It is suggested that this option be checked out and its results compared with other ballistic data.
3. Determine optimum trajectories (inter-orbital and escape) that incorporate both low and high thrust engines operating on the same vehicle.

Bibliography

1. Benny, D.J. "Escape from a Circular Orbit Using Tangential Thrust." Jet Propulsion, 28: 167-169 (March 1958).

2. Bliss, Gilbert, Calculus of Variations. La Salle, Illinois: The Open Court Publishing Company, 1925.

3. Contribution to Astrodynamics, Astrodynamics Analysis for the National Space Surveillance Control Center. Aeronutronic Publication U-880.
Massachusetts: Air Force Command and Control Development Division, Air Research and Development Command, June 1, 1961.

4. Edelbaum, T.N. "Theory of Maximum and Minima," in Chapter 1 of Optimization Techniques, edited by G. Leitmann. East Hartford, Connecticut: Research Laboratories, United Aircraft Corporation, n.d., (Unpublished).

5. Irving, J.H., Power-limited Flight - Optimization in Gravitational Fields. Space Technology lecture of the UCLA Extension, October 7, 1956 (Unpublished).

6. Koerner, T.W., and J.J. Paulson. Nuclear Electric Power for Space Missions. Technical Release Number 34-230. Pasadena, California: Jet Propulsion Laboratory, January 1961.

7. Lawden, D.F. "Optimal Programming of Rocket Thrust Direction." Astronautica Acta, 1: 41-56 (1955).

8. Leitmann, G. "On a Class of Variational Problems in Rocket Flight." Journal of the Aero/Space Sciences, 26: 586-591 (September 1959).

9. Mission Analysis for Electric Propulsion Systems. WADD Technical Report 60-533. Dayton, Ohio: Propulsion Laboratory, Wright Air Development Center, Air Research and Development Command, June 1960.

10. Mission Analysis for Space Vehicles. ASD Technical Report 61-640. Dayton, Ohio: Propulsion Laboratory, Aeronautical Systems Division, Air Force Systems Command, November 1961.

11. Moeckel, W.E., et al. Satellite and Space Propulsion Systems. NASA Technical Note D-285. Cleveland: National Aeronautics and Space Administration, June 1960.

12. Moeckel, W.E., Trajectories with Constant Tangential Thrust in Central Gravitational Fields. NASA Technical Report R-53. Cleveland: National Aeronautics and Space Administration, 1960.

13. Moulton, F.R., An Introduction to Celestial Mechanics (Second Revised Edition). New York: The Macmillan Co., 1958.

14. Orbits with Low Tangential Thrust (G. Shapiro). AFOSR Document Number 1479. Washington, D.C.: Air Force Office of Scientific Research, Air Research and Development Command, September 1961.

15. Perkins, F.M., "Flight Mechanics of Low-Thrust Spacecraft." Journal of the Aero/Space Sciences, 26: 291-297 (May 1959).

16. Reference Manual 709/7090 Fortran Programming System. White Plains, New York: International Business Machines Corporation, 1961.

17. Shield, V.W., Ion Propulsion Mission Requirements and their Effect on Ion Engine Design. WADC Technical Note 59-156. ASTIA Document Number 215829. March 1959.

Appendix A

ASD Numerical Program - Differential Equations of Motion

The equations of motion have been previously defined in Section II of this study as

$$m\left(\ddot{r} - r\dot{\theta}^2\right) = -GM\frac{m}{r^2} + F\sin\beta \tag{3}$$

$$\frac{1}{r}\frac{d}{dt}\left(m r^2\dot{\theta}\right) = F\cos\beta \tag{4}$$

The impressed components of acceleration are defined as follows:

$$A_R = \frac{F}{m}\sin\beta \tag{50}$$

$$A_T = \frac{F}{m}\cos\beta \tag{51}$$

Introducing Eqs (50) and (51) into (3) and (4) and letting $k = GM$ yields

$$\ddot{r} - r\dot{\theta}^2 = -\frac{k}{r^2} + A_R \tag{52}$$

$$\frac{1}{r}\frac{d}{dt}\left(r^2\dot{\theta}\right) = A_T \tag{53}$$

Eqs (52) and (53) are then written for a nonorthogonal reference coordinate system (Ref 10: 9). This system results in single value trajectory variables for any choice of inclination angles ranging from 0 to 90°.

A nonorthogonal coordinate system is represented in Figure 24 (b).

Equations of motion then become

$$\ddot{r} - r\dot{\theta}^2 = -\frac{k}{r^2} + A_R \tag{52}$$

$$\frac{1}{r}\frac{d}{dt}\left(r^2\dot{\theta}\right) = 2\dot{r}\dot{\theta} + r\ddot{\theta} = A_T \tag{53}$$

$$\frac{1}{\rho}\frac{d}{dt}\left(\rho^2\dot{\phi}\right) = 2\dot{\rho}\dot{\phi} + \rho\ddot{\phi} = A_B \tag{54}$$

where A_B represents an acceleration in the direction of $\bar{B}$.

The velocity components are represented by

$$V_R = \dot{r} \tag{55}$$

$$V_T = r\dot{\theta} \tag{56}$$

$$V_B = \rho\dot{\phi} \tag{57}$$

The time differential of Eq (56) yields

$$\dot{V}_T = \dot{r}\dot{\theta} + r\ddot{\theta} \tag{58}$$

Multiplying together Eqs (55) and (56) and dividing by r gives

$$\frac{V_R V_T}{r} = \dot{r}\dot{\theta} \tag{59}$$

Introducing Eq (59) into (58) and the resulting equation into Eq (53) yields

$$\dot{V}_T = A_T - \frac{V_R V_T}{r} \tag{60}$$

The time differential of Eq (55) gives

$$\dot{V}_R = \ddot{r} \tag{61}$$

Squaring Eq (56) and dividing by r yields

$$r \dot{\theta}^2 = \frac{V_T^2}{r} \tag{62}$$

Introducing Eqs (61) and (62) into Eq (52) yields

$$\dot{V}_R = A_R - \frac{k}{r^2} + \frac{V_T^2}{r} \tag{63}$$

The component of V_T along the longitudinal meridian is given by

$$V_\lambda = V_T \cos \jmath \tag{64}$$

or

$$V_\lambda = r \dot{\lambda} \tag{65}$$

where the spherical angle $\jmath$ is measured between the longitudinal meridian and the orbital plane.

Equating (64) and (65) and dividing by r gives

$$\dot{\lambda} = \frac{V_T \cos \jmath}{r} \tag{66}$$

The time differential of Eq (57) gives

$$\dot{V}_B - \dot{\varrho} \dot{\phi} = \varrho \ddot{\phi} \tag{67}$$

Equating Eqs (67) and (54) gives

$$\dot{V}_B = A_B - \dot{\varrho} \dot{\phi} \tag{68}$$

From Figure 24 (b), the radius vector in the local horizontal plane, can be represented as

$$\varrho = r \cos \lambda \tag{69}$$

The time differential of Eq (69) yields

$$\dot{\rho} = \dot{r} \cos\lambda + r \sin\lambda \dot{\lambda} \tag{70}$$

Introducing Eqs (70) (57) (69) into (68) yields

$$\dot{V}_B = A_B - \frac{V_B V_R}{r} + V_B \tan\lambda \frac{V_T \cos \jmath}{r} \tag{71}$$

Also, from Figure 24 (b), V_B can be represented by

$$V_B = V_T \sin \jmath \tag{72}$$

The time differential of Eq (72) gives

$$\dot{V}_B = \dot{V}_T \sin \jmath + V_T \cos \jmath \dot{\jmath} \tag{73}$$

Equating Eqs (71) and (73) and introducing Eq (60) gives

$$A_B - \frac{V_B V_R}{r} + \frac{V_B V_T}{r} \tan\lambda \cos \jmath = \left(A_T - \frac{V_R V_T}{r}\right) \sin \jmath + V_T \cos \jmath \dot{\jmath}$$

or

$$\frac{V_T A_B}{V_T^2 \cos \jmath} - \frac{V_B V_R}{r V_T \cos \jmath} \frac{V_T}{V_T} + \frac{V_B}{r} \tan\lambda - \frac{A_T \sin \jmath}{\cos \jmath V_T} + \frac{V_R}{r} \tan \jmath = \dot{\jmath} \tag{74}$$

Introducing Eq (60) into the second term of Eq (74) yields

$$\frac{V_T A_B}{V_T^2 \cos \jmath} - \frac{V_B}{V_T^2 \cos \jmath}\left(A_T - \dot{V}_T\right) + \frac{V_B \dot{V}_T}{V_T^2 \cos \jmath} - \frac{A_T \sin \jmath}{\cos \jmath V_T} + \frac{V_R \tan \jmath}{r} = \dot{\jmath} \tag{75}$$

Finally, introducing Eqs (72) and (60) into the third term of Eq (75) gives

$$\dot{j} = \frac{V_T A_B - V_B A_T}{V_T^2 \cos j} + \frac{V_B \tan \lambda}{r} \tag{76}$$

From Figure 24 (b), if A_W is the out - of - the orbital plane impressed acceleration, its relation to A_B and A_T is given by

$$A_B = A_T \sin j - A_W \cos j \tag{77}$$

Introducing Eqs (77) and (72) into the first term of Eq (76) yields

$$\dot{j} = -\frac{A_W}{V_T} + \frac{V_B \tan \lambda}{r} \tag{78}$$

Changing the independent variable in Eqs (60) (63) (55) (78) (66) and (56) from time to θ yields the following equations

$$V_T' = A_T \frac{r}{V_T} - V_R \tag{79}$$

$$V_R' = A_R \frac{r}{V_T} - \frac{k}{r V_T} + V_T \tag{80}$$

$$r' = \frac{V_R}{V_T} r \tag{81}$$

$$\lambda' = \cos j \tag{82}$$

$$j' = -\frac{A_W}{V_T^2} r + \sin j \tan \lambda \tag{83}$$

$$t' = \frac{r}{V_T} \tag{84}$$

From Figure 24 (b), the impressed acceleration perpendicular to the orbital plane is given by

$$A_W = \frac{F}{m} \sin \gamma$$

or

$$A_W = A \sin \gamma \tag{85}$$

Substituting Eqs (85) (50) and (51) into Eqs (79) (80) and (83) yields the following sixth order differential system of equations. These equations are given by

$$\dot{V}_T = A \frac{r}{V_T} \cos \gamma \cos \beta - V_R \tag{86}$$

$$\dot{V}_R = A \frac{r}{V_T} \cos \gamma \sin \beta - \frac{k}{r V_T} + V_T \tag{87}$$

$$\dot{r} = \frac{V_R}{V_T} r \tag{81}$$

$$\dot{\lambda} = \cos j \tag{82}$$

$$\dot{j} = - \frac{A}{V_T^2} r \sin \gamma + \tan \lambda \sin j \tag{88}$$

$$\dot{t} = \frac{r}{V_T} \tag{84}$$

These equations are incorporated in the variational approach to trajectory analysis that is fully described in Appendix C.

Appendix B

Normalized Equation of Motion

Normalization of the basic equations of motion is necessary in order to determine those engine parameters that affect the vehicles trajectory. These parameters are also necessary to properly depict in graphical form, the computer results in Section V of this study.

Consider Eq (3) from Section II.

$$m\left(\ddot{r} - r\dot{\theta}^2\right) = -\frac{GMm}{r^2} + F_R \tag{3}$$

where

$$F_R = A_R\, m = F \sin\beta \tag{50}$$

Multiplying Eq (3) by $1/m\, r_o$ yields

$$\frac{\ddot{r}}{r_o} - \frac{r}{r_o}\dot{\theta}^2 = -\frac{GM}{r^2 r_o} + \frac{F_R}{r_o m} \tag{89}$$

The instantaneous vehicle mass is given by

$$m = m_o - \dot{m}\, t = m_o\left(1 - \frac{\dot{m}}{m_o}\, t\right) \tag{90}$$

Introducing Eq (90) into Eq (89) gives

$$\frac{\ddot{r}}{r_o} - \frac{r}{r_o}\dot{\theta}^2 = -\frac{(GM/r_o^3)}{(r^2\ r_o/r_o^3)} + \frac{F_R}{r_o\ m_o\left(1 - \frac{\dot{m}}{m_o}\, t\right)} \tag{91}$$

Introducing nodimensional quantities

$$T_{nd} = \omega_o\, T \tag{16}$$

and

$$\rho = \frac{r}{r_o} \tag{17}$$

where ω_o is taken as the initial orbital angular velocity taken with respect to inertial space. Time is in units of $1/\omega_o$ and distances are in units of the initial radius.

The gravitational attraction force is related by the following equation

$$F = \frac{GM\,m}{r_o^2} = m\,g_o = m\,\omega_o^2\,r_o \tag{92}$$

Introducing Eqs (16) (17) and (86) into Eq (91) and performing the required differentiation in terms of nondimensional parameters yields

$$\frac{d^2\rho}{d\,T_{nd}^2} - \rho\left[\frac{d\,\Theta}{d\,T_{nd}}\right]^2 + \rho^{-2} = \frac{F_R}{m_o\,g_o}\left[\frac{1}{1 - \frac{\dot{m}\,c\,T_{nd}\,g_o}{\omega_o c\,m_o\,g_o}}\right] \tag{93}$$

From Eq (22), the initial thrust acceleration at the reference altitude can also be given by

$$A_o = \frac{A}{g_o} = \frac{F}{W_o} = \frac{F_R}{m_o g_o} = \frac{\dot{m}c}{m_o g_o} \tag{22}$$

Introducing Eq (22) into Eq (93) yields

$$\frac{d^2\rho}{d\,T_{nd}^2} - \rho\left[\frac{d\,\Theta}{d\,T_{nd}}\right]^2 + \rho^{-2} = A_o\left[\frac{1}{1 - \frac{A_o\,T_{nd}g_o}{\omega_o\,c}}\right] \tag{94}$$

The term $(T_{nd}g_o/\omega_o\,c)$ can be simplified by using the definition

of specific impulse in addition to Eq (92) yielding

$$\frac{T_{nd} g_o}{\omega_o c} = \frac{1}{\nabla_2} * T_{nd} \tag{95}$$

where

$$\nabla_2 = \frac{g_e I_{sp}}{\omega_o r_o} = \frac{c}{\bar{V}_{c_o}} \tag{96}$$

Then Eq (94) may be rewritten as

$$\frac{d^2\rho}{d T_{nd}^2} - \rho \left[\frac{d\theta}{d T_{nd}}\right]^2 + \rho^{-2} = A_o \left[\frac{1}{1 - \frac{A_o}{\nabla_2} T_{nd}}\right] \tag{97}$$

Therefore, the vehicles normalized trajectory is determined primarily by the initial thrust acceleration (A_o) and the specific impulse (∇_2) of the engine. This conclusion was also stated by Moeckel (Ref 12: 1).

To obtain a complete general sclution for this study, the electrical power must also be normalized by a parameter ∇_3 and is expressed as:

$$\nabla_3 = A_o \nabla_2 \tag{98}$$

Introducing Eqs (22) and (96) into Eq (98) yields

$$\nabla_3 = \frac{F}{W_o} * \frac{g_E I_{sp}}{\omega_o r_o} \tag{99}$$

Introducing Eq (11) into (99) gives

$$\nabla_3 = \frac{2P}{\omega_o W_o r_o}$$

or (100)

$$\nabla_3 = \frac{2\,(737.6)\,P}{\frac{W_E\ g_o\ \omega_o\ r_o}{g_E}} = \frac{2\,(737.6)\,P}{\frac{W_E\ g_o\ V_{c_o}}{g_E}}$$

where P is the electrical power expressed in KW, W_E is the initial vehicle weight, V_{c_o} is the initial circular velocity at the reference orbit and g_E and g_o represent the acceleration of gravity taken at the surface of the earth and at the initial orbit respectively.

The normalized parameters, A_o, ∇_2 and ∇_3 must be used for obtaining the escape parameters at any reference altitude under consideration and must be used in conjunction with Figures (26) (27) (28) and (29).

To compensate for the new nondimensional time appearing in Eq (97) for any reference altitude other than 1036.5 miles, a correction factor equal to ω_o-1 (radius under consideration) must be applied to the escape parameters obtained from the generalized figures. The escape parameters at the new altitude are given by

$$T_{1_{nd}\ (\text{Radius under consideration})} = \text{C.F.} \times T_{1_{nd}\ (5000)} \quad (101)$$

$$\theta_{(\text{Radius under consideration})} = \text{C.F.} \times \theta_{(5000)} \quad (102)$$

$$\rho_{(\text{Radius under consideration})} = \text{C.F.} \times \rho_{(5000)} \quad (103)$$

where the correction factor is represented by

$$\text{C.F.} = \frac{\omega_o^{-1}}{1143.34} \quad (104)$$

When the radius under consideration corresponds to 5000 miles, the correction factor is equal to unity.

The use of Eqs (101) through (104) are illustrated in the numerical example of this thesis.

Appendix C

Variational Approach to Trajectory Optimization

Consider Eqs (86) (87) (81) (82) (88) and (84) from Appendix A.

$$\dot{V}_T = \frac{A}{V_T} r \cos\gamma \cos\beta - V_R \tag{86}$$

$$\dot{V}_R = \frac{A}{V_T} r \cos\gamma \sin\beta - \frac{k}{rV_T} + V_T \tag{87}$$

$$\dot{r} = \frac{V_R}{V_T} r \tag{81}$$

$$\dot{\lambda} = \cos\jmath \tag{82}$$

$$\dot{\jmath} = \frac{A}{V_T^2} r \sin\gamma + \tan\lambda \sin\jmath \tag{88}$$

$$\dot{t} = \frac{r}{V_T} \tag{84}$$

The problem is to obtain a stationary (extremum) value, or a function of boundary values, subject to the constraints

$$\Phi_1 = \frac{A}{V_T} r \cos\gamma \cos\beta - V_R - \dot{V}_T = 0 \tag{105}$$

$$\Phi_2 = \frac{A}{V_T} r \cos\gamma \sin\beta - \frac{k}{rV_T} + V_T - \dot{V}_R = 0 \tag{106}$$

$$\Phi_3 = \frac{V_R}{V_T} r - \dot{r} = 0 \tag{107}$$

$$\Phi_4 = \cos\jmath - \dot{\lambda} = 0 \tag{108}$$

$$\Phi_5 = \frac{-A}{V_T^2} r \sin\gamma + \tan\lambda \sin\jmath - \dot{\jmath} = 0 \tag{109}$$

$$\Phi_6 = \frac{r}{V_T} - t' = 0 \tag{110}$$

Problem of Mayer

The formulation of trajectory problems with variable end conditions in variational calculus is a problem of Bolza, where a boundary value, or a function of boundary values, D, plus an integral of a function f, is to be extremelized over the interval, Θ_1, to Θ_2 (Ref 10: II-4). The equation can be represented by

$$L = D\ (\Theta_1, \Theta_2) + \int_1^2 f(\Theta, \alpha_1, \alpha_2, y_i, y_i')\, d\Theta \tag{111}$$

where $i = 1 \rightarrow n$ dependent variables.

Equation (111) reduces to Lagranges problem if $D = 0$ and Mayer's problem if $f = 0$.

The constraint equations (105) through (110) may be introduced into the problem, by multiplication of each constraint equation by a Lagrange multiplier, μ_j, and setting

$$f = \sum_{j=1}^{6} \mu_j \Phi_j = 0 \tag{112}$$

since the Mayer formulation was incorporated into the ASD computer program (Ref 10: II-4).

A necessary condition (Ref 2: 130) in variational calculus states that for every minimizing arc, a constant c exists such that the equation

$$\frac{\partial f}{\partial y_i'} = \int_{\Theta_1}^{\Theta_2} \frac{\partial f}{\partial y_i}\, d\Theta + c \tag{113}$$

must be satisfied at every point on the arc.

Taking the differential of Eq (113) with respect to Θ yields the familiar Euler-Lagrange equations.

$$\frac{\partial f}{\partial y_i} - \frac{d}{d\Theta}\left(\frac{\partial f}{\partial y_i'}\right) = 0 \qquad (114)$$

$$i = 1 \rightarrow n$$

Also, an additional condition existing for a minimum at a variable end point is the transversality condition (Ref 8: 587). It is given by

$$dD + \Big(\mu_1 \; V_T' + \mu_2 \; V_R' + \mu_3 \; r' + \mu_4 \lambda' + \mu_5 j' + \mu_6 \; t' - H \; d\Theta\Big)_{\Theta_0}^{\Theta_1} = 0 \qquad (115)$$

Since D is to be minimized, the bracket term must be equal to zero. H represents the first integral since it does not contain Θ explicitly. If D and the boundary conditions do not contain Θ_0 and Θ_1, H is equal to zero.

Introducing constraint Eqs (105) through (110) into Eq (114) yields

$$f = \mu_1 \left(\frac{A\,r}{V_T} \cos\gamma \cos\beta - V_R - V_T'\right) +$$

$$\mu_2 \left(\frac{A\,r}{V_T} \cos\gamma \sin\beta - \frac{k}{r V_T} + V_T - V_R'\right) +$$

$$\mu_3 \left(\frac{V_R}{V_T} r - r'\right) +$$

$$\mu_4 \quad (\cos\gamma - \dot{\lambda}) \; +$$

$$\mu_5 \quad \left(- \frac{A}{V_T^2} \pi \sin\gamma + \tan\lambda \quad \sin\gamma - \dot{\gamma} \right) \; +$$

$$\mu_6 \quad \left(\frac{r}{V_T} - \dot{t}\right) \tag{116}$$

Applying Eq (114) to Eq (116) yields (Ref 10: 13) the Euler-Lagrange equations

$$\dot{\mu}_1 + \mu_2 \left(1 + \frac{k}{rV_T^2}\right) - \mu_3 \frac{V_R}{V_T^2} \quad r \quad - \frac{A_r}{V_T^2} \Bigg[$$

$$(\mu_1 \cos\gamma \cos\beta + \mu_2 \quad \cos\gamma \quad \sin\beta) - \frac{2\mu_5}{V_T} \sin\gamma +$$

$$\frac{\mu_6}{A} \Bigg] = 0 \tag{117}$$

$$\dot{\mu}_2 - \mu_1 + \mu_3 \quad \frac{r}{V_T} = 0 \tag{118}$$

$$\dot{\mu}_3 + \frac{k\mu_2}{r^2 V_T} + \mu_3 \quad \frac{V_R}{V_T} + \frac{A}{V_T} \Bigg[(\mu_1 \quad \cos\gamma \cos\beta +$$

$$\mu_2 \quad \cos\gamma \quad \sin\beta) - \frac{\mu_5}{V_T} \quad \sin\gamma + \frac{\mu_6}{A} \Bigg] = 0 \tag{119}$$

$$\dot{\mu}_4 + \mu_5 \quad \sec^2\lambda \quad \sin\gamma = 0 \tag{120}$$

$$\dot{\mu}_5 - \mu_4 \sin\gamma + \mu_5 \quad \tan\lambda \cos\gamma = 0 \tag{121}$$

$$\dot{\mu}_6 + \dot{A} \frac{r}{V_T} \left[\left(\mu_1 \cos\gamma \cos\beta + \mu_2 \cos\gamma \sin\beta \right) - \frac{\mu_5}{V_T} \sin\gamma \right] = 0 \qquad (122)$$

$$\text{Tan}\,\beta = \frac{\mu_2}{\mu_1} \qquad (123)$$

$$\text{Tan}\,\gamma = - \frac{(\mu_5/V_T)}{\mu_1 \cos\beta + \mu_2 \sin\beta} \qquad (124)$$

The extremal solution is obtained by integrating Eqs (82) (84) (86) (87) (88) (81) and Equations (117) through (122) subject to the boundary conditions arising from Eq (115). The numerical calculation of these equations was accomplished on the IBM 7090 digital computer.

Appendix D

Computer Input Data

Format

The main objective of a format statement is to supply input information to the computer program (Ref 16: 39-45).

Fortran language provides a means of expressing numerical constants and variables into the main computer program. Fortran arthmetric is generally performed with single-precision floating point integers. These integers provide 8 decimal digits of precision and have magnitudes between 10^{-38} and 10^{38} (Ref 16: iii).

The low-thrust computer program incorporates two different conversion forms of numerical data designated by type E or I. Type E pertains to an external floating point decimal and I to an external integer. They are specified in the following forms:

n E b c and n I b

where n, b and c represent fixed constants. Each constant represents:

1. The number of successive fields (n) within each data card.
2. Type of conversion form (E or I) for the field.
3. The width (b) of the field.
4. The number of positions (c) which appear to the right of the decimal point.

Data Cards

All input data are key punched on a general purpose IBM cards and must be in decimal form. Each card has a maximum of 72 characters.

The field width (b) will determine the maximum number of fields for each card. Within each field, all data must appear at the extreme right. Plus signs may be indicated by a + sign or a blank character. Minus (-) signs must be punched. Blanks in numerical fields are regarded as zeros. The start of the exponents may be marked by an E, or by a + or - sign.

For clarity, examples of formal input data are presented in Figure 29.

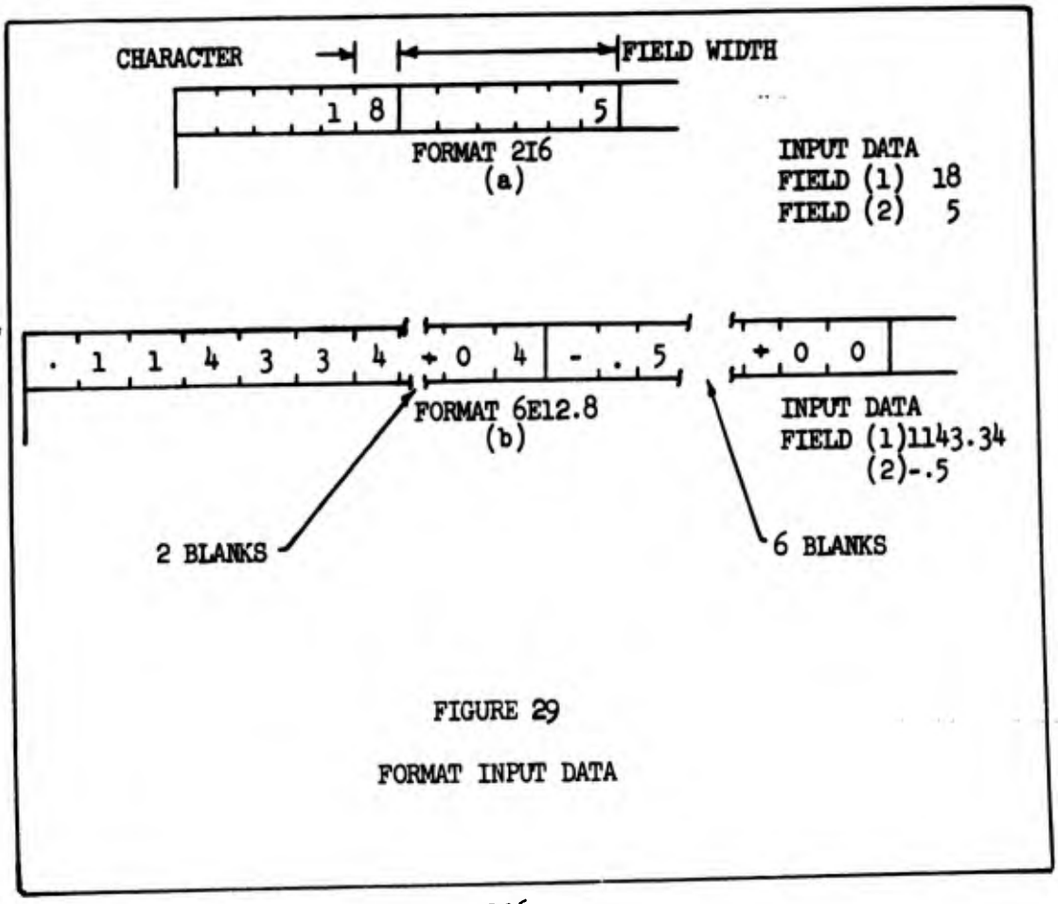

FIGURE 29

FORMAT INPUT DATA

Input Data Low-Thrust Program

The input data cards for each computer run are placed directly in back of the binary deck. Each computer run may consist of a set of cases. If so, the first case will require 7 keypunched IBM data cards plus 5 cards for each option. Each succeeding set will only require 6 data cards plus 5 additional cards for each option.

The input data cards must be placed in the following sequence:

Card 1 (I6)

Field (1) Number of cases to be run.

Card 2 (2I6)

(1) Order of differential equations.

(2) Specifies the number of options to be run in this case.

Card 3 (6E12.8)

(1) Reciprocal of mean motion of reference orbit $\frac{r_o}{\sqrt{c_o}}$

(2) Constant ($45.854 \frac{\text{lbs-sec}}{\text{KW}}$)

(3) Electrical power output (KW) of vehicles power supply

(4) Engine efficiency

$$\text{eff.} = \frac{\text{Jet Power}}{\text{Power supply output}}$$

(5) Powerplant weight franction W_{PP}/W_E

(6) Allowable error (ϵ) in I_{sp}

Card 4 (6E12.8)

(1) Final range angle (θ_f) desired in numerical calculation.

(2) ϵ_M - maximum error in variable due to doubling integration step size divided by the value of variable.

(3) No data required

(4) No data required

(5) Maximum allowable step size

(6) No data required

Card 5 (6E12.8)

(1) No data required

(2) No data required

(3) No data required if printed output of resulting data is required.

(4) Minimum allowable step size

(5) No data required

(6) No data required

Card 6 (6E12.8)

(1) No data required

(2) No data required

(3) No data required

(4) No data required

(5) If thrust is to be optimized, integer is 1. No data required if thrust is given.

(6) Longitude of perigee along the initial orbit in degrees.

Card 7 (6E12.8)

(1) Initial weight normalized with respect to initial weight.

(2) Initial longitude ϕ in degrees

(3) No data required

(4) No data required

(5) Initial energy per unit mass normalized with respect to $v_{c_o}^2$ and is taken as - .5.

(6) Initial value of angular momentum (h) normalized with respect to $v_{c_o}\ r_o$ and is taken as 1.

Card 8 (I6)

(1) Specifies option number

Card 9 (6E12.8)

(1) Specifies initial value θ_o

Card 10 (6E12.8)

Option 4 Thrust Constant - Direction Optimized

(1) Specifies $\frac{F}{W_E}$

Option 5 Specific Impulse Constant - Direction Optimized

(1) Specifies I_{sp}

Option 6 Constant Parameters

(1) Specifies β_o

(2) Specifies $\frac{A}{g_E} = \frac{F}{W_E}$

(3) Specifies γ_o

Option 9 Constant Parameters

(1) Specifies β_o

(2) Specifies $\frac{F}{W_E}$

(3) Specifies γ_o

This card will only specify the data for the specific option mentioned in card number 8. Each additional option will require 5 new cards that are placed directly in back of card number 12. The format of these 5 cards are similar to cards 8 through 12. See Table XVII.

Card 11 (6E12.8)

Used for Options 4 and 5.

Omit for Options 6 and 9.

(1) Specifies β_o

(2) Initial value of μ_3

(3) Initial value of μ_4

(4) Specifies γ_o

Card 12

No data required.

For each additional case, card 1 is omitted and the card sequence stated above is repeated. Table XVII illustrates the data input procedure for 2 cases. The first case is run with 2 options and the last case with 1 option.

It must be emphasized that the procedure outlined above only applies when oblateness and atmospheric drag are omitted from the

DATA							IBM Card No.
2							1
18	2						2
.114334	04.45854	02.10	04.10	1.25	00.10	2	3
.31	05.10	04.10	02.159308	01.20	02.10	1	4
			.10	2			5
.00	01.						6
.10	01.00	01.00	01.00	1-.5	.10	1	7
5							8
.00	01						9
.1000	04						10
	.10	01					11
.00	01						12
5							13
.00	01						14
.50	04						15
	.10	01					16
.00	01						17
18	1						18
.114334	04.45854	02.10	05.10	1.25	00.10	2	19
.31	05.10	04.10	02.159308	01.20	02.10	1	20
			.10	2			21
.00	01						22
.10	01.00	01.00	1.00	1-.5	.10	1	23
5							24
.00	01						25
.5000	04						26
	.10	01					27
.00	01						28

Note: Printed Output 28,998 lines
Computer Time 104.10 min for 7 Runs

TABLE XVII
Input Data for Runs 21-1 through 21-3
7 April 1962

analysis. If the mission dictates that they be included, additional input data are required on the input cards (Ref 10: 36).

Appendix E

Definition of Symbols

A	Engine acceleration
A_o	Nondimensional thrust acceleration or thrust - to - weight ratio taken at reference altitude.
$\bar{B}$	Unit vector in local horizontal plane, perpendicular to $\bar{\rho}$
c	Engine exhaust velocity
C.F.	Correction factor
D	Boundary value to be extremalized
e	Orbit eccentricity
E	Specific mission energy
f	Function whose integral is to be extremalized
F	Engine thrust
g_E	Acceleration of gravity (taken as 32.2011 ft/sec^2)
G	Universal gravitational constant
h	Angular momentum per unit vehicle mass
i	Angle between orbital and equatorial planes
I_{sp}	Specific impulse
j	Angle between orbital and longitudinal meridian planes
J	Propellant utilization factor
k	Gravitational product $G\underline{M}$
KW	Kilo-watts
L	Function to be extremalized

/62-4

, M	Instantaneous vehicle mass
	Mass of central body
N	Mega-watts
	Electrical power output
.	Radius from center of earth to vehicle
⟨	Unit vector in radial direction
⟩	Equatorial radius of earth (taken as 3963.5 stat. miles)
s	Distance traveled on trajectory
T_{nd}	Nondimensional time
T	Time
$\underline{T}$	Perkins time parameter
$\overline{T}$	Unit vector which is tangent and contained within the orbital plane
$\overline{\overline{T}}$	Unit vector perpendicular to radius vector and contained within the orbital plane
V	Orbital velocity
$V.E._{nd}$	Total vehicle energy per unit vehicle mass
W	Vehicle weight
X	Perkins altitude parameter
Y	Perkins velocity parameter
y_i	Generalized dependent variable
α	Specific weight of power plant
β	In-plane throw off angle (See Figure 24a)
γ	Angle between thrust vector and orbital plane (See Figure 24a)

Δ	Incremental change
θ	Range angle
λ	Latitude
μ_j	Lagrange multipliers
ρ	Nondimensional radius vector
ϱ	Radius from polar axis to vehicle in local horizontal plane
ϕ	Longitude
Φ	Constraint equations
ω_o	Initial orbital angular velocity with respect to inertial space
∞	Infinity
∇_2	Del 2 Normalized parameter - I_{sp}
∇_3	Del 3 Normalized parameter - Power

Subscripts

c	Circular
E	Earth's surface
i	Summation indices
j	Summation indices
M	Quantity is calculated from mass considerations
nd	Nondimensional
o	Initial reference orbit
p	Propellant
pp	Power Plant

pl	Payload
st	Structure
1	Escape point

Superscripts

$(\dot{\ })$	Denotes differentiation with respect to independent variable T.
$(')$	Denotes differentiation with respect to independent variable Θ .

GA/PHYS/62-4

Vita

John Joseph Dell was born on [redacted], the son of John S. Dell and Josephine Dell. After completing his work in 1952 at Pulaski Vocational and Technical High School, Bayonne, New Jersey, he enrolled at Newark College of Engineering from which he was graduated with the degree of Bachelor of Science in Mechanical Engineering. After receiving his commission as Lieutenant in the USAF Reserve, he entered active duty in October 1956 assigned to Wright-Patterson Air Force Base, Ohio and eventually held the position of Senior Project Engineer in the field of space propulsion. From this assignment he came to the Air Force Institute of Technology.

Permanent address: [redacted]

Final draft of this thesis was typed by Mrs. Patricia J. Rotterman. The completed thesis was typed by Miss Jo A. Wells.

UNCLASSIFIED